UNIVERSIDADE DE SÃO PAULO

INSTITUTO DE FÍSICA DE SÃO CARLOS

MÔNICA ANDRIOLI CARACANHAS

Vortices and impurities in atomic superfluids:

self-similar expansion and Tkachenko polaron.

São Carlos

2014

MÔNICA ANDRIOLI CARACANHAS

Vortices and impurities in atomic superfluids: self-similar expansion and Tkachenko polaron.

Thesis presented to the Graduate Program in Physics at the Instituto de Física de São Carlos, Universidade de São Paulo to obtain the degree of Doctor of Science.

Concentration area: Basic Physics
Advisor: Prof. Dr. Vanderlei S. Bagnato

Revised Version

(Original version available in the Unity of the Program)

São Carlos

2014

Ficha catalográfica elaborada pelo Serviço de Biblioteca e Informação do IFSC,
com os dados fornecidos pelo(a) autor(a)

Andrioli Caracanhas, Mônica
Vortices and impurities in atomic superfluids: self-similar expansion and Tkachenko polaron. / Mônica Andrioli Caracanhas; orientador Vanderlei Salvador Bagnato - versão corrigida -- São Carlos, 2014.
121 p.

Tese (Doutorado - Programa de Pós-Graduação em Física Básica) -- Instituto de Física de São Carlos, Universidade de São Paulo, 2014.

1. Bose-Einstein condensation. 2. Quantum turbulence. 3. Tkachenko excitations. 4. Polaron. I. Salvador Bagnato, Vanderlei, orient. II. Título.

Aos meus pais.

Acknowledgements

As a thesis supervisor, Professor Vanderlei Bagnato supported me in all stages of this work. He is the initiator of this project and he always gave me constant encouragement and advice, despite his busy schedule. I am especially grateful for his confidence and the freedom he gave me to do this work.

I wish to express my sincere gratitude to Professor Rodrigo Pereira for allowing me to conduct this research under his auspices. He offered me valuable instructions for this study and gave me the opportunity to meet new challenges in my career.

To our foreign collaborators, Professors Alexander Fetter, Victor Romero-Rochín, Vyacheslav Yukalov and Giacomo Roati. Especially thanks to Prof. Fetter, with whom I had a fruitful collaboration. He offered me relevant advice, spent much time to improve publications and he is always open to new illuminating disscussions.

I extend my sincere thanks to all members of our Optics group, to all those who contributed to my success along these years.

I would like to acknowledge the assistance of the postgraduate administrative staff (especially Silvio, Ricardo and Patrícia), the library members (especially Maria Neusa) and the printing-office staff (Ítalo and Denise).

I wish to express my gratitude to Mariana (Mari), Cristina (Cris), Grace and José Dirceu (Di), for all the support that they have been giving to me along these long years of our friendship. They are precious people and I consider myself tremendously lucky to have them on my side!

Without the support of all members of my family, I would never find the courage to overcome all the difficulties during this work. My thanks go to my parents for their confidence and their love during all these years.

This work was supported by Fapesp, CNPq and CAPES.

"Excellence is an art won by training and habituation. We do not act rightly because we have virtue or excellence, but we rather have those because we have acted rightly. We are what we repeatedly do. Excellence, then, is not an act but a habit."

- Aristóteles (384 – 322 a.C.)

"Anyone who has never made a mistake has never tried anything new."

- Albert Einstein (1879–1955)

"Para ser grande, ser inteiro; nada teu exagera ou exclui; ser todo em cada coisa; põe quanto és no mínimo que fazes; assim em cada lago, a lua toda brilha porque alta vive."

- Fernando Pessoa (1888 - 1935)

Abstract

CARACANHAS, M. A. **Vortices and impurities in atomic superfluids:** self-similar expansion and Tkachenko polaron. 2014. 121 p. Thesis (Doctorate in Science) - Instituto de Física de São Carlos, Universidade de São Paulo, São Carlos, 2014.

In this thesis we studied two aspects of Bose-Einstein condensation in dilute gases: (i) the self-similar expansion of a turbulent superfluidity, and (ii) the polaron physics in the context of the superfluid mixtures and vortex lattices. Both analyses are closely related to our experimental trends. Concerning the first subject, we generalized the superfluid hydrodynamic equations to describe the anomalous expansion of a turbulent condensate cloud. The physics behind this characteristic signature of the turbulence could be clarified through the expressions derived in our model, that considered the kinetic energy associated with a tangled vortex configuration. As for the second item, we present the polaron physics of a neutral impurity coupled with the Tkachenko modes of a vortex lattice Bose-Einstein condensate. Through the impurity spectral function, we tracked how the quasiparticle properties varied as a function of the interaction strength toward the lower energy regimes. The spectral function exhibits a Lorentzian broadening for small wave vectors, even at zero temperature, until it starts to reach the low energy fixed point, where it acquires a power law decay. That is the signature of orthogonality catastrophe phenomena, with the breakdown of the quasiparticle picture. We applied canonical unitary transform and renormalization group equations to evaluate the flow of the theory parameters as we go further down in the characteristic energy scales. Finally, we provide preliminary results on the calculation of a system composed of two condensate species, one immersed in a second containing an array of vortices. Making an analogy with superfluids in an optical lattice, we map our Hamiltonian onto a Bose-Hubbard type model and tune the atomic scattering length of the two species to induce a quantum phase transition in the confined cloud. This is a new quantum system which allows investigation beyond the present studies with static optical lattices.

Keywords: Bose-Einstein condensation. Quantum turbulence. Tkachenko excitations. Polaron.

Resumo

CARACANHAS, M. A. **Vórtices e impurezas em superfluidos atômicos:** expansão auto-similar e polaron Tkachenko. 2014. 121 p. Tese (Doutorado em ciências) - Instituto de Física de São Carlos, Universidade de São Paulo, São Carlos, 2014.

Neste projeto de doutorado estudamos dois aspectos em condensados de Bose-Einstein de gases alcalinos diluídos: (i) a expansão auto-similar de um superfluido turbulento, e (ii) a física dos pólarons no contexto de misturas de superfluidos e redes de vórtices. Ambas as análises estão relacionadas com nossas tendências experimentais em átomos frios. Na primeira etapa generalizamos as equações hidrodinâmicas dos superfluidos para descrever a expansão anômala de uma nuvem condensada turbulenta. A física por detrás dessa assinatura característica da natureza turbulenta da nuvem pôde ser compreendida através das equações derivadas em nosso modelo, que considerou a energia cinética advinda de uma configuração de vórtices enovelados. Na segunda parte do trabalho abordamos a física do pólaron, analisando as propriedades de uma impureza neutra acoplada com os modos Tkachenkos de um condensado de Bose-Einstein contendo uma rede de vórtices. Através da função espectral da impureza, pudemos acompanhar a evolução das propriedades de quase-partícula em função da magnitude do parâmetro de interação, à medida que caminhávamos em direção ao regime de baixas energias do sistema. A função espectral apresentou inicialmente um alargamento do seu perfil Lorentziano para baixos valores dos momentos da impureza e das excitações, mesmo a temperatura zero. Ao atingir a proximidade de um ponto fixo de baixas energias, porém, o espectro passa a adquirir um perfil de decaimento com lei de potência. Trata-se de uma assinatura do fenômeno da catástrofe de ortogonalidade, com a quebra da natureza de quase-particula do sistema. Aplicamos uma transformação canônica com operadores unitários e técnicas de grupo de renormalização para avaliar o fluxo das " constantes " da teoria à medida que diminuíamos as escalas de energia características do nosso sistema. Na etapa final apresentamos alguns resultados preliminares sobre o sistema de duas espécies de condensado sobrepostas, uma delas contendo a rede de vórtices. Por meio de uma analogia com superfluidos em redes ópticas, mapeamos nosso Hamiltoniano em um modelo Bose-Hubbard e variamos o comprimento de espalhamento atômico das espécies envolvidas para induzir a transição de fase quântica naquela aprisionada na rede. Mostramos que essa nossa nova configuração quântica de rede permite investigações que vão além daquelas estudadas com redes ópticas estáticas.

Palavras-chaves: Condensação de Bose-Einstein. Turbulência quântica. Modos de Tkachenko. Polaron.

List of Figures

List of abbreviations and acronyms

BEC	Bose–Einstein condensation/condensate
GPE	Gross-Pitaevskii equation
TF	Thomas–Fermi approximation
QUIC	Quadrupole and Ioffe configuration
TOF	Time–of–flight
LLL	Lowest–Landau–level
TM	Tkachenko modes
RG	Renormalization group
OC	Orthogonality catastrophe
RF	Radio–frequency
BH	Bose–Hubbard
MI-SF	Mott–insulator superfluid
EBH	Extended Bose–Hubbard

Contents

1 Introduction

1.1 BEC in dilute atomic vapor

The phenomenon known as Bose-Einstein condensation (BEC) was predicted by Einstein in 1924. In a system of particles obeying Bose statistics and whose total number is conserved, in his calculations there should be a temperature below which a finite fraction of all the particles condense into the same one-particle state. Based on the ideas of Bose related to photons, Einstein's original prediction was for a noninteracting gas, a system felt by some of his contemporaries to be perhaps pathological. This scenario changes, however, shortly after the observation of superfluidity in liquid ^4He below the λ temperature ($2.17\,K$) (1). Fritz London suggested that, despite the strong interatomic interactions, BEC was indeed occurring in this system and was responsible for the superfluid properties; his suggestion has survived until now and forms the basis for our modern understanding of the superfluid phase (2). In 1995 BEC was realized in a system very different from ^4He, namely, dilute atomic alkali gases trapped by magnetic fields (3). Over the last few years these systems have been the subject of an explosion of research, both experimental and theoretical (4, 5).

Contrary to the superfluid liquid helium, that consists of a high density atomic system with complicated nonlocal interactions, the weakly interacting Bose gas condensate behaves like a system of point particles with simple local interactions. For the latter, there is a mean field treatment given by the Gross Pitaevskii equation (GPE) (6, 7). The GPE is a practically exact model in the limit of zero temperature, where essentially all of the atoms exist in the Bose-Einstein condensate phase. In many experiments the condensate exists at well below the BEC transition temperature such that this approximation is justified. Extensions of the GPE to include the effect of thermal atoms provide a more complete (albeit not exact) physical model of a real BEC (8). It successfully describes many properties of trapped condensate clouds such as the dynamics (free expansion and

collective modes) and the low energy excitations, including collective excitations, solitons and vortices singularities (6); even the superfluid turbulence in such a system has been the subject of many theoretical papers, which are based on simulations of the GPE to generate and track the evolution of the turbulent regime (9, 10).

Besides of being an easily superfluid system to dealt when compared to the liquid helium counterpart, there is a growing interest in the field of cold atoms associated with other aspects of it. Atomic physics experiments with quantum degenerate Bose and Fermi gases are characterized by the distinguishing features that we have: a detailed microscopic understanding of the Hamiltonian of the systems realized in the laboratory, and complete control of the system parameters via external fields. In particular, atoms can be trapped and their motion controlled in magnetic and optical traps, allowing for example, the realization of quantum gases with different dimensionality at effectively zero temperature. In addition, atoms have many internal states which can be manipulated using laser light and can be employed as a probe of the gas properties, and their collisional properties can be tuned with magnetic and optical Feshbach resonances (3, 7). That made possible the production of the two component BECs, which was the first attempt to nucleate vortices in this system. Latter techniques to generate vortex singularities come with the rotational anisotropic bulk experiment (attractive dipole potential created by a stirring laser beam) and also the phase imprinting method (phase profile imprinted onto the condensate via laser beams) (5). A new chapter in this history starts with the artificial Gauge fields technique, that is in the way to produce an ordered vortex array in the BEC (11).

In the early days of atomic BEC experiments, the main focus was to investigate condensate properties of matter waves like coherence, as described theoretically by the Hartree-Fock-Bogoliubov mean field theory for weakly interacting quantum gases (7). More recently, emphasis has shifted to strongly interacting systems, which are much more in line with present interests in theoretical condensed matter physics. As mentioned before, not only the external potential, but also the interaction and now the kinetic terms (gauge fields) can be well controlled in the BEC system. These new techniques developed to manipulate the cold atoms turn this field a great "toolbox" to probe the concepts de-

veloped in the nuclear physics, condensate matter and quantum computation fields. The BEC can reproduce condensed matter Hamiltonians, for example, with most experimental simulations coming with the introduction of the BECs in optical lattices (4). This leads to Hubbard type lattice models, where one can engineer various types of Hamiltonians for $1D$, $2D$ and $3D$ Bose and Fermi systems, which can be controlled by varying external field parameters. In addition, the field of the cold atoms has generated problems and ideas specific to these novel systems.

This scenario illustrates the importance of the field that this doctorate's project belongs to. The models developed here closely follow our experimental group observations and our future trends in the laboratory. Moreover, the study realized in this thesis, including the experimental proposals to probe the developed theory, is relevant in the context of Bose-Einstein condensate mixtures, since it requires the application of the most recent and successful techniques in this field: the advances in cooling mechanisms to produce binary condensates, Feshbach resonance technique to control the interaction parameters and artificial Gauge fields to selectively nucleate vortex lattices in one of the atomic species.

1.2 Thesis outline

In section 2, we described the turbulent superfluid system. Particularly, the superfluid hydrodynamic model (formalism equivalent to the GPE equation) was generalized to explain the anomalous behavior of the free expanding turbulent condensate cloud observed in the São Carlos Optics Group experiments.

Following the latest trends in our experiments, in the remaining sections of the thesis we deal with the topic of two species BEC.

In section 3, we analyzed the properties of impurities immersed in a vortex lattice formed by ultracold bosons in the mean field quantum Hall regime. Besides the effects of a periodic lattice potential that come with the interspecies atomic repulsion, the impurity is dressed by collective modes of the lattice (Tkachenko modes) with parabolic dispersion.

We keep the analysis of the single impurity-vortex lattice system toward lower temperature regimes, until the break of the previous polaronic quasiparticle picture. The latter phenomenon was demonstrated by the appearance of a power law decay in the impurity's Spectral Function.

The model for the two superfluid system started to be built in section 4, after its stability properties had been established within the single impurity case. The polaron superfluid in a vortex lattice Bose-Einstein condensate system was mapped onto a Bose-Hubbard type Hamiltonian. Then, we investigated a quantum phase transition in the confined cloud by tuning the atomic scattering length of the two species. We described how this new quantum system allows novel phenomena beyond the present studies with static optical lattices.

The summary of the main results and the conclusions for each chapter of the thesis are presented in section 5.

2 Self-Similar expansion of a turbulent cloud

2.1 Definition of BEC and GPE formalism

Bose-Einstein condensation was first described for an ideal gas of free bosons, with mass m and density n. The chemical potential μ is obtained from the conditions

$$n_{\mathbf{k}} = \frac{1}{e^{\beta(\varepsilon_{\mathbf{k}}-\mu)}-1}$$
$$\sum_{\mathbf{k}} n_{\mathbf{k}} = n,$$

where the boson occupation $n_{\mathbf{k}}$ has $\varepsilon_{\mathbf{k}} = k^2/2m$ and $\beta = (k_B T)^{-1}$. In a dimension $d > 2$, μ reaches 0 at a temperature T_c such that

$$\int d\varepsilon\ \rho(\varepsilon)\ \frac{1}{e^{\beta_c \varepsilon}-1} = n$$

where we have the one particle density of states $\rho(\varepsilon) \sim \varepsilon^{d/2-1}$. The existence of a finite value for this integral reflects the saturation of the occupation number of particles in the excited states. Then, below T_c, a macroscopic number of particles N_0 accumulates in the lowest state, with μ locked to zero giving the maximum value for the occupation distribution of the excited states. When $d \leq 2$ the integral above diverges and Bose-Einstein condensate does not occur, since we will have $T_c = 0$.

These conclusions hold for an uniform infinite system. The condensation at low dimensions can be restored, however, if the system is put in a confining potential $V \sim r^{\nu}$ (12) that changes the accessible region for the particles. A particle with energy ε can occupy a volume of radius $L \sim \varepsilon^{1/\nu}$, and the correspondent density of states will now behave as $\rho(\varepsilon) \sim L^d \varepsilon^{d/2-1} = \varepsilon^{d/\eta+d/2-1}$. We can alter η to make the integral convergent and T_c finite.

The original argument of Einstein to treat the condensation process assumes the absence of interactions. We would like to generalize here the definition of BEC to an interacting system. A generally applicable definition of BEC was given by Penrose and Onsager (1956), starting with the diagonal form of one-particle density matrix of the system (13).

Considering a system consisting of a large number N of spinless bosonic particles (without internal degrees of freedom). It may have arbitrary interparticle interactions and be subject to a general time-dependent single-particle potential. Any pure many-body state of the system at time t can be written in the form $\psi_N(\mathbf{r}_1, \mathbf{r}_2, ..., \mathbf{r}_N)$, were $\mathbf{r}_i$ describes the coordinates of the particle i. This function ψ_N is symmetric under exchange of any pair ij, and can be used to define the single-particle density matrix for this system

$$\rho_1(\mathbf{r}, \mathbf{r}', t) = N \int d\mathbf{r}_2 ... d\mathbf{r}_N \; \psi_N(\mathbf{r}_1, \mathbf{r}_2, ..., \mathbf{r}_N) \; \psi_N^*(\mathbf{r}_1', \mathbf{r}_2, ..., \mathbf{r}_N) \tag{2.1}$$

Here, $\rho_1(\mathbf{r}, \mathbf{r}', t)$ is basically the probability amplitude, at time t, to find a particular particle at $\mathbf{r}$ times the amplitude to find it at $\mathbf{r}'$, averaged over the behavior of all the other $N-1$ particles. Since it is a Hermitinan matrix $\rho_1(\mathbf{r}, \mathbf{r}') = (\rho_1(\mathbf{r}', \mathbf{r}))^*$, there is a complete set of orthogonal eigenfunctions $\varphi_\alpha(\mathbf{r}, t)$ of ρ_1, for any given t, that allows we rewrite it in a diagonal form $\rho_1(\mathbf{r}, \mathbf{r}', t) = \sum_\alpha n_\alpha(t) \varphi_\alpha^*(\mathbf{r}, t) \varphi_\alpha(\mathbf{r}', t)$, with the natural normalized orbitals $\int d^2r \, |\varphi_\alpha(\mathbf{r}, t)|^2 = 1$.

Returning to the statement "a macroscopic number of particles occupies a single oneparticle state", the existence of a BEC depends on the magnitude of the n_α compared to N:

1. If all the eigenvalues n_α of ρ_1 at time t are of order unity (none of order N), then we say the system is "normal" at time t (i.e. not Bose-condensed).
2. If there is exactly one eigenvalue of order N, with the rest all of order unity, then we say the system exhibits "simple BEC".
3. If there are two or more eigenvalues of order N, with the rest of order unity, then we say it exhibits "fragmented BEC".

We can make the definition rigorous by taking an appropriate thermodynamic limit; e.g. for a gas of atoms moving freely in space in volume V, we can consider the limit $N \to \infty$,$V \to \infty$,$N/V = const.$, $T = const.$; then the limiting value for n_α of order N is reflected in a constant value of the fraction n_α/N, while the statement that "n_α is of order unity" means that $lim(n_\alpha/N) \to 0$.

Genuine Bose-Einstein condensation is not an ideal gas effect; it necessarily implies

interacting particles. For an interacting system of bosons, there is only one eigenvalue of ρ_1 that has $\mathcal{O}(N)[n_0 \sim N]$, and the system is a BEC described by a single particle wave function. We remark that the essential role played by the interaction between the particles is due to the exchange interaction energy contribution that appears when we deal with condensate in more than one state. That makes condensate fragmentation energetically costly (14); then the condensate particles accumulate in a single state and there are no condensate particles shared between different degenerate states.

A general system of bosons with mass m interacting through a potential $V_{int}(\mathbf{r})$ and moving in an external potential $V_{ext}(\mathbf{r},t)$ is described by the Hamiltonian (6, 7)

$$\hat{H} = \int d^3r\, \hat{\psi}^\dagger(\mathbf{r},t)\left[\frac{-\hbar^2}{2m}\nabla^2 + V_{ext}(\mathbf{r},t)\right]\hat{\psi}(\mathbf{r},t)$$
$$+ \int d^3r\, d^3r'\, \hat{\psi}^\dagger(\mathbf{r},t)\hat{\psi}^\dagger(\mathbf{r}',t)V_{int}(\mathbf{r}-\mathbf{r}')\hat{\psi}(\mathbf{r},t)\hat{\psi}(\mathbf{r}',t). \qquad (2.2)$$

Just as in a magnetic material described by an isotropic Heisenberg model, the Hamiltonian is invariant under simultaneous rotation of all the spins, so in a Bose system described by standard creation and annihilation operators $\hat{\psi}(\mathbf{r})$, $\hat{\psi}^\dagger(\mathbf{r})$ it is invariant under the global $U(1)$ gauge transformation $\hat{\psi}(\mathbf{r}) \to \hat{\psi}(\mathbf{r})\, e^{i\phi}$, $\hat{\psi}^\dagger(\mathbf{r}) \to \hat{\psi}^\dagger(\mathbf{r})\, e^{-i\phi}$. At first sight, symmetry forbids either the expectation value $\langle \mathbf{S} \rangle$ of the magnetization of the magnetic material, or the corresponding quantity $\langle \hat{\psi} \rangle$ in the Bose system, to take a finite value. Nevertheless, we know that if the material in question is ferromagnetic, then when it is below its Curie temperature and we take the thermodynamic limit, in the presence of infinitesimal symmetry breaking fields, the quantity $\langle \mathbf{S} \rangle$ indeed takes a finite (macroscopically large) value, and thus the direction of the magnetization is a well defined quantity. Similarly, it is argued in the Bose case when one is below the Bose condensation temperature and takes the thermodynamic limit in a similar way, $\langle \hat{\psi} \rangle$ (order parameter) becomes finite (in this case proportional to $N^{1/2}$) and its phase ϕ thus become well defined. The Bose condensate is said possess a "spontaneous broken gauge symmetry" (13).

In the spirit of a mean-field theory, Pitaevskii (15) (1961) and Gross (1963) (16) independently derived an equation for the condensate wave function by approximating $\hat{\psi}(\mathbf{r})$ in the equation of motion, $i\hbar\, \partial_t \hat{\psi}(\mathbf{r},t) = [\hat{\psi}(\mathbf{r},t), \hat{H} - \mu\hat{N}]$, by its expectation value

$\langle\hat{\psi}(\mathbf{r},t)\rangle = \psi_0(\mathbf{r},t)$ over a coherent state, where μ is the chemical potential and $\hat{N}$ is the number operator. That comes with the replacement of a quantum degree of freedom by its classical approximation.

To justify this approximation, we can consider again the diagonal form of the single particle density matrix ρ_1. Since $\rho_1(\mathbf{r},\mathbf{r}',t) = \langle\hat{\psi}(\mathbf{r},t)^\dagger\hat{\psi}(\mathbf{r}',t)\rangle$ (6), that gives the possibility of identify the field operator as a linear combination of the density matrix eigenfunctions, that is, $\hat{\psi}(\mathbf{r},t) = \sum_\alpha \varphi_\alpha(\mathbf{r},t)\hat{a}_\alpha$, where $\hat{a}^\dagger_\alpha$, $\hat{a}_\alpha$ are the annihilation and creation operators of a particle in the state φ_α (single particle wave function for general interacting and nonuniform operator). As the field obeys, for a fixed time t, the commutator relation $[\hat{\psi}(\mathbf{r}),\hat{\psi}^\dagger(\mathbf{r}')] = \delta(\mathbf{r}-\mathbf{r}')$ and $[\hat{\psi}(\mathbf{r}),\hat{\psi}(\mathbf{r}')] = 0$, then we can derive the equivalent relation $[\hat{a}_\alpha,\hat{a}^\dagger_\beta] = n_\alpha\ \delta_{\alpha,\beta}$ and $[\hat{a}_\alpha,\hat{a}_\beta] = 0$. Also, from the definition of ρ_1 we found $\langle\hat{a}^\dagger_\alpha\hat{a}_\beta\rangle = \delta_{\alpha\beta}\ n_\alpha$. Upon condensation, we have that $n_0 = \langle\hat{a}^\dagger_0\hat{a}_0\rangle$ will assume a macroscopically large value N_0. On the other hand, the commutator $\left[\hat{a}_0,\hat{a}^\dagger_0\right] = 1$ continues to be of $\mathcal{O}(1)$. Thus, it seems reseanable to neglect all commutators of the zero operator $\hat{a}_0$ in comparison with its expectation value.

The wave function $\varphi_0(\mathbf{r},t)$ relative to the macroscopic eigenvalue n_0 plays a crucial role in the theory of BEC and characterizes the so-called wave function of the condensate. To characterize that, it is useful separate in the field operator $\hat{\psi}$ the condensate from the other components

$$\hat{\psi}(\mathbf{r},t) = \varphi_0(\mathbf{r},t)\hat{a}_0 + \sum_{\alpha\neq 0}\varphi_\alpha(\mathbf{r},t)\hat{a}_\alpha. \tag{2.3}$$

The introduction of BEC trough Bogoliubov consist in replace the operator $\hat{a}_0$ by $\sqrt{N_0}$, that is the classical approximation justified above. It is equivalent to treat the macroscopic component $\varphi_0(\mathbf{r},t)\hat{a}_0$ as a classical field $\psi_0(\mathbf{r},t) = \sqrt{N_0}\varphi_0(\mathbf{r},t)$. Additionally, we can have a residual field $\hat{\delta}\psi(\mathbf{r},t) = \sum_{\alpha\neq 0}\varphi_\alpha(\mathbf{r},t)\hat{a}_\alpha$.

The Gross-Pitaevskii equation (GPE) reads

$$i\hbar\,\partial_t\psi_0(\mathbf{r},t) = \left[\frac{-\hbar^2}{2m}\nabla^2 - \mu + V_{ext}(\mathbf{r},t) + \int d^2r'\,V_{int}(\mathbf{r}-\mathbf{r}')|\psi_0(\mathbf{r}',t)|^2\right]\psi_0(\mathbf{r},t). \tag{2.4}$$

The use of the Gross-Pitaevskii equation (2.4) to describe the interacting boson system assumes a small BEC depletion, i.e., $N_0 \simeq N$. This is a good approximation in the

absence of strong correlations and at low temperatures. Thus, it is particularly suitable for dilute ultracold gases (6,7), for which the interparticle potential range is much smaller than the interparticle distance. In these systems, interactions are well described by the pseudopotential $V_{int}(\mathbf{r}) \simeq g\,\delta(\mathbf{r})$, where the effective interaction g includes the influence of short-wavelength degrees of freedom that have been eliminated.

Let us turn to the consequences of the GPE, setting $V_{ext}(\mathbf{r},t) = V_{ext}(\mathbf{r})$ and considering the many-body ground state evolution through a phase factor $\psi_0(\mathbf{r},t) = \psi_0(\mathbf{r})\, e^{-i\mu t}$. Substituting this form into Eq. (2.4) yields the time-independent GPE

$$\mu\psi_0(\mathbf{r}) = \left[\frac{-\hbar^2}{2m}\nabla^2 + V_{ext}(\mathbf{r}) + g|\psi_0(\mathbf{r})|^2\right]\psi_0(\mathbf{r}). \tag{2.5}$$

Now we specialize to the case of a free single-particle system, $V_{ext}(\mathbf{r}) = 0$, focusing on a small but nonzero coupling constant g. In particular, the ground state will be the spatially constant, macroscopically occupied zero-momentum state ψ_0. This uniform GPE equation reveals much about the nature of the system:

- For $\mu < 0$ (i.e. above the condensation threshold of the non-interacting system), the equation exhibits only the trivial solution $\psi_0 = 0$. This means that no stable condensate amplitude exist.
- Below the condensation threshold ($\mu \geq 0$), the equation is solved by any configuration with $|\psi_0| = \sqrt{\mu/g}$. - The equation couples only to the modulus of ψ_0. That is, the solution of the stationary phase equation is continuously degenerate: each configuration $\psi_0 = \sqrt{\mu/g}\, e^{i\phi}$ with $\phi \in [0, 2\pi]$ is a solution.

As in the condensate matter physics (17), given a theory with globally G invariant action, two scenarios are possible: either the ground states share the invariance properties of the action or they do not. The two alternatives are illustrated in the this example of the Bose system. For $\mu < 0$, the action has a single ground state at $\psi_0 = 0$. This state is trivially symmetric under the action of $G = U(1)$. However, for positive μ, i.e. in the situation discussed above, there is an entire manifold of degenerate ground states,

defined through the relation $|\psi_0| = \sqrt{\mu/g}$. These ground states transform into each other under the action of the gauge group. However, none of them is individually invariant. The above definition confirmed our previous argumentation that the $U(1)$ symmetry group was spontaneously broken.

Locking of the phase means fluctuation of the particles number N and the appearance of the Bogoliubov excitations on top of the condensate. Interacting boson systems support excitations with a dispersion that strongly deviates from the free-particle dispersion $\varepsilon_0(k) = \hbar^2 k^2/2m$. To compute the excitation spectrum, as derived by Bogoliubov, we determine a quadratic Hamiltonian from Eq. (2.2) in terms of $\delta\hat{\psi}(\mathbf{r}) = \hat{\psi}(\mathbf{r}) - \sqrt{N_0}$ and $\delta\hat{\psi}^\dagger(\mathbf{r}) = \hat{\psi}^\dagger(\mathbf{r}) - \sqrt{N_0}$ and keep only the (leading) terms up to $\mathcal{O}(N_0)$. Its linearized form describes the condensate excitations, which, for an uniform gas, has a dispersion of the form $\varepsilon(k) = \sqrt{\varepsilon_0(k)[\varepsilon_0(k) + 2gn_0]}$, with $n_0 = N_0/V$ the atomic density and g is the strength of the interaction. Note that, in the $|\mathbf{k}| \to 0$ limit, the excitations above the BEC state are linearly dispersing phonons: $\varepsilon(k) \simeq \hbar s|\mathbf{k}|$, where $s = \sqrt{gn_0/m}$. From the point of view of the spontaneous breakdown of the $U(1)$ symmetry, the phonons are the Goldstone modes of the broken-symmetry phase (17). We remark that these virtual excitations of particles out of the condensate are enough to lift the degeneracy of the ground state, favoring the pure state condensates (14).

2.2 Superfluid dynamic equations

In this part we introduce the superfluid hydrodynamic equations. The physical content of the GPE may be revealed by reformulating it as a pair of hydrodynamic equations, which are expressions of the conservation laws for particle number and for total momentum. That can be derived by setting $\psi_0(\mathbf{r}, t) = \sqrt{n(\mathbf{r}, t)}\, e^{i\theta(\mathbf{r},t)}$ in Eq. (2.4). Separating the real and imaginary parts of the resulting system we obtain the equations

$$\partial_t\theta + \left(\frac{\hbar(\nabla\theta)^2}{2m} + \frac{1}{\hbar}[V_{ext} + gn] - \frac{\hbar}{2m}\frac{\nabla^2\sqrt{n}}{\sqrt{n}}\right) = 0,$$
$$\partial_t n + \frac{\hbar}{m}\nabla\cdot(n\nabla\theta) = 0. \tag{2.6}$$

In Eq. (2.6), the first equation describes a potential flow with velocity potential $\mathbf{v}(\mathbf{r},t) = (\hbar/m)\nabla\theta(\mathbf{r},t)$. That equation tells us that the system adjusts to spatial fluctuations of the density by a dynamical phase fluctuation. The second equation represents a continuity equation, where the particle current is given by $\mathbf{j}(\mathbf{r},t) = n(\mathbf{r},t)\mathbf{v}(\mathbf{r},t)$. A current flow with non-vanishing divergence is accompanied by dynamical distortions in the density profile. The most remarkable feature of these equations is that, for a uniform density ($V_{ext} = 0$), they possess steady state solutions with non-vanishing current flow. Setting $\partial_t\theta = \partial_t n = 0$, we obtain the conditions $\delta n = 0$ and $\nabla \cdot \mathbf{j} = 0$, i.e. below the condensation temperature, a configuration with an uniform density profile can support a steady state divergenceless (super)current.

Steady state current flow in normal environments is prevented by the mechanism of energy dissipation, i.e. particles constituting the current flow scatter off imperfections inside the system, converting part of their energy into the creation of elementary excitations (macroscopically, the conversion of kinetic energy into the creation of excitations manifests itself as heat production). Apparently, this mechanism is inactivated in superfluid states of matter, i.e. the current flow is dissipationless. No energy can be exchanged if there are no elementary excitations to create. Then, to avoid dissipative loss of energy, the excitations of the system have to be energetically high-lying, so that the kinetic energy stored in the current-carrying particles is insufficient to create them. There is an argument due to Landau showing that a linear excitation spectrum (the long wavelength Bogoliubov sound wave spectrum derived in the previous section) indeed is suffices to stabilize dissipationless transport in superfluids, if the fluid velocity is inferior to the characteristic sound velocity (7).

Let us conclude with important consequences related to the superfluid velocity field $\mathbf{v}$. In any region of space where $n(\mathbf{r},t)$ is nonzero (so that $\mathbf{v}(\mathbf{r},t)$ is everywhere defined) we have $\nabla \times \mathbf{v}(\mathbf{r},t) = 0$. Since ψ_0 is single valued, the change of its phase over any close path must be a multiple of 2π. That gives the Onsager-Feynman quantization

condition for the circulation (6)

$$\begin{aligned} \triangle\theta = \oint_C \nabla\theta \cdot d\ell = \kappa\, 2\pi \\ \rightarrow \oint_C \mathbf{v} \cdot d\ell = \kappa h/m, \end{aligned} \tag{2.7}$$

with κ an integer value. The explicit occurrence of $\hbar$ in this formula reminds us that the superfluid velocity is essentially a macroscopic manifestation of a quantum-mechanical object.

2.3 Turbulence in atomic BECs

The study of turbulence in quantum fluids goes back to early thermal counterflow experiments, where the superfluid and the normal component travel in opposite directions, producing a turbulent regime (18). Feynman characterized the turbulent regime in a superfluid as a tangle of quantized vortices (19). Vinen verified this scenario in his experiments with ^{4}He (18), where the resulting dissipation was connected to the friction of the vortex lines with the normal fluid. Recently, the experimental observation of quantized vortices and turbulence in condensates of trapped atomic vapors (20,21) contributes to the Feynman picture of turbulence; also, it confirms the superfluid nature of the BEC.

The possibility of studying turbulence in an alternative superfluid to liquid helium is very attractive and may still create new exciting possibilities. Atomic Bose-Einstein condensates (BEC) are a highly tunable system that holds much promise for the development of theoretical and experimental insights into some of the unanswered questions surrounding the theory of quantum turbulence (22). First of all, the relatively low density of trapped atomic superfluids allows a clearer visualization of the vortex geometry as well as the direct observation of the distribution of vortices and other effects related to few vortices. Vortex reconnections (23), which can change the topology of the vortex lines, always play an important role in quantum turbulence and there is a lack of understanding about the microscopic details previously observed and studied in liquid helium.

New effects due to the finite aspects of the superfluids (22), that might not be

present in homogeneous systems like helium, will appear in these atomic trapped systems. Those effects might be remarkable concerning the evolution of the turbulent regime and its decay, generating thermal atoms, which can be easily detected and better studied in their dynamical aspects. The finite size effects may place limits on the maximum number of allowed vortices existing in the superfluid cloud before evolving to turbulence. This fact may have dramatic implications on the dynamical behavior of the turbulent states.

Atomic BECs are currently the most accessible system in which to study the small scale properties of turbulent vortex flow. Theoretical investigations have begun to build up a picture of vortex dynamics and the processes contributing to the forcing and decay of turbulence at small scales (24–26) and there is a favorable scenario for experimental verification of those mechanisms in atomic BECs. At large scales, the features of classical turbulence are an emerging feature of quantum turbulence (27), suggesting that research with BEC systems may provide insight into some of the outstanding questions of turbulence. The study and understanding of turbulence in Bose-Einstein condensation of trapped neutral atoms is still at the very beginning, but has a great potential to become an important and exciting research field.

2.4 Anomalous expansion of a turbulent cloud

In recent work, the turbulent state of a ^{87}Rb condensate was observed under the application of oscillatory perturbations to the trapping magnetic field (20, 21). These experiments showed the possibility to create a turbulent state in an ultracold atomic alkaline system starting from a normal BEC.

An up view of our experimental apparatus is showed in Fig. 1a. The magnetic field is given by a QUIC (Quadrupole and Ioffe configuration) trap (28), composed of a quadrupole field generated by two coils operating in anti-Helmholtz configuration and an Ioffe coil. The latter creates a bias field that eliminates the zero values in the magnetic field of the quadrupole. The overall trapping potential felt by the BEC cloud can be approximated by a harmonic potential, which frequencies are related with atomic magnetic

Figure 1 – Experimental apparatus (a) and oscillatory perturbation scheme (b)

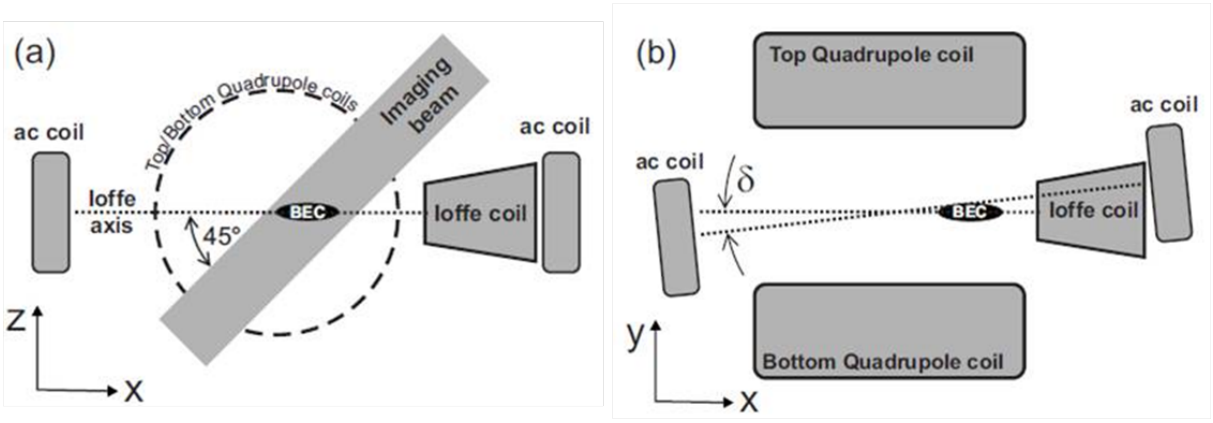

Source: HENN et al. (20)

Figure 2 – Density profile of the atomic condensate cloud, obtained using absorption imaging of the ^{87}Rb atomic cloud after 15 ms of time-of-flight: (a) single vortex in an ordinary condensate, where the cloud dimension is 60 μm × 80 μm; (b) density distribution of a turbulent condensate, with dimension 300 μm × 100 μm.

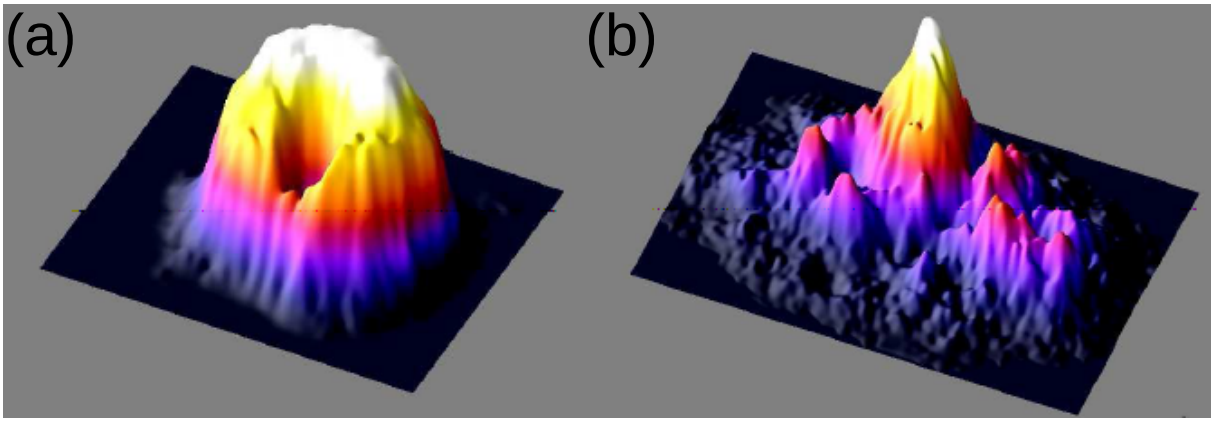

Source: CARACANHAS et al. (29)

moment and the magnetic field intensity (7,28). For our large number atomic sample, the equilibrium configuration of the trapped BEC comes from the competition between the trap potential and the repulsive atomic interaction (7). The cigar shaped cloud profile showed in Fig. 1 is due to our axial symmetric trap configuration, with lower confinement along the symmetry axes direction (represented by x in the scheme of Fig. 1, but that will be treat in the following as z axes), with $\omega_z/\omega_\rho \sim 0.1$. Figure 2 shows absorption images from a single vortex Thomas-Fermi (TF) BEC and a turbulent cloud generated in these experiments (the oscillatory magnetic field perturbation is generated by the misaligned ac coils illustrated in Fig. 1b). A lot of vacancies can be clearly observed in the density

Figure 3 – Absorption Image of the ^{87}Rb cloud during the free expansion: (a) shows a classical thermal (non-condensed) cloud expansion, for which the value of aspect ratio tends to unity; (b) an anisotropic expansion of an ordinary BEC, without vortices, where there is an inversion of the initial aspect ratio; (c) expansion of a condensate in the turbulent regime, where the aspect ratio seems fixed.

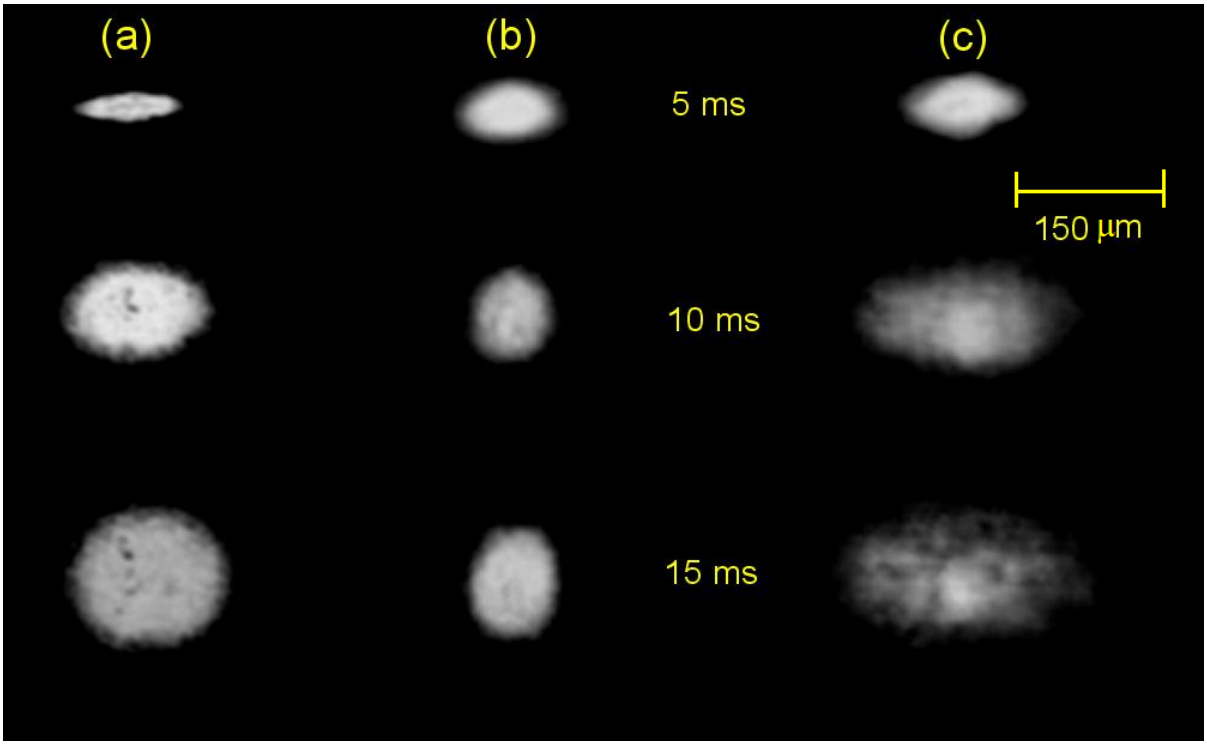

Source: CARACANHAS et al. (29)

profile of the turbulent cloud. They indicate where the vorticity is concentrated during the imaging process (image beam represented in Fig. 1a).

The most common diagnostic of trapped atomic clouds is done by imaging it after the cloud is released from the trap, that is, during the free expansion. That makes it easy to identify the differences between a thermal and a Bose-condensed cloud. The thermal cloud shows a gaussian profile that evolves to an isotropic density distribution at long times of expansion. Otherwise, in the Thomas-Fermi regime (7) (dense and interacting large BEC cloud), the quantum cloud shows a profile that reflects the shape of the confining trap. Then, for a cigar-shaped trap, for example, the BEC cloud expands dramatically faster in the radial than in the axial direction, mostly due to the strongest repulsive interaction between the atoms (for an ideal BEC we could expected this same behavior, since the quantum pressure also increases with the spatial confinement). That causes

the signature inversion of the BEC cloud aspect ratio during the free expansion. These expansion dynamics can be seen respectively in columns (a) and (b) of Fig. 3. Considering now a turbulent BEC cloud, besides the evidences of the tangled vortices configuration given by the vacancies in the density profile absorption image in Fig. 2, we observed that the cloud dynamics also differed from the thermal and the BEC samples due to the presence of vorticity. In fact, for the cigar shaped trap used in (21), the turbulent condensate expands with a nearly constant aspect ratio once released from its confinement and does not display the aspect ratio inversion observed in a TF condensate. In Fig. 3 c we show this evolution, clearly self-similar, of the turbulent cloud.

To characterize the anomalous expansion of the turbulent sample, we developed a generalized expansion model based on the Lagrangian approach. The kinetic term contribution of a tangle vortex configuration was added to the system Lagrangian and the Euler-Lagrange equations were derived to describe the dynamics of the turbulent cloud. The aspect-ratio calculations agreed with the experimental results, showing that the physics behind the anomalous expansion of the turbulent system was well explained by our model (30). Further details are reviewed below. Before that, we introduce the rotational hydrodynamic model to characterize the effect of the vortices over the free expansion of the cloud.

2.5 Rotational Hydrodynamic equation

The original hydrodynamic approach was successfully employed to describe the collective modes dynamics and the vortex free condensate expansion (6); now its rotational version comes to deal with the vortex lattice BEC dynamics (31).

As defined in the introduction, the rotational velocity field of the superfluid should be zero. Otherwise, considering the integral in Eq. (2.7), we can define a closed path C on which ψ_0 is everywhere finite, but which envelops a region in which the latter vanishes. For this particular situation, we can have the rotational velocity field non zero above the enclosed singularity (6, 7). This scenarios apply to a path taken around the singularity

of a vortex GPE solution (5). For example, considering a cylindrical coordinate system $\mathbf{r}(\rho, \theta, \phi)$), the vortex wave function, with a straight line singularity along z, is given by

$$\Phi(\mathbf{r}) = \sqrt{n} e^{i\kappa\phi} f(\rho)$$

Now we have a GPE solution with a space dependent phase, which velocity field profile can be determined from Eq. (2.7) as

$$\mathbf{v}(\mathbf{r}, t) = \frac{\kappa\hbar}{m\rho}\hat{\phi}. \tag{2.8}$$

As expected, that gives a rotational velocity field with

$$\nabla \times \mathbf{v} = \frac{\kappa\hbar}{m}\delta^{(2)}(\mathbf{r})\ \hat{\mathbf{z}}. \tag{2.9}$$

Considering now an array of vortices aligned along z. We can determine the circulation that comes from the contribution of all vortex lines inside a closed path, establishing a mean vorticity Ω ($= \frac{h}{2m} n_V$ (5)) for the enclosed area, so that $\nabla \times \mathbf{v} = 2\mathbf{\Omega}$. Basically we associate a classical fluid behavior for the superfluid system due to its high angular velocity (= high density non overlaping-vortex lines n_V). This is a well-known approximation applied before to treat the dynamics of a BEC cloud with an array of vortices (31). We will describe further properties of the vortices lattice system in the next chapter, emphasizing here that such approximation for the vortex array superfluids enable us to derive their rotational version of the Euler equation

$$\partial_t \mathbf{v} + \nabla\left(\frac{1}{2}mv^2 + V_{ext} + gn\right) = m\mathbf{v} \times (\nabla \times \mathbf{v}).$$

We conclude this part by introducing the rotational hydrodynamic equations, which were applied in (29) to solve the expansion dynamics of the turbulent cloud. Here we briefly describe some of the results obtained in that reference, since they are important material for our most recent model for the turbulent superfluid dynamics, that will be treated in the next section.

As in the variational method, in the Thomas-Fermi (TF) hydrodynamic approach we started defining an ansatz to the condensate wave function. That has a couple of

parameters, which dynamic equations are obtained after substitute the ansatz in the hydrodynamic equations. We considered for the density and velocity field

$$n(\mathbf{r},t) = n_0(t)\left(1 - \frac{x^2}{R_x^2(t)} - \frac{y^2}{R_y^2(t)} - \frac{z^2}{R_z^2(t)}\right),$$

$$\mathbf{v}(\mathbf{r},t) = \frac{1}{2}\nabla\left(b_x(t)x^2 + b_y(t)y^2 + b_z(t)z^2\right) + \mathbf{\Omega}(t)\times\mathbf{r}, \tag{2.10}$$

with the TF radius R_i for the density profile and velocity field phase coefficient b_i. That last is associated to the irrotational component of the velocity field, and, according with Eq. (2.10), was complemented by a rotational component, with vorticity $\Omega(t) = \frac{\hbar}{m}\frac{N_V}{R_y(t)R_z(t)}$, associated to the presence of a vortex array in our system (with N_V vortices). The latter was considered aligned perpendicularly to the symmetry axis of the initial trapped cloud, that has the cigar shaped profile Fig. 4. Using the hydrodynamic equations constrains: particle number conservation and stability of the initial solution, translated in the relation $b_i = \frac{\dot{R}_i}{R_i}$ and the additional irrotational velocity field $\alpha(t)\nabla(xy)$, with $\alpha(t) = \frac{R_y^2(t)-R_z^2(t)}{R_y^2(t)+R_z^2(t)}\,\Omega(t)$, we could combined the time evolution equation for R_i and b_i to obtain the second order equations for the TF cloud dimensions

$$\begin{aligned}
\ddot{R}_x - \frac{15N\hbar^2 a_s}{m^2}\frac{1}{R_x^2 R_y R_z} &= 0\\
\ddot{R}_y - \frac{15N\hbar^2 a_s}{m^2}\frac{1}{R_y^2 R_x R_z} &= 4\left(\frac{N_V\hbar}{m}\right)^2\frac{1}{\left(R_y^2+R_z^2\right)^2}R_y\\
\ddot{R}_z - \frac{15N\hbar^2 a_s}{m^2}\frac{1}{R_z^2 R_x R_y} &= 4\left(\frac{N_V\hbar}{m}\right)^2\frac{1}{\left(R_y^2+R_z^2\right)^2}R_z.
\end{aligned} \tag{2.11}$$

We showed that the centrifugal force resulted form the vortex lattice velocity field diminishes the atomic repulsive interaction force effects, that originally dictates the shape of the expanded cloud. Figure 4 illustrates the aspect ratio deceleration obtained for our particular vortex array orientation, obtained with the numeric solution of the system in Eq. (2.11).

From these considerations we conclude that the vortex alignment could bring the desired effect to explain the anomalous behavior of the turbulent cloud. In spite of the vortex lines be a main ingredient to characterized the turbulence in quantum fluids, we

Figure 4 – Aspect-ratio evolution during the free expansion of a normal and a vortex array BEC cloud with vorticity along the the x-axis (perpendicular to the symmetry axis). The vorticity is normalized by the radial trap frequency ω_ρ. To keep the system stability we have to constrain $\Omega < \omega_\rho$. For $\Omega = 0.7\omega_\rho \rightarrow N_V \sim 70$

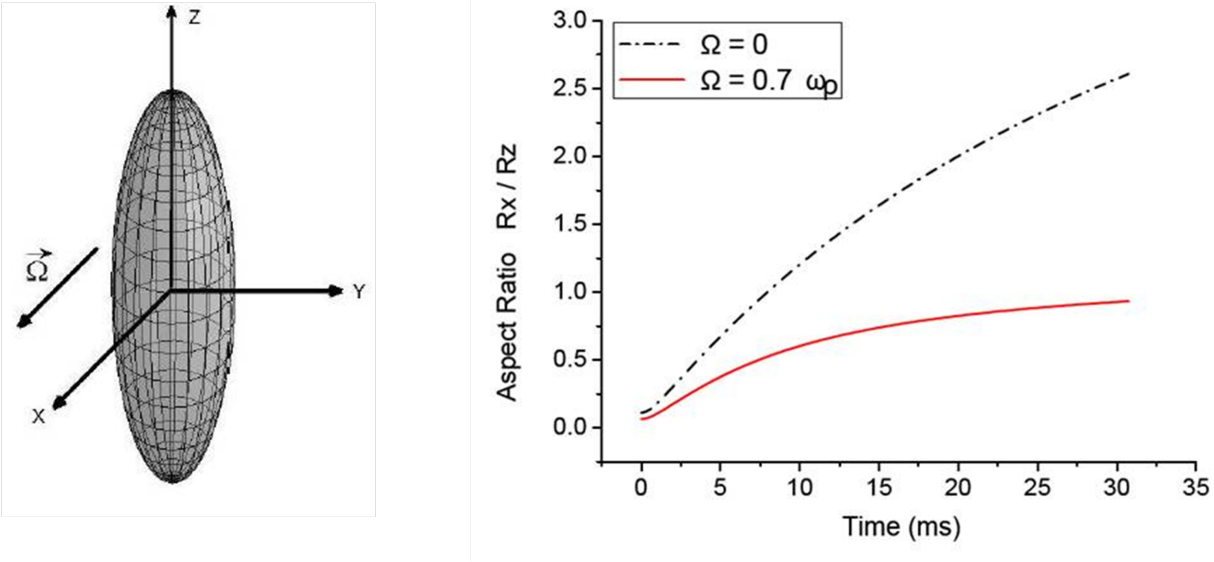

Source: CARACANHAS et al. (29)

did not expect that a vortex lattice modeling could give more than a qualitative insight for our experimental results. Next, we will describe our Lagrangian model, where we attempt to obtain a quantitative agreement with our experimental data.

2.6 Lagrangian with isotropic vorticity

After having presented our main problem in section 2.4 and described our first theoretical approach to deal with this system (section 2.5), here we applied variational principle to derive the dynamic equations for the expansion of a turbulent condensate cloud. Our time-dependent equations for the radius were derived from the action principle

$$\delta \int_{t_1}^{t_2} \mathcal{L}\, dt = 0, \tag{2.12}$$

where the Lagrangian $\mathcal{L}$ is

$$\mathcal{L} = \int d^3r \left[i\frac{\hbar}{2}\left(\psi^* \frac{\partial \psi}{\partial t} - \psi \frac{\partial \psi^*}{\partial t}\right) - \varepsilon[\psi]\right]. \tag{2.13}$$

The energy density $\varepsilon[\psi]$ is given by

$$\varepsilon[\psi] = \frac{\hbar^2|\nabla\psi|^2}{2M} + V_{ext}|\psi|^2 + \frac{1}{2}g|\psi|^4, \tag{2.14}$$

with the repulsive atomic contact interaction $g = 4\pi\hbar^2 a_s/M$, where a_s is the s-wave scattering length and M the atomic mass; $V_{ext}(\boldsymbol{r})$ gives the external confining potential.

In the variational principle Eq. (2.12), the variations of ψ (or ψ^*) are arbitrary, apart from the requirement that they vanish at $t = t_1$, $t = t_2$, and on any spatial boundaries for all t. With a physically motivated choice of trial function ψ, this variational principle provides the foundation for approximate solutions of dynamical problems. In this context, we consider the Thomas-Fermi (TF) trial function for ψ in Eq. (2.15)

$$\psi(\vec{r},t) \;=\; e^{iS(\vec{r},t)} \prod_{j=x,y,z} e^{i\beta_j M\, x_j^2/2\hbar}\, \sqrt{n_0}\left(1 - \sum_{j=x,y,z}\frac{x_j^2}{R_j^2}\right)^{1/2} \Theta\left(1 - \frac{x^2}{R_x^2} - \frac{y^2}{R_y^2} - \frac{z^2}{R_z^2}\right), \tag{2.15}$$

including the velocity arising from the random vortices (with a phase S) and the overall expansion (with a phase ϕ, here parametrized by the three quantities β_j); the variational parameters being the TF radius R_j and the phase β_j associated with the irrotational velocity potential $\phi_j = \beta_j\, M\, x_j^2/2\hbar$, that leads to a linear velocity field $u_j = \beta_j\, x_j$, with $j = x, y, z$. Note that the induced expansion velocity is strictly irrotational. The normalization integral of $\psi(\vec{r},t)$ yields

$$n_0 = \frac{15N}{8\pi}\frac{1}{R_x R_y R_z}, \tag{2.16}$$

where N represents the total number of atoms in the cloud.

With this ansatz we generalize the usual formalism, including the kinetic energy associated with tangled vortex configuration in the system Lagrangian. Applying the trial function in Eq. (2.13) provides

$$\begin{aligned}\mathcal{L} = &-\frac{NM}{14}\left(R_x^2\dot{\beta}_x + R_y^2\dot{\beta}_y + R_z^2\dot{\beta}_z\right) - \frac{NM}{14}\left(\beta_x^2 R_x^2 + \beta_y^2 R_y^2 + \beta_z^2 R_z^2\right)\\ &-\frac{NM}{2}\langle\upsilon_0^2\rangle - \frac{NM}{2}\langle\delta\upsilon^2\rangle - \frac{15}{7}\frac{\hbar^2\, a_s\, N^2}{M}\frac{1}{R_x R_y R_z}.\end{aligned} \tag{2.17}$$

Above, we considered the rotational velocity field

$$\frac{\hbar}{M}\nabla S = \upsilon_0 + \delta\upsilon, \tag{2.18}$$

where υ_0 is the cloud center of mass motion induced by the vorticity, while $\delta\upsilon$ is the additional local velocity associated with the individual vortices. In Eq. (2.17) we assumed that the time derivative of S is negligible (slow vortex motion) and only considered velocities squares without the cross terms (uncorrelated υ_0 and $\delta\upsilon$). The mean values $\langle\cdots\rangle$ are evaluated with a single-particle wave function $\varphi = N^{-1/2}\psi$.

We can calculate the term $\langle\delta\upsilon^2\rangle$ for the energy of the individual vortices integrating the local vortex line energy density (6, 7) (the square of Eq. (2.8) with $\kappa = 1$, multiplied by the atomic mass density "M n") in the radial direction from the vortex core size ξ to the maximum radius ℓ. That latter corresponds to the effective intervortex separation for a given randomly oriented vortex configuration, for which we associated the energy per unit length

$$\frac{\pi n\hbar^2}{M}\ln\left(\frac{\ell}{\xi}\right). \tag{2.19}$$

Assuming that there is a mean vortex line length L per unit volume, the total energy from the tangled vortices will be

$$E_{vort} = \frac{\pi\, N\,\hbar^2}{M}\, L\, \ln\left(\frac{\ell}{\xi}\right). \tag{2.20}$$

We scale L with the inverse squared length, so

$$L(R) \propto (R_x^2 + R_y^2 + R_z^2)^{-1}. \tag{2.21}$$

This choice leads to dynamical equations that look like a generalization of those previously in Eq. (2.11), as we will be seen.

When the vortex energy in Eq. (2.20) is substituted into Eq. (2.17), we obtain the system Lagrangian

$$\mathcal{L} = -\frac{NM}{14}\left(R_x^2\dot{\beta}_x + R_y^2\dot{\beta}_y + R_z^2\dot{\beta}_z\right) - \frac{NM}{14}\left(\beta_x^2R_x^2 + \beta_y^2R_y^2 + \beta_z^2R_z^2\right) - N\,U(R_x, R_y, R_z),$$

where the effective potential U is given by

$$U(R_x, R_y, R_z) = \frac{M}{2}\langle\upsilon_0^2\rangle + \frac{15}{7}\frac{a_s\hbar^2N}{M}\frac{1}{R_xR_yR_z} + \frac{\pi\hbar^2}{M}\frac{L_0(R_{x0}^2 + R_{y0}^2 + R_{z0}^2)}{R_x^2 + R_y^2 + R_z^2}\ln\left(\frac{\ell}{\xi}\right), \tag{2.22}$$

with L_0 being the initial value of the vortex line density. The Lagrangian equations $(d/dt)(\partial\mathcal{L}/\partial\dot{\beta}_j) = \partial\mathcal{L}/\partial\beta_j$ for β_j are straightforward and yield $\beta_j = \dot{R}_j/R_j$, which enforces the conservation laws. Correspondingly, the Lagrangian equation $\partial\mathcal{L}/\partial R_j = 0$ for R_j simplifies because $\beta_j^2 + \dot{\beta}_j = \ddot{R}_j/R_j$. Some algebra yields the basic result $\frac{1}{7}M\ddot{R}_j = -\partial U/\partial R_j$, or more explicitly (ignoring the mean velocity $\langle v_0^2\rangle$ and treating the slowly varying logarithm as constant), it yields the dynamical equation for $j = x, y, z$

$$\ddot{R}_j = 14\pi \frac{\hbar^2}{M^2} \frac{L_0(R_{x0}^2 + R_{y0}^2 + R_{z0}^2)R_j}{(R_x^2 + R_y^2 + R_z^2)^2} \ln\left(\frac{\ell}{\xi}\right) + 15 \frac{\hbar^2 a_s}{M^2} \frac{N}{R_j R_x R_y R_z}. \tag{2.23}$$

According with the equation above, the rapid expansion of the turbulent cloud arises from two sources: the isotropic vorticity and the repulsive atomic interaction, given respectively by the first and second terms in the right-hand side of Eq. (2.23). For large times, when the expansion yields large values for the mean radii, the vortex term dictates the cloud dynamics due to its particular scaling with the inverse radius (three inverse powers, whereas the interaction term has four inverse powers). When the vortex term dominates over the interaction (at long times), the equations acquire a simple form, with $\ddot{R}_j/R_j$ independent of the index j, that leads to the asymptotic scale invariance (self-similarity).

Finally we solved the system of differential equations Eq. (2.23) to obtain the evolution of the aspect ratio for both the vortex-free and the turbulent cloud. Returning to the initial value of the vortex line density $L_0 = L_0^T/V_0$, we can estimate the total vortex line extension $L_0^T = \bar{R}_0 N_V$ ($\bar{R}_0 = \sqrt{R_{0x}^2 + R_{0y}^2 + R_{0z}^2}$), where N_V represents the number os vortices inside the cloud of initial volume V_0. Starting with the initial cloud configuration (stationary solution of Eq. (2.23), when we included the trap potential V_{ext}), we calculated the aspect ratio dynamics in Fig. 5 (experimental parameters in the legend). While the vortex-free condensate shows the aspect ratio inversion, the turbulent condensate rapidly achieves an asymptotic value less than one. Hence we have an inhibition of the inversion due to self-similar expansion.

Besides the calculation of the cloud aspect-ratio, with the hydrodynamic equations we can also track the evolution of interaction and kinetic energy of the cloud during the free

expansion. For a vortex free condensate, it is well known that the energy from the repulsive atomic interaction is decisive to the cloud shape *in situ*, dominating its aspects during the free expansion (6). The energy functional associated with the turbulent system, however, presents the competition between this repulsive interaction and the extra kinetic energy provided by the vortices. That new aspect of the turbulent cloud can be seen in Fig. 6 (see also the inset, with the energy balance of a normal BEC), with the energy functionals calculated from the solution of the dynamic equations. It is possible demonstrate that

Figure 5 – Aspect-ratio evolution during the free expansion of a normal and a turbulent BEC. The inset represents the time window in the experiments ($10 < \tau < 30 \rightarrow 4 < t < 18\ ms$). Points represent the experimental values and the solid lines our theoretical calculation. The parameters are from our experiment with ^{87}Rb: trap frequency: $\omega_x = \omega_y = \omega_\rho = 2\pi \times 207\,Hz$ and $\omega_z = 2\pi \times 23Hz$; number of atoms: $N = 10^5$; scattering length: $a_s = 100a_0$. We chose N_V that maximized the effects of the vortex tangled $[N_V = 8\pi\, N\, a_s/(e\, \bar{R}_0)]$.

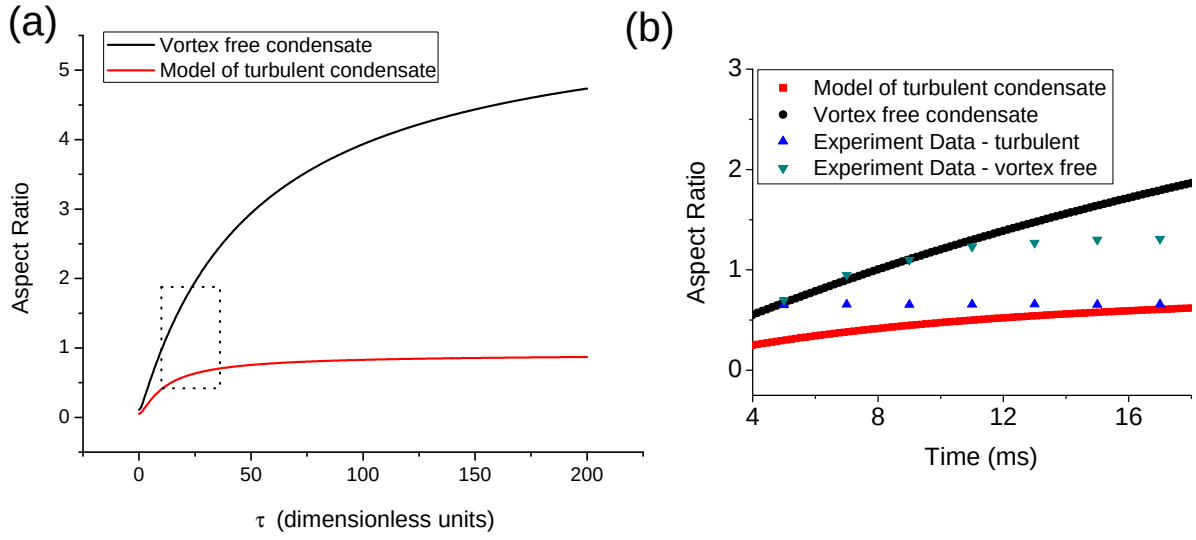

Source: CARACANHAS et al. (30)

the asymmetry of the trap V_{ext} contributes to balance the cloud energy between kinetic (vortex rotational field) and interaction. In the context of the turbulent cloud in a cigar shape trap, the vortex kinetic contribution has a crucial role in the expansion, since it attenuates the effects of the interaction energy that, for our cigar shape trap configuration, affects mainly the more confined direction. The inhibition of the aspect ratio inversion (21) of the turbulent cloud is related to an increment in the expansion velocity along the less confined direction (symmetry axes). That could be explained by an preferential

alignment of the vortices lines along the short axes, due to lower line bending probability. Then, the centrifugal contribution (perpendicular to the line direction) of such "partial aligned" bundle of lines affects mainly the axial direction.

Figure 6 – Evolution of interaction and kinetic energy of the cloud during the free expansion.

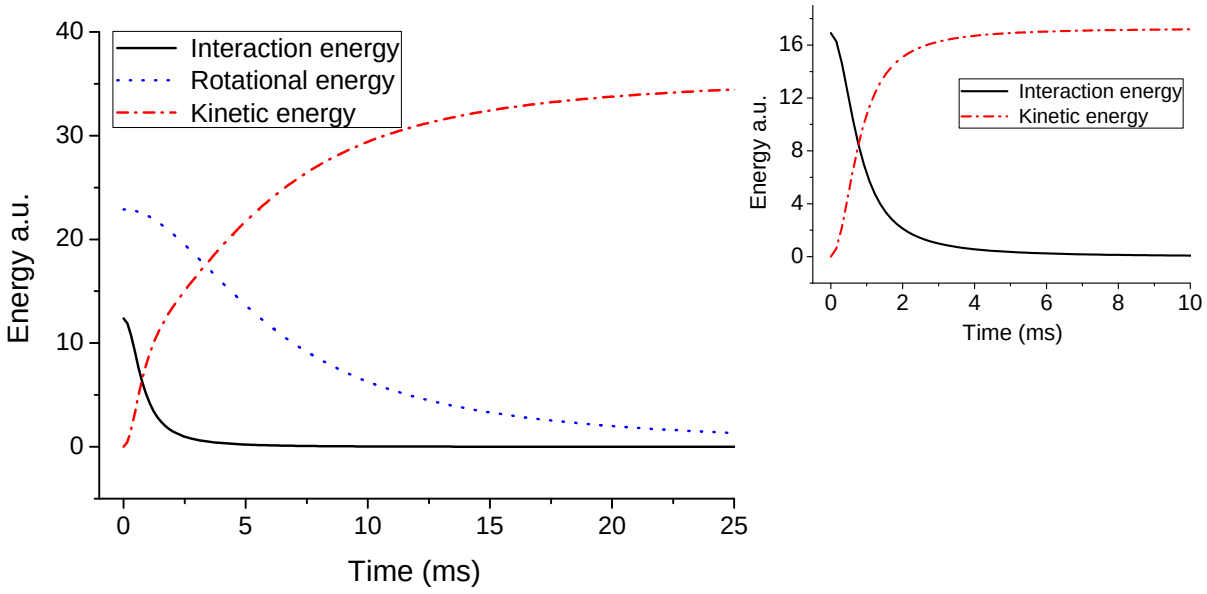

Source: elaborated by the author

2.7 Frozen Modes

In this section we applied again the generalized Lagrangian formalism, but to explain the apparent suppression of the collective modes dynamics in a harmonic trapped turbulent cloud. The collective modes of a BEC cloud can be determined through the linearization of the correspondent Euler-Lagrange dynamic equations (32, 33). In the following, we linearize our dynamic equations in Eq. (2.23), including the trap potential, and solve the resulting system to extract the normal frequencies of the low energy collective modes. Particularly, for a cigar shape trap geometry, we easily obtained analytical expressions for the modes frequencies (32). Those were compared with the collective mode frequencies of a normal BEC cloud. We concluded that the higher magnitude of the former represent a further obstacle to excite this particular mode in the vortex tangled BEC.

Assuming $N_V = 8\pi\, N\, a_s/(e\,\bar{R}_0)$ (30) and for the trap aspect ratio $\lambda = \omega_z/\omega_\rho$, we used $\tau = \omega_\rho t$ and $R_i = l_r \tilde{R}_i$ $(l_r = \sqrt{\hbar/M\omega_\rho})$ in Eq. (2.23) to obtain the dimensionless system of differential equations

$$\begin{aligned}
\ddot{\tilde{R}}_x + \tilde{R}_x &= \frac{P_r}{\tilde{R}_x^2\,\tilde{R}_y\,\tilde{R}_z} + \frac{P_v\,(\tilde{R}_{0x}^2+\tilde{R}_{0y}^2+\tilde{R}_{0z}^2)}{(\tilde{R}_{0x}\,\tilde{R}_{0y}\,\tilde{R}_{0z})}\;\frac{\tilde{R}_x}{(\tilde{R}_x^2+\tilde{R}_y^2+\tilde{R}_z^2)^2}\\
\ddot{\tilde{R}}_y + \tilde{R}_y &= \frac{P_r}{\tilde{R}_y^2\,\tilde{R}_x\,\tilde{R}_z} + \frac{P_v\,(\tilde{R}_{0x}^2+\tilde{R}_{0y}^2+\tilde{R}_{0z}^2)}{(\tilde{R}_{0x}\,\tilde{R}_{0y}\,\tilde{R}_{0z})}\;\frac{\tilde{R}_y}{(\tilde{R}_x^2+\tilde{R}_y^2+\tilde{R}_z^2)^2}\\
\ddot{\tilde{R}}_z + \lambda^2\tilde{R}_z &= \frac{P_r}{\tilde{R}_z^2\,\tilde{R}_x\,\tilde{R}_y} + \frac{P_v\,(\tilde{R}_{0x}^2+\tilde{R}_{0y}^2+\tilde{R}_{0z}^2)}{(\tilde{R}_{0x}\,\tilde{R}_{0y}\,\tilde{R}_{0z})}\;\frac{\tilde{R}_z}{(\tilde{R}_x^2+\tilde{R}_y^2+\tilde{R}_z^2)^2},
\end{aligned} \tag{2.24}$$

where $P_r = 15\,N\,a_s/l_r$ and $P_v = (48\pi/e)\;(N\,a_s/l_r)$. Now we can linearize the system Eq. (2.24) with

$$\begin{aligned}
\tilde{R}_x &= \tilde{R}_{0x} + \delta_x(\tau),\\
\tilde{R}_y &= \tilde{R}_{0y} + \delta_y(\tau),\\
\tilde{R}_z &= \tilde{R}_{0z} + \delta_z(\tau),
\end{aligned} \tag{2.25}$$

where $\tilde{R}_{i0}$ corresponds to the stationary solution in the trap and δ_i is the deviation around this equilibrium value. In an extremely cigar shaped trap ($\lambda \ll 1$), we have $(\tilde{R}_{0x}^2+\tilde{R}_{0y}^2+\tilde{R}_{0z}^2) \sim \tilde{R}_{0z}^2$. That simplifies the stationary equations ($\ddot{R}_i = 0$) of Eq. (2.24), which can be written with cylindrical coordinates

$$\begin{aligned}
\tilde{R}_{0\rho} &= \frac{P_r}{\tilde{R}_{0\rho}^3\,\tilde{R}_{0z}} + \frac{P_v}{\tilde{R}_{0\rho}\,\tilde{R}_{0z}^3}\\
\lambda^2\tilde{R}_{0z} &= \frac{P_r}{\tilde{R}_{0z}^2\,\tilde{R}_{0\rho}^2} + \frac{P_v}{\tilde{R}_{0^2}^2\,\tilde{R}_{0z}^2}.
\end{aligned} \tag{2.26}$$

This system provides the approximate solution

$$\begin{aligned}
\tilde{R}_{0\rho} &= \left[\frac{P_r\,\lambda^{2/3}}{(P_r+P_v)^{1/3}}\,\frac{1}{1-\frac{P_v\,\lambda^2}{(P_r+P_v)}}\right]^{3/10} \sim \frac{P_r^{3/10}\,\lambda^{1/5}}{(P_r+P_v)^{1/10}}\\
\tilde{R}_{0z} &= \frac{(P_r+P_v)^{1/3}}{\lambda^{2/3}}\,\frac{1}{\left[\frac{P_r\,\lambda^{2/3}}{(P_r+P_v)^{1/3}}\,\frac{1}{1-\frac{P_v\,\lambda^2}{(P_r+P_v)}}\right]^{1/5}} \sim \frac{(P_r+P_v)^{2/5}}{P_r^{1/5}\,\lambda^{4/5}}.
\end{aligned} \tag{2.27}$$

After substitute Eq. (2.25) in (2.23), the coefficients of the linear terms in δ can be applied to constructed the matrix $(\delta_\rho,\, \delta_z)$ of the resulting system. The characteristic polynomial of this matrix was determined and its roots provided the collective mode frequencies

$$\tilde{\omega}_b = \sqrt{2 - \frac{P_v\,\lambda^2}{(P_v + P_r)}} \sim \sqrt{2} \tag{2.28}$$

and

$$\tilde{\omega}_q = \frac{1}{\sqrt{2}}\frac{1}{(P_v + P_r)}\left[A_1 - \sqrt{A_2}\right]^{1/2} \tag{2.29}$$

with $A_1 = (3\,\lambda^2 + 4)\,P_v^2 + (6\,\lambda^2 + 8 + 8\,\lambda^4)\,P_r\,P_v + (3\,\lambda^2 + 4)\,P_r^2$ and $A_2 = (16 - 40\,\lambda^2 + 25\lambda^4)\,P_v^4 + (-136\,\lambda^2 + 48\,\lambda^6 + 208\,\lambda^4 + 64)\,P_r\,P_v^3 + (350\,\lambda^4 + 96 - 168\,\lambda^2 + 64\,\lambda^8)\,P_r^2\,P_v^2 + (-48\,\lambda^6 - 88\,\lambda^2 + 64 + 176\,\lambda^4)\,P_r^3\,P_v + (-16\,\lambda^2 + 9\,\lambda^4 + 16)\,P_r^4$.

Those solutions are associated respectively with the breathing (ω_b) and the quadrupole (ω_q) modes (6, 7). While the breathing mode corresponds to in phase oscillation of the radial and axial radius of the condensate, the quadrupole mode is associated to the out of phase oscillation of these widths. For $P_v = 0$, that is, without the vortex contribution, we recover the expected values for an usual TF BEC (32, 33)

$$\tilde{\omega}_b = \sqrt{2} \tag{2.30}$$

and

$$\tilde{\omega}_q = \frac{1}{\sqrt{2}}\left[3\,\lambda^2 + 4 \pm \sqrt{-16\,\lambda^2 + 9\,\lambda^4 + 16}\right]^{1/2} \tag{2.31}$$

Finally, for our extreme cigar shape tap $\lambda \ll 1$, the limit of Eq. (2.29) gives the frequency

$$\tilde{\omega}_q \to \frac{1}{\sqrt{2}}\left[5 + \frac{3\,P_v}{(P_v + P_r)}\right]^{1/2}\lambda \tag{2.32}$$

that is

$$\omega_q = \tilde{\omega}_q\,\omega_\rho = \frac{1}{\sqrt{2}}\left[5 + \frac{3\,P_v}{(P_v + P_r)}\right]^{1/2}\omega_z. \tag{2.33}$$

Considering our experimental parameters for P_v and P_r (20), we find ω_q 20% higher than the value expected for a normal BEC in this same trap conditions. That contributes to explain the "freezing" of this collective oscillation of the turbulent cloud. In the real

system, however, we can not disregard the presence of the thermal cloud, mainly after submitting the BEC to the oscillatory perturbation. The thermal atoms generate friction in the vortex tangle system due to the their scattering with the vortex filaments. This energy dissipative process can also inhibit the cloud collective modes.

2.8 Summary

We modeled the anomalous expansion of a condensate in the turbulent regime. The expressions developed here clarify the physics behind the self-similar free expansion, which is a crucial and characteristic signature of turbulence in the trapped system, as seen in experiments. Although very phenomenological in nature, our model shows that the behavior of the expansion depends intrinsically on the amount and distribution of vorticity present in the sample.

3 Impurity in a Vortex Lattice

3.1 Tkachenko polaron

3.1.1 Polaron History

The problem of the motion of an electron in an ionic crystal has been of interest ever since the solid state physics began to developed in the early 1930's. The interest in this problem has continued to the present day since it provides a simple model of particles interacting with a quantum field and serves as a test ground for new methods (34). Besides that, it is relevant for applied physics superconductors. The fate of a single impurity interacting with its environment determines the low-temperature behavior of many condensed matter systems. Polarons are central to the understanding of colossal magnetoresistance materials (35), and they affect the spectral function of cuprates, the parent material of high-T_c superconductors (36). Another famous impurity problem is the Kondo effect, where immobile spin impurities give rise to an enhanced resistance in metals below the Kondo temperature (37). Following, we give a brief overview of the studies that drive us to this quasiparticle state.

In 1933, Landau pointed out that the most energetically favorable state of an electron in a polar lattice can be either a freely moving particle in an undistorted (or slightly distorted) lattice, or a trapped particle in a strongly distorted lattice (38). Pekar pushed this concept and developed a macroscopic model where the polar lattice is described as a dielectric continuous medium (39). His works are focused on this new quasiparticle, composed of a localized electron and the potential well of the distorted lattice, for which Pekar coined the term polaron. Up to this point, the concept of self-trapping was fully equivalent to localization. The idea of the polaron as a mobile free charge carrier was presented in a subsequent paper and the effective mass of the polaron was calculated by Landau and Pekar. Pekar's polaron describes an electron interacting with optical phonons

of frequency ω. Due to finite phonon frequencies, ion polarizations can follow electron motion if it moves sufficiently slow. This situation gives polarons with wave functions and corresponding lattice distortions spread over many lattice sites, propagating through the lattice as free electrons but with an enhanced effective mass. The size of the trapped state is large enough that the discreteness of the lattice can be ignored, and a continuous dielectric medium can be used instead, hence a large or continuous polaron.

The Fröhlich (40) model has a starting point similar to the Pekar polaron, with the electron in the periodic potential of the three-dimensional lattice treated through the bare effective mass approximation and the ionic crystal approximated by a continuous dielectric medium. However, this time the polarization was treated in a proper quantum mechanical way, that is, in the second quantized form, where the ionic displacement was described by phonons. When the polaron binding energy E_p (lattice deformation energy due to the electron presence) is larger than the half-bandwidth, zt of the electron band, all states in the Bloch bands are dressed by phonons. That occurs if we increase the coupling to phonons such that the polaron radius becomes comparable with the lattice constant (sites separation) and the carriers are described as small or lattice polarons. Then, the continuum approximation is no longer justified and we have to move on to the lattice models. Basically, an increase coupling will give a crossover from Bloch states of band electrons (parabolic dispersion) or large polarons propagating with almost bare mass in a rigid lattice to heavily dressed Bloch states of small polarons propagating with an exponentially enhanced effective mass (34).

The most studied lattice model is the Holstein, that is focus on optical phonons approximated by dispersionless Einstein phonons with $\omega(q) = \omega$ and with the simpler Holstein coupling $g(q) = g$. We define two dimensionless parameters to describe the various regimes of the lattice polaron, as opposed to the single dimensionless coupling constant of the large polaron. First is the adiabaticity ratio ω/t, with the particles tunneling rate t. The second parameter is the dimensionless electron-phonon coupling constant $g = E_p/zt$. Besides the Holstein coupling, the possible forms of electron phonon couplings include the polar, or Fröhlich coupling discussed above with $g(q) = 1/|q|$ and the deformation

coupling with $g(q) = |q|$.

In 1957, in an attempt to understand the role of back flow in the roton feature of the helium superfluid dispersion (41), Feynman and Cohen studied a different polaron: an impurity atom in a condensed ^4He superfluid. The polarons, in this sense, can be defined as the excitations created through the interaction of the impurity with the BEC atoms.

3.1.2 Polaron in Ultracold Atoms

To review the subject of polaron in ultracold atoms, we chose to summarize selective works that illustrate the particularities of this system.

An important experiment in this research area is given in (42), where a small concentration of spin-down impurities was immersed in a spin-up Fermi sea of ultracold atoms. In contrast to the electron moving in a phonon bath, a bosonic environment, the impurity there interacts with a fermionic environment, the Fermi sea of electrons. In this system the interaction strength is characterized by the ratio of the inter particle distance, that is a function of spin-up Fermi wave vector, to the atomic scattering length. The scenario for a single impurity was the following: for weak attraction, the impurity propagates freely in the spin-up medium of density and experiences the familiar attractive mean field energy shift. However, as the attractive interaction grows, the impurity can undergo momentum changing collisions with environment atoms, and thus starts to attract its surroundings. The impurity "dressed" with the localized cloud of scattered fermions constitutes the Fermi polaron. Dressing becomes important once the mean free path of the bare impurity in the medium becomes comparable to the distance between environment particles. The dressed impurity can move freely through the environment, with an energy shifted away from the simple mean field result. This polaronic state is stable until, for strong attraction, equivalent to a deep effective potential well, the spin-down impurity will bind exactly to one spin-up atom, thus forming a tightly bound molecule.

In the experiment described above, they used the Feshbach resonance technique (7) to modify the strength of the contact interaction between the impurity and the background

atoms. Also, they applied radio Frequency spectroscopy (43–45) to explore the excitation spectrum of the system and identify the polaron formation (i.e. the appearance of a distinguishable peak in the impurity spectrum that differs from the background spectrum). This technique will be further detailed in the end of this section. An important remark here it is the higher control of the model parameters when the theory is made with this ultracold atomic system. Particularly, for the polaron problem, we can explore not only different coupling regimes, but also engineer new kinds of momentum dependence for the coupling parameter, as will be shown in our project later on. Other important advance bring by the cold atoms community is the optical trap (7). To deal with our next example, we have to explain some properties of a variety of optical trap called optical lattice (4).

There is no doubt that the optical lattice device represents an enormous development in the atomic vapors Bose-Einstein condensates field. This lattice is made with counter-propagating laser beams that produce periodic trap potentials for the BEC atoms. The laser parameters: intensity, frequency and polarization direction, can be controlled in a very wide range yielding a versatile trap geometry. Optical lattices are ideally suited to produce and study one and two dimensional BECs with the remaining degrees of freedom frozen. They also allow to alter the ratio of kinetic to interaction energy significantly with respect to magnetically trapped BEC, leading to the experiment where an optical lattice was used to adiabatically transform a BEC into a Mott insulating state (4). In spite of all flexibility introduced with this trapped system, it has a serious limitation to simulate condensed matter systems: the lack of phonons, that is, the ions vibrations of a crystal. Since the most interesting phenomena in condensed matter physics involve phonons, is desirable to introduce them in a controlled way into optical lattices.

Returning to the context of polaron in ultracold atoms, there is a theoretical proposal to compensate this absence of lattice phonons in the optical lattices. It has been suggested that immersing an optical lattice into a BEC leads to intraband phonons, which induce the formation of polarons. The idea is to study the transport properties of bosonic atoms in an optical lattice, when they are dressed by the Bogoliubov coherent phonon modes of a second, not trapped, species background (46). The latter do not see the lattice

and its density fluctuation provides the polaronic effective tunneling and self-interaction of the trapped species. Besides that, it was also suggested to use an interband darkstate laser transition associated with the intraband phonon scattering in this system as a mechanism to cool the atomic sample in the optical lattice (47).

3.1.3 Vortex Lattice

As mentioned in the abstract of this thesis, in our analysis we consider the impurity bosonic species trapped in a vortex lattice BEC. The vortex array configuration was first observed in a dilute-gas BEC by the group of Ketterle (MIT) in 2001 (48), followed by the experiments of Cornell's group, that observed the normal excitations of the lattice (49) (see Fig. 7), that is, vortex lines oscillations that characterizes the low energy Tkachenko modes (50–52). The array configuration appears after the appropriate angular momentum

Figure 7 – Tckachenko mode: long-wavelength transverse lattice excitations of the vortex lines.

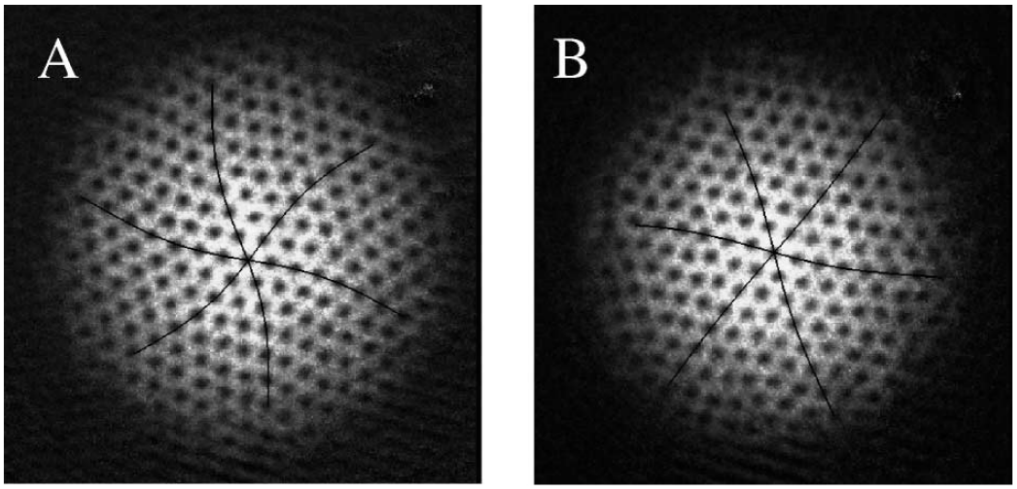

Source: CORNELL et al. (49)

being transferred to the superfluid sample. Once established, this configurations proved to be stable, including its normal modes (53), with a rotational frequency close to, but below, the external trap confining potential (54). We started describing this system in section 2, but now we will analyze its properties; in particular the vortex lattice collective modes, that represent our phonons.

In 1955, Feynman predicted that a superfluid can rotate when pierced by an array of quantized singularities or vortices. Some years later, Abrikosov demonstrated that such vortices in a type II superconductor organize into a triangular crystalline lattice due to their mutual repulsion. Not surprisingly, Abrikosov lattice has an associated rigidity. In 1966, Tkachenko proposed that a vortex lattice in a superfluid would support transverse elastic modes. He published two remarkable papers (55, 56) on the behavior of arrays of straight vortices in an unbounded rotating incompressible irrotational fluid as a model for superfluid ^4He. The first paper shows that a triangular lattice has the lowest energy of all simple lattices with one vortex per unit cell. The second paper studies small perturbations of a general lattice, showing that the square lattice is unstable for waves in certain directions, but that the triangular lattice is stable for all normal modes. For the triangular structure, he also determines the dispersion relation of the small-amplitude normal modes of a vortex lattice, along with the corresponding eigenvectors, for a given wave vector q lying in the xy plane perpendicular to rotational frequency Ω. Considering the vortex cell radius to be $l = \sqrt{\hbar/M\Omega}$, he shows that at long wavelengths $ql \ll 1$, the wave is predominantly transverse with a linear dispersion relation $\omega(q) = c_T\, q$, where $c_T = 1/2\sqrt{\hbar\Omega/M}$ is the speed of propagation with M the atomic mass. This long-wavelength motion is effectively a transverse phonon in the vortex lattice.

The radial expansion of rapidly rotating BECs means that the condensate is essentially two dimensional. Thus, bending modes of the vortices are irrelevant, but the nonzero compressibility of these atomic gases requires a significant modification to Tkachenko's analysis. Sonin (1987) (50) and Baym (2003) (51) generalized Tkachenko's result to find a new long-wavelength expression $\omega(q) = c_T\, q\sqrt{s^2q^2/(4\Omega^2 + s^2q^2)}$ where $s = \sqrt{gn/M}$ is the speed of sound. This expression assumes an infinite uniform system, but some authors (51, 52) also included the nonuniformity of the trapped BEC. If $sq \geq \Omega$, the short-wavelength or incompressible limit, then this expression reduces to Tkachenko's $\omega(q) \propto c_T\, q$. Otherwise, for the long-wavelength or compressible limit $sq \ll \Omega$, the mode becomes soft with $\omega(q) \propto q^2$. Dispersion becomes quadratic owing to hybridization with sound waves. This soft collective-mode spectrum has important consequences for stability

of the vortex lattice at large wavelengths (57).

For a vortex array system, in the long wave limit, it has been showed that, besides the quadratic Tkachenko mode, there is a gapless inertial mode with $\omega \sim 2\Omega$ (58). Considering the two linear dispersion modes, the longitudinal and optical phonon excitations, which results from the translational symmetry breaking of a $2D$ solid, we conclude that the Tkachenko mode with quadratic dispersion has to be counted as two linear dispersion modes (59).

Another way to justify the quadratic dispersion is relating the Tkachenko mode as Goldstone modes, allowed in non relativistic systems (59), which appear with the symmetry breaking ground states (17). An analogy here can be made with the spontaneous magnetization that appears in the Heisenberg ferromagnetic model. The momentum operator $\hat{S}$, which commutes with the system hamiltonian, has non zero expectation value in this particular spin aligned (e.g. z direction) fundamental state. The excitation around this ground state are Goldstone modes called magnons, which are well defined excitation of the momentum operator $\hat{S}_z$ with quadratic dispersion. Similarly, in the vortex lattice system we have the vortex aligned state breaking the symmetry of the angular momentum operator. Here, however, the number of the Tkachenko excitations is not conserved, since they are not well defined excitations of the operator $\hat{L}_z$ (the vortex lattice breaks the translational symmetry in the plane of the lines).

3.1.4 Tkachenko polaron model

We consider a two component superfluid mixture, one with an Abrikosov vortex array (48). The bosons are strongly confined in the z direction by an external trapping potential (occupying the ground state of the z harmonic well with frequency ω_0) and we have to deal with a $2D$ problem in the xy plane. The bosons are confined in this plane by

the harmonic trap $V_{ext}(\mathrm{r})$. For this system we have the Hamiltonian $H = H_A + H_B + H_{int}$,

$$
\begin{aligned}
H_A &= \int d^2r \left[\hat{\psi}_A^\dagger \frac{(-i\hbar\nabla - \mathbf{A})^2}{2m_A} \hat{\psi}_A + V_{ext}(\mathrm{r})\, \hat{\psi}_A^\dagger \hat{\psi}_A + \frac{g_A}{2} (\hat{\psi}_A^\dagger \hat{\psi}_A)^2 \right], \\
H_B &= \int d^2r \left[\hat{\psi}_B^\dagger \frac{(-i\hbar\nabla)^2}{2m_B} \hat{\psi}_B + \frac{g_B}{2} (\hat{\psi}_B^\dagger \hat{\psi}_B)^2 \right], \\
H_{int} &= g_{AB} \int d^2r\, \hat{\psi}_A^\dagger \hat{\psi}_A \hat{\psi}_B^\dagger \hat{\psi}_B,
\end{aligned}
\tag{3.1}
$$

where each species is described by the creation (destruction) operator $\hat{\psi}_i$ ($\hat{\psi}_i^\dagger$). The intra and inter repulsive contact interaction for this $2D$ system is given respectively by $g_i = \frac{2\sqrt{2\pi}\,\hbar^2\, a_i}{m_i l_0}$ and $g_{ij} = \frac{\sqrt{2\pi}\,\hbar^2\, a_{ij}}{\mu\, l_0}$, with the reduced mass $\mu = \frac{m_i m_i}{m_i + m_j}$ and the axial oscillator length $l_0 = \sqrt{\frac{\hbar}{m_A \omega_0}}$ ($l_0 \gg a_i$). In order to induce a vortex lattice in the majority species in the laboratory frame, keeping the impurity species with nearly free dispersion, we consider an artificial vector potential $\mathbf{A}$ (11) corresponding to an effective uniform magnetic field $\mathcal{B}^*$ that couples selectively to A atoms (60). Had we considered a rotating trap, the Hamiltonian in the rotating frame would contain an effective magnetic field that couples to both species, leading to the undesirable effect of Landau quantization of the impurity energy levels. This is why we need a selective gauge field to realize our model in the laboratory frame. The essential idea of implementing artificial gauge fields for neutral atoms is to produce Berry phases by combining the internal atomic structure with carefully engineered optical potentials, for instance via spatial gradients of detuning or Rabi frequency (61). Thus the gauge field is species specific because it depends on internal atomic degrees of freedom.

At critical array vorticity Ω, when the harmonic oscillator length of $V_{ext}(\mathrm{r})$ coincides with the magnetic length $l = \sqrt{\frac{\hbar}{m_A \Omega}}$, the residual radial trap vanishes and one then has an infinite plane geometry. In the regime of weak interactions $g_A n_A \ll \hbar\Omega$ ($\Omega = \mathcal{B}^*/m_A$), i.e. the mean-field quantum Hall regime (62,63), we can assume all particles of A in the same macroscopic quantum state: a linear superposition of the lowest Landau Level eigenstates that gives the vortex solution for species A. The minimum energy configuration corresponds to the Abrikosov vortex Lattice described by $\psi_A(z) = \sqrt{n_A}\varphi_A(z)$, where the normalized function $\varphi_A(z) = (2\varsigma)^{1/4}\ \vartheta_1(\sqrt{\pi\varsigma}z, \rho)\ e^{z^2/2}\ e^{-|z|^2/2}$ with the Jacobi delta function ϑ_1 ($z = x + iy$; $\rho = \exp(i\pi\tau)$ with $\tau = u + i\varsigma$, $u = -1/2$ and $\varsigma = \sqrt{3}/2$)

gives the triangular configuration for the vortex singularities (64).

In the polaron problem, we focus on a single B atom (very dilute species B), weakly interacting with the majority of the atoms with average two-dimensional density $n_A = N_A/\mathcal{S}$, where N_A is the total number of atoms distributed over an area $\mathcal{S}$. Before advancing with the model, a few remarks about the vortex system stability are in order. First, we keep our system at $T = 0$. Then, in spite of not having a phase coherence system, with part of the atoms A outside the condensate state, we still have a well established vortex lattice density profile (57). We also have the mean field quantum Hall regime, with the number of vortices well below the number of atoms of species A (large filling factor $\upsilon = N_A/N_V \gg 1$). Neither the quantum fluctuation nor the thermal one will affect the vortex lattice stability inside this particular regime considered here. The diluteness of species B ($N_B \ll N_A$) allows us to disregard the interaction effects over stability properties of the background vortex lattice species.

In the above scenario, we can apply the Bogoliubov transform in $\hat{\psi}_A$ to derive the excitations around the vortex lattice fundamental state. Thus, we include that quantum fluctuations in the mean field approximation for A, $\hat{\psi}_A = \psi_A + \delta\hat{\psi}_A$, with the field fluctuation

$$\delta\hat{\psi}_A(\mathbf{r}) = \frac{1}{\sqrt{\mathcal{S}}}\sum_{\mathbf{q}\in \mathrm{BZ}}\left[u_{\mathbf{q}}(\mathbf{r})a_{\mathbf{q}} - v_{\mathbf{q}}(\mathbf{r})a^{\dagger}_{\mathbf{q}}\right], \tag{3.2}$$

where $a_{\mathbf{q}}$ is the annihilation operator for the Tkachenko mode (TM) with wave vector $\mathbf{q}$ defined in the Brillouin zone of the triangular lattice.

After substituting the transformed field operator $\hat{\psi}_A(\mathbf{r})$ in Eq. (3.1), we separate H in the correspondent orders of fluctuation $\delta\hat{\psi}_A(\mathbf{r})$ to isolate the Hamiltonian for the impurity interacting with the TM background

$$H = H_A^{(0)} + H_A^{(1)} + H_A^{(2)} + H_B + H_{int}^{(0)} + H_{int}^{(1)} + \mathcal{O}(\delta\hat{\psi}_A^n), \;\; n \geq 3. \tag{3.3}$$

The gran-canonical formalism $\left(K = H - \sum_i \mu_i \int d^2r\ \hat{\psi}_i^{\dagger}\,\hat{\psi}_i\right)$ provides for the system hamiltonian

$$\begin{aligned} K &= [H_A^{(2)} - \mu_A\hat{N}_A] + [H_B + H_{int}^{(0)} - \mu_B\hat{N}_B] + [H_{int}^{(1)}] \\ &= K_A^{BOG} + K_B + H_{imp-ph}. \end{aligned} \tag{3.4}$$

To deduce the Tkachenko excitation spectrum ω_q, we diagonalized the second order term in fluctuation field $(H_A^{(2)} - \mu_A \delta\hat{\psi}_A^\dagger \delta\hat{\psi}_A)$, based on references (64, 65). The values of $u_{\mathbf{q}}(\mathbf{r})$ and $v_{\mathbf{q}}(\mathbf{r})$ in Eq. (3.2) comes from solution of the correspondent Bogoliubov-de Gennes equations, that gives the TM phonon hamiltonian K_A^{BOG}. For $q \ll l^{-1}$ ($l = \sqrt{\hbar/m_A\Omega}$), we can approximate $u_{\mathbf{q}}(\mathbf{r}) \approx \varphi_A(\mathbf{r}) c_{1\mathbf{q}} e^{i\mathbf{q}\cdot\mathbf{r}}$ and $v_{\mathbf{q}}(\mathbf{r}) \approx \varphi_A(\mathbf{r}) c_{2\mathbf{q}} e^{-i\mathbf{q}\cdot\mathbf{r}}$ where $c_{1\mathbf{q}} \approx \sqrt{(\chi_q/\tilde{\omega}_q + 1)/2}$ and $c_{2\mathbf{q}} \approx \sqrt{(\chi_q/\tilde{\omega}_q - 1)/2}$, with $\tilde{\omega}_q \approx \kappa\sqrt{\eta}(ql)^2/4$ and $\chi_q \approx \kappa[1 - (ql)^2/4 + (\eta+1)(ql)^4/32]$ (Abrikosov lattice constants: $\kappa \approx 1.1592$ and $\eta \approx 0.8219$). The collective modes have dispersion relation $\hbar\omega_q = \tilde{\omega}_q \, n_A g_A \approx \hbar^2 q^2/2M$, where $M = \frac{1}{2\kappa\sqrt{\eta}} \frac{\hbar\Omega}{n_A g_A} m_A$ is the Tkachenko boson mass.

Let us now turn to the interspecies interaction H_{int} in Eq. (3.1). The zero order term in $\delta\hat{\psi}_A$

$$H_{int}^{(0)} = \int d^2r \, V(\mathbf{r}) \hat{\psi}_B^\dagger(\mathbf{r}) \hat{\psi}_B(\mathbf{r}), \tag{3.5}$$

with $V(\mathbf{r}) = n_A g_{AB} |\varphi_A(\mathbf{r})|^2$, accounts for the static lattice potential of the Abrikosov lattice seen by the impurities. This is analogous to the periodic potential produced by laser beams in optical lattices (4). But here the potential stems from the density-density interaction g_{AB}, which makes it energetically more favorable for B atoms to be located near vortex cores, where the density of A atoms vanishes. We can compare the recoil energy $E_R = \hbar^2/2m_B\xi^2$, where ξ is the vortex core size, with the lattice potential depth $V_0 = n_A g_{AB}$. In the mean field quantum Hall regime, $\xi \sim l$ (5), thus $E_R \sim (m_A/m_B)\hbar\Omega$. The shallow lattice limit $E_R \gg V_0$ is more natural if $m_A \sim m_B$ and $g_{AB} \sim g_A$, that will be the regime explored in this section. But we recall that the deep lattice limit can also be achieved by selecting heavier impurity atoms and by increasing g_{AB}.

The combination of the periodic potential (3.5) with the kinetic energy in H_B in Eq. (3.1) leads to Bloch bands for the impurity. For weak interactions, we can project into the lowest band and write $\hat{\psi}_B(\mathbf{r}) \sim \frac{1}{\sqrt{\mathcal{S}}} \sum_{\mathbf{k}} \Phi_{\mathbf{k}}(\mathbf{r}) b_{\mathbf{k}}$, where $\Phi_{\mathbf{k}}$ is a Bloch wave function and $b_{\mathbf{k}}$ annihilates a B atom with wave vector $\mathbf{k}$ in the Brillouin zone. In the long wavelength limit, the lowest band dispersion becomes $\varepsilon_{\mathbf{k}} \approx \hbar^2 k^2/2m_B^*$, where m_B^* is the effective impurity mass. Hereafter we set $m_B^* = m$ to lighten the notation. It is interesting to

compare m with the Tkachenko mode mass M. If $m \sim m_A$, we expect $m < M$ in the mean field quantum Hall regime.

To first order in $\delta\hat{\psi}_A$, the term generated by H_{int} is the impurity-phonon interaction ($H^{(1)}_{int} = H_{imp-ph}$). Using the mode expansion in Eq. (3.2), we obtain

$$H_{imp-ph} = \frac{1}{\sqrt{\mathcal{S}}} \sum_{\mathbf{k},\mathbf{q}} g_{\mathbf{k},\mathbf{q}}\, b^\dagger_{\mathbf{k}+\mathbf{q}} b_{\mathbf{k}} (a_{\mathbf{q}} + a^\dagger_{-\mathbf{q}}), \tag{3.6}$$

with impurity-phonon coupling

$$g_{\mathbf{k},\mathbf{q}} = \sqrt{n_A} g_{AB} (c_{1\mathbf{q}} - c_{2\mathbf{q}}) \times \int_{s_V} \frac{d^2r}{\pi l^2}\, \Phi^*_{\mathbf{k}+\mathbf{q}}(\mathbf{r}) \Phi_{\mathbf{k}}(\mathbf{r}) |\varphi_A(\mathbf{r})|^2 e^{i\mathbf{q}\cdot\mathbf{r}}. \tag{3.7}$$

We have reduced the integral in Eq. (3.7) to the unit cell s_V occupied by a single vortex with area πl^2, using the lattice translational symmetry (see appendix A.1). Since we focus on the "large polaron" regime (66), we take the continuum limit in Eq. (3.7) expanding it for small wave vectors $k, q \ll l^{-1}$. The dependence on particle momentum $\mathbf{k}$ disappears as the dominant effect in the impurity-phonon interaction is the slow oscillation of the potential (67). As a result, the coupling simplifies to

$$g_{\mathbf{k},\mathbf{q}} \approx \lambda_q = \lambda\, q, \tag{3.8}$$

where

$$\lambda \approx \eta^{1/4} \left(\frac{\upsilon}{8\pi}\right)^{1/2} g_{AB} \int_{s_V} \frac{d^2r}{\pi l^2}\, |\Phi_0(\mathbf{r})|^2 |\varphi_A(\mathbf{r})|^2, \tag{3.9}$$

with the filling factor $\upsilon = \pi n_A l^2$. The linear momentum dependence in Eq. (3.8) stems from the small-q limit of $c_{1\mathbf{q}} - c_{2\mathbf{q}}$. For comparison, the same factor yields $\lambda_q \propto \sqrt{q}$ in homogeneous BECs (46, 47).

We finally obtain the two dimensional Tkachenko polaron model hamiltonian (68)

$$H = \sum_{\mathbf{q}} \frac{\hbar^2 q^2}{2M}\, \hat{a}^\dagger_{\mathbf{q}}\, \hat{a}_{\mathbf{q}} + \sum_{\mathbf{k}} \frac{\hbar^2 k^2}{2m}\, \hat{b}^\dagger_{\mathbf{k}}\, \hat{b}_{\mathbf{k}} + \frac{1}{\sqrt{S}} \sum_{\mathbf{k},\mathbf{q}} \lambda\ |\,\mathbf{q}\,|\ \hat{b}^\dagger_{\mathbf{k}}\, \hat{b}_{\mathbf{k}+\mathbf{q}}\, (\hat{a}_{\mathbf{q}} + \hat{a}^\dagger_{-\mathbf{q}}), \tag{3.10}$$

where the quadratic dispersion relation of the Tkachenko modes and the impurity kinetic energy are given respectively by first and second terms of Eq. (3.10), with the correspondent Tkachenko excitations $\hat{a}_{\mathbf{q}}$ ($\hat{a}^\dagger_{\mathbf{q}}$) and impurity $\hat{b}_{\mathbf{k}}$ ($\hat{b}^\dagger_{\mathbf{k}}$) creation (destruction) operators in momentum state. The coupling between them is given by the last term of the Hamiltonian, with $\lambda = (2\pi)^{-1/2} \eta^{1/4} g_{AB}\, \upsilon^{1/2}$.

Figure 8 – (a) Impurity self-energy (a) and vertex correction Feynman diagram (b). The solid and wavy lines represent free impurity and Tkachenko mode (phonon) propagators, respectively.

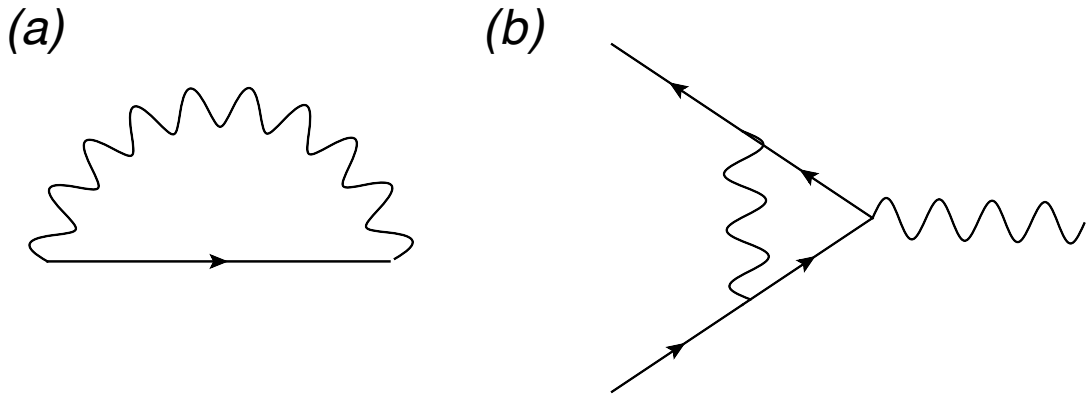

Source: elaborated by the author

3.1.5 Weak coupling regime

In order to describe both the energy and the decay of the polaron, it is natural to use diagrammatic many-body theory. The Green's function of the impurity particle is $G(\mathbf{k},\omega) = [\omega - \varepsilon_{\mathbf{k}} - \mathrm{Re}\Sigma(\mathbf{k},\omega) - i\mathrm{Im}\Sigma(\mathbf{k},\omega)]^{-1}$ where $\Sigma(\mathbf{k},\omega)$ is the self-energy. That real part describes the energy shift of the minority particle due to the interactions with the medium. We start considering the weak coupling limit of Eq. (3.10), where the lowest order diagram that contributes to the self-energy contains one Tkachenko mode in the intermediate state Fig. 8a. This gives the retarded self-energy (69)

$$\Sigma^{(1)}_{Ret}(\mathbf{k},\omega) = \int \frac{d^2q}{(2\pi)^2} \frac{|\lambda_q|^2}{\omega - \varepsilon_{\mathbf{q}} - \varepsilon_{\mathbf{k}+\mathbf{q}} + i\delta}. \tag{3.11}$$

The energy of the polaron is found as solutions to the implicit equation $E_{\mathbf{k}} \simeq \varepsilon_{\mathbf{k}} + \mathrm{Re}\Sigma(\mathbf{k}, E_{\mathbf{k}})$ and the quasiparticle residue at a given pole is found from $Z_{\mathbf{k}}^{-1} = 1 - \left(\frac{\partial \mathrm{Re}\Sigma}{\partial\omega}\right)\Big|_0$. Also, the effective mass of the polaron can be obtained with $\frac{m_0}{m^*} = Z_{\mathbf{k}}\left[1 + m_0\left(\frac{\partial^2\Sigma}{\partial k^2}\right)\Big|_0\right]$. These quasiparticles may be thought of as free particles with renormalized masses, spectral weights and decay rate $\gamma_{\mathbf{k}} = -Z_{\mathbf{k}}^{-1}\,\mathrm{Im}\Sigma(\mathbf{k}, E_{\mathbf{k}})$. For weak coupling, we can expand the self-energy around the polaron pole and write the Green's function as (69)

$$G(\mathbf{k},\varepsilon) \approx \frac{Z_{\mathbf{k}}}{\varepsilon - E_{\mathbf{k}} + i\gamma_{\mathbf{k}}}. \tag{3.12}$$

According to Eq. (3.11), the imaginary part of $\Sigma(\mathbf{k},\varepsilon)$ is given by

$$\mathrm{Im}\Sigma(\mathbf{k},\varepsilon) = -\frac{\lambda^2\mu^2}{2\hbar^4}\left(\delta\varepsilon + \frac{\mu\hbar^2k^2}{m^2}\right)\theta[\varepsilon - \varepsilon_{min}(k)], \tag{3.13}$$

where $\delta\varepsilon = \varepsilon - \hbar^2k^2/2m$ is the energy distance from the mass shell, the reduced mass is $\mu = mM/(m+M)$, $\theta(x)$ is the Heaviside step function and $\varepsilon_{min}(k)$ is the lower threshold imposed by kinematic constraints. The perturbative result gives $\varepsilon_{min}(k) = \hbar^2k^2/2(m+M)$, which corresponds to the kinetic energy of the center of mass for two particles with masses m and M and total momentum $\hbar\mathbf{k}$. We expect that this cutoff in the imaginary part disappears as higher order self-energy diagrams are included.

The real part of the self-energy reads

$$\mathrm{Re}\Sigma(k,\varepsilon) = \frac{\lambda^2\mu^2}{\pi\hbar^4}\left[|\delta\varepsilon| - \left(\delta\varepsilon + \frac{\mu\hbar^2k^2}{m^2}\right)\ln\left|\frac{\Lambda}{f(k,\varepsilon)}\right|\right], \tag{3.14}$$

where Λ is a high-energy cutoff (of order $\hbar^2/2ml^2$) and $f(k,\varepsilon) = (\mu\hbar^2k^2/2m^2)\theta(\delta\varepsilon) + [\varepsilon - \varepsilon_{min}(k)]\theta(-\delta\varepsilon)$. We have omitted in Eq. (3.14) a constant term of order Λ that amounts to a non-universal shift in the polaron ground state energy.

Two remarks about Eqs. (3.13) and (3.14) are in order. The first remark is that the impurity decay rate $\gamma_{\mathbf{k}} \propto k^2$ is nonzero for any $k > 0$. This is a direct consequence of the quadratic dispersion of Tkachenko modes, since there is always available phase space for the decay of the single particle respecting energy and momentum conservation. As a result, polarons moving through the vortex lattice experience a dissipative force. The second remark is that the scaling of the decay rate $\gamma_{\mathbf{k}} \sim k^2 \sim \varepsilon_{\mathbf{k}}$ signals that the polaron is only marginally coherent. This is consistent with the infrared logarithmic singularity in the real part $\mathrm{Re}\Sigma(\mathbf{k},\varepsilon_{\mathbf{k}}) \sim \varepsilon_{\mathbf{k}}\ln|\Lambda/\varepsilon_{\mathbf{k}}|$ for $\varepsilon_{\mathbf{k}} \ll \Lambda$.

According to the Landau theory for quasiparticles in a Fermi liquid (70), they become well defined (long lifetime excitations) as we consider low energetic system close to the Fermi level, with the reduction of the phase space available for quasiparticle scattering. That statement can be translated as follow: for $k \to k_F$, the quasiparticle width in the system excitation spectra should go to zero quicker than the quasiparticle energy, the latter representing the peak position of this spectra. That is true in the a Fermi liquid

theory, where the particle-hole excitation in the Fermi level gives the quasiparticle (core-hole) decay rate $\gamma_{\mathbf{k}} \propto \varepsilon_{\mathbf{k}}^2$. Our particular situation here is a border (or marginal) condition of such criteria, since the ratio between the decay rate and the quasiparticle energy does not vary with the momentum. We should also expect such marginal coherence properties of the TM quasiparticle from a simple scaling analysis of the interaction term in the system Hamiltonian Eq. (3.10). That will be calculated next, after a brief introduction to the renormalization group method.

3.1.6 RG equations and marginal Interaction

We start defining the renormalization groups analyze (RG) (17,71,72). Considering the path integral representation of the system with macroscopic degree of freedom given by the field $\phi(\mathbf{x}, t) = \phi(x)$. For the system partition function we have

$$Z = \int D\phi \, e^{-S(\phi)} \tag{3.15}$$

RG transform consists in integrating the high energetic degrees of freedom (short distances or high momentum values) to produce an equivalent low energy model. A subsequent scaling transformation is applied in the integrated system to recover the original scales. Such process, that is, the fast fields integration following by scaling, results in the renormalization of the coupling constants for the remaining slow fields effective Hamiltonian. This procedure will be exemplified below (72).

Considering first the Fourier components of the field

$$\phi(x) = \int \frac{d^D k}{(2\pi)^D} \, e^{ikx} \tag{3.16}$$

with $k = (\mathbf{k}, \omega)$. Now we will integrate the highest Fourier components of the field ($\phi_>$) to produce an effective action for the lowest ($\phi_<$)

$$\begin{aligned} Z &= \int D\phi_< D\phi_> \, e^{-S(\phi_< + \phi_>)} \\ &= \int D\phi_< \, e^{-S_{eff}(\phi_<)} \end{aligned} \tag{3.17}$$

where

$$S_{eff}(\phi_<) = \int D\phi_> \, e^{-S(\phi_< + \phi_>)}. \tag{3.18}$$

In Eq. (3.17), we integrate the degrees of freedom inside a certain sector in momentum space $\Lambda/b < |\mathbf{k}| < \Lambda$ (high momentum cutoff Λ), with $b > 1$. It will be equivalent to average over the short distance scale $b\,a$ in the real space (a being the lattice constant, with $\Lambda = a^{-1}$) and the resulting theory will be explicitly cutoff dependent. Then we have to rescale the lengths and time in order to restore the original units; we rescale the momentum as $k' = kb$ to recover $|k'| < \Lambda$. We can repeat these steps, with a new high energy cutoff $\Lambda' \equiv \Lambda/b < \Lambda$, to derive, at the tree level approach (71), the RG equations for the theory couplings close to a fixed point.

The fixed point is characterized by the invariance of the action under RG transform, that is $S^*_{eff}(\phi_<) = S^*_{eff}(\phi)$. The system in the fixed point stays invariant under the change of space/time scale associated with the transformation. Since for each system we can attribute a length scale ξ to determine the field correlations, particularly, for the fixed point such loss of scale can be defined by $\xi = 0$ or $\xi = \infty$ (17). The latter, non trivial condition, describes a system at criticality or phase transition (quantum or thermal).

Let us consider a system close to the critical point and a set of operators $\{\phi_n(x)\}$ and correspondents coupling constants $\{\lambda_n\}$

$$S(\phi) = S^*(\phi) + \int d^D x \sum_n \lambda_n \phi_n(x). \tag{3.19}$$

After apply the RG transformation over this system, that is, integrate the high energy modes $\Lambda \to b\Lambda$ ($b < 1$), we rescale the length $x \to x/b$. The action $S^*(\phi)$ remains invariant while the field operator transforms with a scale dimension Δ_n, so

$$\int d^D x \sum_n \lambda_n \phi_n(x) = \int d^D x \sum_n b^{-D} b^{\Delta_n} \lambda_n \phi_n(x) \tag{3.20}$$

This RG transform is equivalent to a rescaling of the coupling constant

$$\lambda'_n = b^{-D+\Delta_n} \lambda_n = \lambda_n(b). \tag{3.21}$$

With $b \to 1^-$, we can write $b = e^{-\delta\ell}$ ($\lambda_n(b) = e^{(D-\Delta_n)\delta\ell}\ \lambda_n$) and with the differential change for the coupling constant construct the tree level Beta-function

$$\begin{aligned} \lambda_n(b) - \lambda_n &= \delta\ell\ (D - \Delta_n)\lambda_n, \\ \to \beta(\lambda_n) = \frac{\partial \lambda_n}{\partial \ell} &= (D - \Delta_n)\lambda_n + ... \end{aligned} \tag{3.22}$$

That gives the evolution of the effective coupling constants of the model upon changing length or time scales.

We can use these scaling analysis to prove that our interaction term is a marginal operator. The field ϕ is an integrable variable in the definition of the action, then it can be rescaled arbitrarily. We choose a term of the Hamiltonian to represents the free theory parameter to rescale this field. That is equivalent to select a term in the action which governs the behavior of the free theory, and require that it be strictly invariant under RG step. It renders the leading operator in the action scale invariant. The scaling of r and t is defined basing on the dynamic exponent z given by the model dispersion relation $\omega(q)$ ($q \to bq; \omega \to b^z\omega$).

To apply the considerations above, we switch our model to a functional integral formalism, starting from the Hamiltonian in second quantization Eq. (3.10). Switching to first quantization in the Hilbert space of a single impurity ($\sum_{\mathbf{k}} b^\dagger_{\mathbf{k}} b_{\mathbf{k}} = 1$), we can write

$$H_{imp} = \frac{\mathbf{P}^2}{2m}, \tag{3.23}$$

where $\mathbf{P}$ is the impurity momentum operator. Moreover,

$$H_{imp-ph} = \frac{\lambda}{\sqrt{\mathcal{S}}} \sum_{\mathbf{q}} q \, (a_{\mathbf{q}} + a^\dagger_{-\mathbf{q}}) \sum_{\mathbf{k}} |\mathbf{k}+\mathbf{q}\rangle\langle\mathbf{k}|. \tag{3.24}$$

The operator acting on the impurity Hilbert space in Eq. (3.24) is recognized as $\sum_{\mathbf{k}} |\mathbf{k}+\mathbf{q}\rangle\langle\mathbf{k}| = e^{i\mathbf{q}\cdot\mathbf{X}}$, where $\mathbf{X}$ is the impurity position operator. Thus we can write (to simplify the notation we denote $\omega_q = q^2/2M$, adopting $\hbar = 1$ in the rest of the text)

$$\begin{aligned} H_{imp-ph} &= \frac{\lambda}{\sqrt{\mathcal{S}}} \sum_{\mathbf{q}} q \, (a_{\mathbf{q}} + a^\dagger_{-\mathbf{q}}) e^{i\mathbf{q}\cdot\mathbf{X}}, \\ &= \frac{\lambda}{\sqrt{\mathcal{S}}} \sum_{\mathbf{q}} \frac{q^2}{\sqrt{2M\omega_q}} (a_{\mathbf{q}} + a^\dagger_{-\mathbf{q}}) e^{i\mathbf{q}\cdot\mathbf{X}} \\ &= -\lambda \nabla^2 \phi(\mathbf{X}), \end{aligned} \tag{3.25}$$

where we define the dimensionless scalar field from Tkachenko modes

$$\phi(\mathbf{r}) = \sum_{\mathbf{q}} \frac{1}{\sqrt{2\mathcal{S}M\omega_q}} (a_{\mathbf{q}} + a^\dagger_{-\mathbf{q}}) e^{i\mathbf{q}\cdot\mathbf{r}}. \tag{3.26}$$

We also introduce the momentum canonically conjugate to $\phi(\mathbf{r})$

$$\Pi(\mathbf{r}) = -i \sum_{\mathbf{q}} \sqrt{\frac{M\omega_q}{2\mathcal{S}}} (a_{\mathbf{q}} - a^\dagger_{-\mathbf{q}}) e^{i\mathbf{q}\cdot\mathbf{r}}, \tag{3.27}$$

so that $[\phi(\mathbf{r}), \Pi(\mathbf{r}')] = i\delta(\mathbf{r}-\mathbf{r}')$. The free phonon Hamiltonian can be cast in the field theory form

$$H_{ph} = \frac{1}{2M}\int d^2r \left[\Pi^2 + \frac{1}{4}(\nabla^2\phi)^2\right] + \text{const.} \tag{3.28}$$

Therefore the Hamiltonian for a single impurity coupled to the Tkachenko field reads

$$H = \frac{\mathbf{P}^2}{2m} + \frac{1}{2M}\int d^2r \left[\Pi^2 + \frac{1}{4}(\nabla^2\phi)^2\right] - \frac{\tilde{\lambda}}{\mu}\nabla^2\phi(\mathbf{X}), \tag{3.29}$$

where $\tilde{\lambda} = \mu\lambda$, with $\mu = mM/(m+M)$, is the dimensionless coupling constant. A particular configuration of the system at time τ is specified by $\mathbf{X}(\tau), \phi(\mathbf{r}, \tau)$.

That the impurity-phonon interaction in Eq. (3.10) is marginal can be seen by writing down the partition function $Z = \int \mathcal{D}\mathbf{X}\,\mathcal{D}\phi\, e^{-S[\mathbf{X},\phi]/\hbar}$ with the effective Euclidean action

$$S = \int d^2r d\tau \left[\frac{M}{2}(\partial_\tau\phi)^2 + \frac{1}{8M}(\nabla^2\phi)^2\right] + \int d\tau \left[\frac{m}{2}(\partial_\tau\mathbf{X})^2 - \frac{\tilde{\lambda}}{\mu}\nabla^2\phi(\mathbf{X})\right]. \tag{3.30}$$

The action in Eq. (3.30) is invariant under the RG transformation (71) with scale factor $b > 1$: $\mathbf{r}' = b^{-1}\mathbf{r}$, $\tau' = b^{-z}\tau$, $\phi' = \phi$, $\mathbf{X}' = b^{-1}\mathbf{X}$, with dynamical exponent $z = 2$. Once more, we verified that the quadratic dispersion of the Tkachenko bosons associated with linear momentum coupling with the impurity gives a marginal operator H_{imp-ph}.

3.1.7 Interaction Flow

Having established that the impurity-phonon coupling constant $\tilde{\lambda}$ is marginal, we proceed by calculating the quantum correction to scaling. At one-loop level, the renormalization of $\tilde{\lambda}$ is given by the vertex-correction diagram in Fig. 8b. Integrating out high-energy modes, we obtain the perturbative RG equation (see appendix A.2)

$$\frac{d\tilde{\lambda}}{d\ln(\Lambda_0/\Lambda)} = \frac{\tilde{\lambda}^3}{\pi}. \tag{3.31}$$

Let us denote by m_0 the bare mass (i.e. without logarithmic corrections). The effective mass m^* that will give the polaron dispersion $E_{\mathbf{k}} \approx \varepsilon^*_{\mathbf{k}} = k^2/2m^*$ is related to the self-energy, Eq. (3.11), and can be expanded to order λ^2 as

$$\frac{m^*}{m_0} \approx 1 - \left(\frac{\partial\Sigma}{\partial\omega}\right)\Big|_0 - m_0\left(\frac{\partial^2\Sigma}{\partial k^2}\right)\Big|_0 \tag{3.32}$$

which gives

$$m^* \approx m_0 + \frac{2\lambda^2\mu^3}{\pi} \ln\left(\frac{\Lambda}{\varepsilon_{\mathbf{k}}}\right). \tag{3.33}$$

That yields the impurity mass renormalization

$$\frac{dm}{d\ln(\Lambda_0/\Lambda)} = \frac{2\tilde{\lambda}^2\mu}{\pi}. \tag{3.34}$$

Interestingly, similar RG equations occur in another two-dimensional system, namely graphene with unscreened Coulomb interactions (73). But while in graphene the interaction is marginally irrelevant, in our case Eqs. (3.31) and (3.34) show that $\tilde{\lambda}$ flows to strong coupling and the polaron mass increases. We interpret this result as a sign that the "large polaron", defined from a small value of the bare coupling constant $\tilde{\lambda}_0$, becomes surprisingly heavy and strongly damped at small wave vectors. In conclusion, our effective coupling constant λ corresponds to a marginally relevant interaction.

3.1.8 Anomalous broadening of spectral function

How can we experimentally probe the effects of our marginally relevant interaction? The answer comes with the investigation of the system spectral function $A(k,\omega)$; that gives the distribution of energies ω in the system when a particle with momentum $\mathbf{k}$ is added or removed from it. For the non-interacting system, $A_0(\mathbf{k},\omega)$ is simply a δ function peaked at the energy $\varepsilon_{\mathbf{k}}$

$$\begin{aligned} A_0(\mathbf{k},\omega) &= \delta(\omega - \varepsilon_{\mathbf{k}}) \\ &= -\frac{1}{\pi}\mathrm{Im}\frac{1}{\omega - \varepsilon_{\mathbf{k}} + i\delta} = -\frac{1}{\pi}\mathrm{Im}\, G_0(\mathbf{k},\omega). \end{aligned} \tag{3.35}$$

The first step of the second line is just a simple mathematical rewriting of the delta function. In the second line the Green's function G_0 for non-interacting particles is introduced. Here we have defined the so-called retarded Green's function, with δ small and positive. More generally, the single-particle Green's function $G(\mathbf{k},\omega)$ is defined in terms of the correlation function of particle creation and annihilation operators (69). For our present purpose, it is sufficient to note that $A(\mathbf{k},\omega)$ is the spectral representation of the complex

function $G(\mathbf{k},\omega)$

$$G(\mathbf{k},\omega) = \int_{-\infty}^{\infty} dx \, \frac{A(\mathbf{k},x)}{(\omega - x + i\delta)}. \tag{3.36}$$

$A(\mathbf{k},\omega)$ has a clear physical meaning, and it can be deduced through radio frequency spectroscopy (a cold atom version of the electron angle resolved photoemission experiments), as will be discussed later on.

In the problem with interactions, however, $G(\mathbf{k},\omega)$ will differ from $G_0(\mathbf{k},\omega)$. This difference can be quite generally defined through the single-particle self-energy function $\Sigma(\mathbf{k},\omega)$

$$G(\mathbf{k},\omega)^{-1} = G_0(\mathbf{k},\omega)^{-1} - \Sigma(\mathbf{k},\omega). \tag{3.37}$$

Eq. (3.36) ensures the relation between $G(\mathbf{k},\omega)$ and $A(\mathbf{k},\omega)$

$$A(\mathbf{k},\omega) = -\frac{1}{\pi}\mathrm{Im}\, G(\mathbf{k},\omega). \tag{3.38}$$

With this preliminary scenario, let us consider then the signature effect of our marginal relevant interaction. As mentioned before, that could be probed through the ratio between the decay rate $\gamma_{\mathbf{k}}$ and the energy $E_{\mathbf{k}}$ of the quasiparticle peak.

To analyze this impurity-phonon interaction effect at energy scales $\Lambda \gg \Lambda_0 \; e^{-\pi/2\lambda_0^2\mu_0^2}$ (appendix A.2), we can apply RG improved perturbation theory and replace the bare constants (λ_0 and m_0) in the lowest order result for the self-energy by their renormalized values. We are interested in the logarithmically divergent terms that govern the renormalization of the quasiparticle weight $Z_{\mathbf{k}}$, the coupling constant λ and the effective mass in the dispersion $\varepsilon^*_{\mathbf{k}}$. These infrared singularities stem from differentiating the pre factor of the logarithm in the real part of the self-energy with respect to ω and k. According to section 3.1.5, we can compute the field renormalization

$$Z_{\mathbf{k}}^{-1} \approx 1 + \frac{\lambda^2\mu^2}{\pi} \, \ln\left(\frac{\Lambda}{\varepsilon_{\mathbf{k}}}\right). \tag{3.39}$$

Therefore the quasiparticle weight $Z_{\mathbf{k}}$ decreases logarithmically as k decreases in the weak coupling regime.

Also from 3.1.5 (Eq. 3.13), the lowest order result for the imaginary part of the self-energy can be written as

$$\mathrm{Im}\Sigma(k,\varepsilon_{\mathbf{k}}) \approx -\frac{\lambda_0^2 m_0 M^3 k^2}{2(m_0+M)^3}. \tag{3.40}$$

The logarithmic singularities in the imaginary part of Σ appear at fourth order in perturbation theory, stemming from both, vertex corrections (renormalization of λ) and self-energy corrections in the internal impurity line (renormalization of m). We obtain the RG improved decay rate by replacing λ_0 and m_0 in Eq. (3.40) by λ and m^*, including the field renormalization as in Eq. (3.39). The ratio between the renormalized decay rate and the renormalized dispersion becomes

$$\begin{aligned}\frac{\gamma^*_{\mathbf{k}}}{\varepsilon^*_{\mathbf{k}}} &= \frac{\lambda^2 Z_{\mathbf{k}} (m^*)^2 M^3}{(m^*+M)^3} \\ &\approx \frac{\lambda_0^2 m_0^2}{(1+\varrho)^3}\left[1+\frac{\lambda_0^2 m_0^2(5+\varrho^2)}{\pi(1+\varrho)^4}\ln\frac{\Lambda}{\varepsilon_{\mathbf{k}}}\right],\end{aligned} \tag{3.41}$$

where we expanded to first order in the logarithmic correction. The coefficient of the logarithmic term is positive for any value of mass ratio $\varrho = m_0/M$, thus the relative width $\gamma^*_{\mathbf{k}}/\varepsilon^*_{\mathbf{k}}$ of the quasiparticle peak increases with decreasing k. That manifest as an anomalous broadening of the spectral function at small k and low enough temperatures $T \ll \varepsilon_{\mathbf{k}}$. In comparison with impurities dressed by optical or acoustic phonons, in this coupling regime the Tkachenko polaron is distinguished by a Lorentzian quasiparticle peak with a finite width for arbitrarily small k, even at zero temperature (74).

So far we have neglected the Beliaev energy damping of Tkachenko modes (65). Within a perturbative approach with a dressed phonon propagator, it is easy to verify that a finite decay rate for Tkachenko modes leads to further broadening of the polaron spectral function. Remarkably, the result that the Tkachenko mode decay rate scales as $\Gamma_{\mathbf{q}} \propto q^2$ suggests that the nonlinear (cubic) phonon decay process considered in Ref. (65) is also marginal. However, $\Gamma_{\mathbf{q}}/\hbar\omega_{\mathbf{q}} \sim 1/\upsilon$, whereas for the polaron decay rate $\gamma_{\mathbf{k}}/E_{\mathbf{k}} \sim \lambda^2 \sim \upsilon$ according to Eq. (3.8). Therefore, our results are valid in the mean field quantum Hall regime, where $\upsilon \gg 1$.

3.2 Orthogonality catastrophe (OC)

In the last section we derived an effective polaron Hamiltonian for a neutral impurity coupled with the Tkachenko modes of a vortex lattice Bose-Einstein condensate. That contains a marginal impurity-phonon interaction which gives the broadening of the Lorentzian polaron spectral function for small impurity momenta. Now, through the impurity spectral function, we track how the polaron properties vary as function of the interaction strength toward the lower energy regime.

3.2.1 Brief introduction to OC

Let us start with the phenomenological Landau theory to treat the conduction electrons in solids (70, 75). That was successful in dealing with the strong interaction between the conduction electrons, treated as free quasiparticles. His theory was adequate for high charge density system at $T = 0$, where the screening of the Coulomb interaction applies. As we know, the Fermi liquid description is valid as long as the excitation spectrum of the system retains a coherent single particle piece, given by a finite quasiparticle weight $Z > 0$. When the evaluation of Z reduces to an overlap between two orthogonal states wavefunction, however, the system is classified as a singular Fermi liquid. Before explain such argument in the context of the Landau theory, we start introducing the orthogonality catastrophe phenomena.

That history involves Anderson (76), describing the ground state of N electrons when disturbed by an infinity massive charge. He showed that the later acts as a localized instantaneous potential, creating a phase shift in the single particle wave function of each electron, that do not overlap completely with the original orbitals anymore. After introduce the localized potential, however, the consequence for the many body wave function should be more drastic. Since it represents the Slater determinant of N shifted single electrons orbitals, we expect that its projection with the original ground state many body wave function (without perturbation) goes to zero in the thermodynamic limit ($N \to \infty$).

The OC phenomenon was applied latter by Mahan (77) to justify the x-ray edge singularity that appears in the line shape for absorption spectra of metals near the threshold (lower absorption x-ray frequency), that is closely related to the Anderson OC. The x-ray creates a hole in the atomic core level and a particle in the conduction band above the Fermi level. That hole will produce an additional localized potential (screening Coulomb interaction) for the conduction electrons, changing the system many body configuration as in the Anderson's example. The term "catastrophe" was then designed to describe a forbidden x-ray transition due to the orthogonality between the initial and the final states of the conducting electrons. The sudden switch on of the core-hole potential excite the system by creating an infinite number of low energy electron-hole pairs in the conduction band. Those excitations, however, break the original system symmetry, allowing the forbidden transition to be observed.

Now we will do a parallel with Landau theory, considering the additional of a charge particle with total momentum $\mathbf{k}$ in a system of N conduction electrons. We can construct a perturbative solution for the wavefunction of $N+1$ interacting electrons, respecting the conservation laws (energy, momentum, spin and particles number) (78)

$$|\psi^{N+1}_{\mathbf{k},\sigma}\rangle = Z^{1/2}_{\mathbf{k}} c^{\dagger}_{\mathbf{k},\sigma}|\psi^{N}\rangle + \sum_{\mathbf{k_i},\sigma_i} \alpha(\mathbf{k_i},\sigma_i) c^{\dagger}_{\mathbf{k}_3}\, c_{\mathbf{k}_2} c^{\dagger}_{\mathbf{k}_1} \delta_{\mathbf{k},\mathbf{k}_1-\mathbf{k}_2+\mathbf{k}_3}\, |\psi^{N}\rangle + ... \tag{3.42}$$

That solution can be decomposed as a sum of a bare particle of momentum $\mathbf{k}$ created in the original system of N interacting state (coherent piece with quasiparticle amplitude $Z_{\mathbf{k}}$), plus a series expansion of multiples particle-hole excitations with a fixed total momentum $\mathbf{k}$. The Landau theory breaks down when $Z_{\mathbf{k}}$ becomes zero. In other words, in addition of a single particle or a hole, the system creates a divergent number of particle-holes pairs so that the leading term does not have a finite weight in the thermodynamic limit.

In this part of the thesis we explored the low energy regime of a neutral impurity atom interacting with the Tkachenko modes background. We have found before that the self-energy allowed we characterize this system as a "marginal Fermi liquid". The singular behavior of our system in the infrared is reflected by the polaron weight Z, since it is related with the real part of the self-energy. We will show here that another important result of this interaction is the orthogonality catastrophe phenomenon (OC), that comes

with impurity self-localization. The impurity Greens function will present branch cuts rather than poles, and the OC signature comes with the power law dependence of the impurity spectral function.

In the following, we summarize the main results obtained in the previous section, where we treated the weak coupling regime. Next we analyze lower energy regimes, applying the canonical transform in Hamiltonian to extract the singular spectral function for the OC. The RG flux of the theory parameters between the weak and low energy coupling fixed points, associated with a variational methodology to treat residual interaction, allowed the determination of spectral function for all coupling strength inside the low energy interval.

3.2.2 Tkachenko phonon - impurity Hamiltonian

The two dimensional Tkachenko polaron model is given by the equation (3.10), where the Tkachenko excitations and the impurity creation (destruction) in the momentum state are given respectively by the operators $\hat{a}_{\mathbf{q}}$ ($\hat{a}^{\dagger}_{\mathbf{q}}$) and $\hat{b}_{\mathbf{k}}$ ($\hat{b}^{\dagger}_{\mathbf{k}}$). The first term of Eq. (3.10) represents the quadratic dispersion relation of the Tkachenko modes, the effective mass M of the Tkachenko boson can be expressed in terms of the vortex array filling factor $\upsilon = \pi n_A l^2$, where n_A is the majority species density and $l = \sqrt{\hbar/m_A\Omega}$ the vortex separation in the array with uniform vorticity Ω. The second term represents the impurity kinetic energy, with effective mass m of the minority species due to the vortex lattice. The coupling between them is given by the last term of the Hamiltonian, where $\lambda = (2\pi)^{-1/2}\eta^{1/4} g_{AB}\, \upsilon^{1/2}$, with g_{AB} the $2D$ inter-species interaction and the constant $\eta \approx 0.8219$ characteristic of the Abrikosov vortex lattice.

As showed before, the effective low energy system hamiltonian is associated with an increasing coupling with the background phonons. At weak coupling, we obtained a renormalizable quantum field theory with a marginally relevant interaction, that is reflected in the anomalous broadening of the impurity excitation spectrum. That is an unusual behavior guaranteed by the quadratic dispersion of the Tkachenko modes.

We intend to show here another consequence that comes with this soft modes dispersion, that is the appearance of OC in the Tkachenko excitation background due to the impurity perturbation. The new features associated with our model is not only the occurence of OC in a bosonic cold atoms background, since until now this phenomenon has just been considered for impurities in a degenerate Fermi sea (79–81), but also the possibility of study the transient regime toward the OC (82–84). In the cold atomic experiments with optical lattice, the latter localizes the impurity in specific positions to induce the OC (79). In our case, the interaction with the background vortex lattice is enough to induce the spontaneous localization of the impurity and then produce OC. Experimental techniques (45,79,81) were already developed to detect the OC and can be easily adapted to our particular situation.

3.2.3 RG analysis

We found that the coupling constant λ is marginally relevant in the weak coupling limit ($e^{-\pi/4\tilde{\lambda}_0^2} \ll kl \ll 1$). The impurity mass m also increases with the RG flow. In addition, there is the field renormalization in Eq. (3.39), where the logarithmic correction stems from coupling between an impurity and bosonic modes with a constant density of states, that is, bosons with parabolic dispersion in $2D$. According to Eq. (3.33) and Eq. (3.39), in the infrared limit, that is, for $k \to 0$ we will have $m^* \approx \frac{2\lambda^2\mu^3}{\pi} \ln\left(\frac{\Lambda}{\varepsilon_{\mathbf{k}}}\right)$ and $Z_{\mathbf{k}} \approx \exp\left[-\frac{\lambda^2\mu^2}{\pi} \ln\left(\frac{\Lambda}{\varepsilon_{\mathbf{k}}}\right)\right] = \left(\frac{\varepsilon_{\mathbf{k}}}{\Lambda}\right)^{\frac{\lambda^2\mu^2}{\pi}}$. These aspects of the theory in low energy regimes resemble the x-ray edge problem explored in the introduction. The quasiparticle resulted from the dressing of the core-hole with the low energetic particle-hole excitations has a quasiparticle weight $Z = (\omega/\omega_c)^{\alpha_{orth}}$ (85); the cutoff ω_c has the order of the Fermi level width and α_{orth} is proportional to the square of the coupling between the core- hole impurity and the conduction electrons. The core-hole propagator vanishes for long times (low energy regimes) as $D(t) \sim (1/\omega_c t)^{\alpha_{orth}}$.

Pursuing the analogy with the x-ray edge problem, here we assume the RG flow from the weak coupling to a low energy fixed point where $m \to \infty$. According to RG

dynamic equations in (68), the first is an unstable weak coupling fixed point (marginal relevant interaction) reflecting increasing effective mass and coupling constant of the polaron. Assuming monotonic evolution of m for lower values of k, however, we expect that λ asymptotically approaches a critical value ($\lambda \to \lambda_c$), that is, the RG flow of λ should have an infrared cutoff associated with the divergent polaron mass. The latter could be classified as a stable fixed point. Now we are mainly interested in find this fixed point and determine the Greens function (and the correspondent spectral function) of the impurity close to this point, for $\varepsilon_{\mathbf{k}} \ll \Lambda\, e^{-\pi/2\mu_0^2\lambda_0^2}$.

In order to analyze the polaron spectrum in this regime, we generalize the RG flow equations including the quasiparticle weight evolution $Z_{\mathbf{k}}$ to determine the effective parameters of the theory. The perturbative RG equations (β *function* (71)) around the low energy fixed point were derived considering lowest order correction diagrams (the one-phonon, Fig. 8a, and three point vertex diagrams, Fig. 8b) with renormalized $G(\mathbf{k},\omega) = Z_{\mathbf{k}}/\omega$ for the internal lines impurity Green function; that corresponds to neglect the polaron pole near the fixed point, as $m \to \infty$.

These Feynman diagrams were integrated in momentum space limited by a UV cut off Λ. Considering the infinitesimal reduction of the cut off ($\Lambda' = \Lambda\, e^{-d\ell}$ with $d\ell \ll 1$), that is, diminishing the momentum shell to integrate out the fast modes, we derive the flow equations for the theory parameters. With $\tilde{\lambda} = M\lambda$ and $m = M\tilde{m}$, those equations can be rewritten as

$$\begin{aligned}
\frac{dZ_{\mathbf{k}}}{d\ell} &= -\frac{\tilde{\lambda}^2\, Z_{\mathbf{k}}}{\pi}\left(\frac{\mu}{M}\right)^2, \\
\frac{d\tilde{\lambda}}{d\ell} &= \frac{\tilde{\lambda}^3 Z_{\mathbf{k}}^2}{\pi}\left(\frac{\mu}{M}\right)^2, \\
\frac{d\tilde{m}}{d\ell} &= 2\,\frac{\tilde{\lambda}^2}{\pi}\left(\frac{\mu}{M}\right)^3.
\end{aligned} \tag{3.43}$$

We can immediately solve the first two equations to find the asymptotic limit $\lambda_c = e^{1/2}\lambda_0$ for $Z \to 0$. It confirms the validity of disregarding higher order corrections in the RGs (see

Figure 9 – RG Flow - The original problem, with bare parameters, corresponds to the starting point in the diagram ($Z = 1$). The length along the flow direction is essentially a measure of how many energy scales have been integrated out, with the regions towards which the flow points being the effective parameters of the model at lower and lower energies.

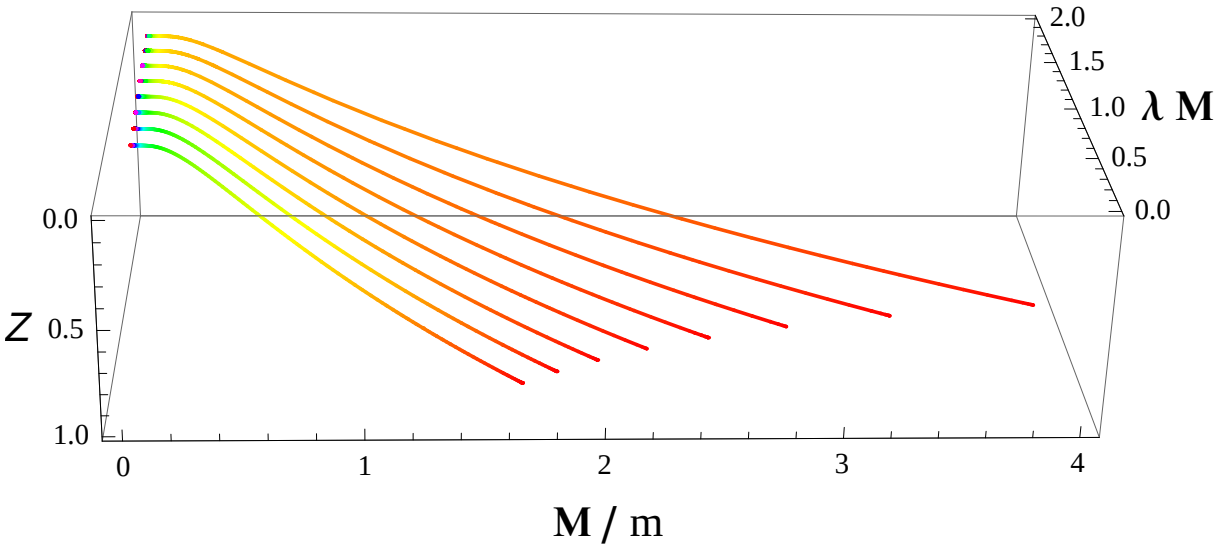

Source: elaborated by the author

appendix A.3), since λ does not differ significantly from the bare constant of the theory, that is kept in the weak coupling regime. Figure (9) shows the flow in a renormalization group diagram. Particularly here, the parameters flow toward a line of fixed points. A fixed line usually corresponds to a class of models which have some asymptotic behavior, e.g. an exponent, which varies continuously. As example, we have the Kosterlitz Thouless phenomenon (86) or even to the non singular Fermi liquid ferromagnetic Kondo problem (87). For the latter, an interesting generalization is given by the spin less finite range interaction model developed in (88). Their RG equation gives the low energy physics dominated by the orthogonality catastrophe as the spin-flip operator (or hybridization between the impurity and conduction electron orbital in the original Anderson model) goes to zero. In our case, that will be the impurity kinetic term that goes to zero in the fixed line, preventing further fluctuations of the impurity potential.

3.2.4 Dispersionless impurity Spectral Function

The low-energy physics dominated by the orthogonality catastrophe has been solved by renormalization group methods Fig. 9. But simple arguments based on the x-ray edge singularity give the correct qualitative physics of the low energy fixed point, as will be showed next, with the spectral function calculation. First we try the simplest possible approximation and neglect the kinetic energy of the impurity in Eq. (3.10). In this case of infinite mass, the model can be solved exactly by an unitary transformation (69)

$$U = \exp\left[\frac{\alpha}{\sqrt{S}}\sum_{\mathbf{k},\mathbf{q}}\frac{1}{q}\,\hat{b}^{\dagger}_{\mathbf{k}}\,\hat{b}_{\mathbf{k}+\mathbf{q}}\,(\hat{a}_{\mathbf{q}}-\hat{a}^{\dagger}_{-\mathbf{q}})\right]. \tag{3.44}$$

This is analogous to the Lang-Firsov transformation used in the small polaron regime for lattice models with strong electron-phonon interaction (69). This transformation equally applies to the Frohlich (continuous) model in the intermediated coupling regimes (40). Using the identity $e^{-S}\hat{O}e^{S} = \hat{O} + [S,\hat{O}] + \frac{1}{2!}[S,[S,\hat{O}]] + ...$, we calculate the phonon dislocation ($\alpha_q = \alpha/q$)

$$\begin{aligned} e^{-S}\hat{a}_{\mathbf{q}}e^{S} &= \hat{a}_{\mathbf{q}} - \frac{1}{\sqrt{S}}\sum_{\mathbf{k},\mathbf{q}}\alpha_q\,\hat{b}^{\dagger}_{\mathbf{k}}\,\hat{b}_{\mathbf{k}-\mathbf{q}} \\ e^{-S}\hat{a}^{\dagger}_{\mathbf{q}}e^{S} &= \hat{a}^{\dagger}_{\mathbf{q}} - \frac{1}{\sqrt{S}}\sum_{\mathbf{k},\mathbf{q}}\alpha_q\,\hat{b}^{\dagger}_{\mathbf{k}}\,\hat{b}_{\mathbf{k}+\mathbf{q}}. \end{aligned} \tag{3.45}$$

Choosing $\alpha = 2M\lambda$ eliminates the impurity-phonon coupling of the transformed H

$$U^{\dagger}HU = \sum_{\mathbf{q}}\frac{q^2}{2M}\,\hat{a}^{\dagger}_{\mathbf{q}}\,\hat{a}_{\mathbf{q}} + const. \tag{3.46}$$

We can verify the orthogonality between the final $|\tilde{0}\rangle$ and initial phonon vacuum state $|0\rangle$, that is, the background state with and without the impurity. Those are related by the canonical transform $|\tilde{0}\rangle = U|0\rangle$; thus for one localized impurity the projection $\langle 0|\tilde{0}\rangle$ gives

$$\langle 0|\exp\left[\frac{\alpha}{\sqrt{S}}\sum_{\mathbf{q}}\frac{1}{q}\,(\hat{a}_{\mathbf{q}}-\hat{a}^{\dagger}_{-\mathbf{q}})\right]|0\rangle \propto e^{-\frac{\alpha^2}{S}\sum_{\mathbf{q}}\frac{1}{q^2}}. \tag{3.47}$$

The sum can be converted to an integral $\frac{\alpha^2}{S}\sum_{\mathbf{q}}\frac{1}{q^2} \to \frac{\alpha^2}{2\pi}\int\frac{dq}{q}$ and the overestimated projection value, with the lower bound $q_{min} = \frac{2\pi}{L}$, gives $\langle 0|\tilde{0}\rangle = 0$ for an infinite system

($L \to \infty$). As in the Anderson proposal we had the orthogonality between the Fermi sea ground state with and without the particle-hole excitation, in the thermodynamic limit $N \to \infty$, here the orthogonality comes from the infinite number of Tkachenko modes excited in the phonon vacuum by the localized impurity. We note that the new vacuum $|\tilde{0}\rangle$ is built by a coherent superposition of TM phonons.

Considering $\psi_B(\mathbf{r},t) = \frac{1}{\sqrt{S}} \sum_{\mathbf{k}} e^{i\mathbf{k}.\mathbf{r}}\, \hat{b}_{\mathbf{k}}(t)$, it is easy to show that

$$\begin{aligned} \tilde{\psi}_B(\mathbf{r},t) &= e^{-S}\psi_B(\mathbf{r},t)e^{S} = \psi_B(\mathbf{r},t)\; e^{\alpha Y(\mathbf{r},t)} \\ \tilde{\psi}^{\dagger}_B(\mathbf{r},t) &= e^{-S}\psi^{\dagger}_B(\mathbf{r},t)e^{S} = \psi^{\dagger}_B(\mathbf{r},t)\; e^{-\alpha Y(\mathbf{r},t)}, \end{aligned} \tag{3.48}$$

where we have the phonon displacement operator $Y(\mathbf{r},t) = \frac{1}{\sqrt{S}} \sum_{\mathbf{q}} q^{-1} e^{i\mathbf{q}\cdot\mathbf{r}} (\hat{a}_{\mathbf{q}} - \hat{a}^{\dagger}_{-\mathbf{q}})$. The impurity Green's function becomes

$$\begin{aligned} G(\mathbf{r},t) &= -i\theta(t)\, \langle \tilde{\psi}_B(\mathbf{r},t)\tilde{\psi}^{\dagger}_B(\mathbf{0},0)\rangle \\ &= -i\theta(t)\, \langle \psi_B(\mathbf{r},t)\psi^{\dagger}_B(\mathbf{0},0)\rangle \langle e^{\alpha Y(\mathbf{r},t)} e^{-\alpha Y(\mathbf{0},0)}\rangle. \end{aligned} \tag{3.49}$$

The unitary transformation decouples the impurity and phonon operators, as showed in Eq. (3.49), where the first and second brackets correspond to the mean values taken with the impurity and phonon ground state respectively. Since the problem is now noninteracting, we can calculate the exact propagators. For the first term we have

$$\langle \psi_B(\mathbf{r},t)\psi^{\dagger}_B(\mathbf{0},0)\rangle = \frac{1}{S}\sum_{\mathbf{k}}\; e^{i(\mathbf{k}.\mathbf{r} - \varepsilon_{\mathbf{k}} t)} \langle \hat{b}_{\mathbf{k}}(0)\hat{b}^{\dagger}_{\mathbf{k}}(0)\rangle. \tag{3.50}$$

Using $e^{A+B} = e^{A}\; e^{B}\; e^{-[A,B]/2}$ for the second term, with $A = \alpha Y(\mathbf{r},t)$, $B = -\alpha Y(\mathbf{0},0)$ and $\frac{[A,B]}{2} = -i\frac{\alpha^2}{S}\sum_{\mathbf{q}} \frac{e^{i\mathbf{q}.\mathbf{r}}}{q^2} \sin\omega_q t$, we find

$$\langle e^{\alpha Y(\mathbf{r},t)} e^{-\alpha Y(\mathbf{0},0)}\rangle = e^{\alpha^2 I(\mathbf{r},t)}, \tag{3.51}$$

with $I(\mathbf{r},t) = \frac{1}{2\pi}\int \frac{dq}{q}\, [\exp(-i\omega_q t)\; J_0(qr) - 1]$.

For impurity infinite mass ($\varepsilon_{\mathbf{k}} \to 0$ and $t > 0$)

$$G(\mathbf{r},t) = -i\,\delta(\mathbf{r})\; e^{\alpha^2 I(t)}, \tag{3.52}$$

where $I(t) \approx -\frac{1}{4\pi}\left[\gamma + \ln(i\omega_q t)\right]$ with the Euler constant γ. The propagator of $Y(\mathbf{r}, t)$ is logarithmic, thus it gives rise to an additional power-law decay in the impurity Green's function, as expected from the orthogonality catastrophe, that is

$$G(\mathbf{r}, t) \propto \delta(\mathbf{r})\, t^{-\alpha^2/4\pi}. \tag{3.53}$$

Notice that $\alpha^2/4\pi = M^2\lambda^2/\pi = \mu^2\lambda^2/\pi$ since $\mu = M$ for $m \to \infty$. This seems consistent with the coefficient of the logarithmic correction in Eq. (3.39), coming from the weak coupling regime and also reflected in the $Z_{\mathbf{k}}$ exponent for k in the low energy fixed point. The orthogonality induced by the self localization of the impurity (89) leads to the decay of the correlation function with this non-universal exponent.

Taking the Fourier transform of (3.53) gives a power-law singularity in the spectral function

$$A(\mathbf{k}, \omega) \sim \omega^{\alpha^2/4\pi - 1}. \tag{3.54}$$

The actual value of $\alpha^2/4\pi$ determines the singular properties at low energy. In a renormalization group language, for $\alpha^2/4\pi < 1$, the flows impinge on the line of fixed points and we obtain a continuous set of exponents.

3.2.5 Spectral function for Finite mass impurity

When m is finite, the unitary transformation in Eq. (3.46) does not diagonalize the Hamiltonian exactly because the transformation of the impurity kinetic energy generates an additional interaction. Nonetheless we can use a variational approach that fixes the parameter of the unitary transformation by minimizing the polaron ground state energy (see section III-A of (90)). Starting with the transformation of Eq. (3.10)

$$\tilde{H} = U^\dagger H U = \tilde{H}_{imp} + \tilde{H}_{ph} + \tilde{H}_{imp-ph}, \tag{3.55}$$

where

$$\tilde{H}_{imp} = \sum_{\mathbf{k}} \frac{k^2}{2m} \hat{b}^\dagger_{\mathbf{k}} \hat{b}_{\mathbf{k}} + \frac{1}{\sqrt{S}} \sum_{\mathbf{k},\mathbf{q}} \alpha_q \left[\frac{k^2}{2m} - \frac{|\mathbf{k}-\mathbf{q}|^2}{2m} \right] \hat{b}^\dagger_{\mathbf{k}} \hat{b}_{\mathbf{k}-\mathbf{q}} (\hat{a}_{\mathbf{q}} - \hat{a}^\dagger_{-\mathbf{q}})$$
$$+ \frac{1}{2S} \sum_{\mathbf{k},\mathbf{q},\mathbf{q}'} \alpha_{\mathbf{q}} \alpha_{\mathbf{q}'} \left[\frac{k^2}{2m} - 2\frac{|\mathbf{k}-\mathbf{q}|^2}{2m} + \frac{|\mathbf{k}-\mathbf{q}-\mathbf{q}'|^2}{2m} \right] \hat{b}^\dagger_{\mathbf{k}} \hat{b}_{\mathbf{k}-\mathbf{q}-\mathbf{q}'} (\hat{a}_{\mathbf{q}} - \hat{a}^\dagger_{-\mathbf{q}})(\hat{a}_{\mathbf{q}'} - \hat{a}^\dagger_{-\mathbf{q}'}), \tag{3.56}$$

$$\tilde{H}_{ph} = \sum_{\mathbf{q}} \frac{q^2}{2M} \hat{a}^\dagger_{\mathbf{q}} \hat{a}_{\mathbf{q}} - \frac{1}{\sqrt{S}} \sum_{\mathbf{q},\mathbf{k}} \alpha_q \frac{q^2}{2M} \hat{b}^\dagger_{\mathbf{k}} \hat{b}_{\mathbf{k}-\mathbf{q}} (\hat{a}_{\mathbf{q}} + \hat{a}^\dagger_{-\mathbf{q}}) + \frac{1}{S} \sum_{\mathbf{q},\mathbf{k}} \alpha_q^2 \frac{q^2}{2M} \hat{b}^\dagger_{\mathbf{k}} \hat{b}_{\mathbf{k}}, \tag{3.57}$$

and

$$\tilde{H}_{imp-ph} = \frac{1}{\sqrt{S}} \sum_{\mathbf{q},\mathbf{k}} \lambda_q \, \hat{b}^\dagger_{\mathbf{k}} \hat{b}_{\mathbf{k}-\mathbf{q}} (\hat{a}_{\mathbf{q}} + \hat{a}^\dagger_{-\mathbf{q}}) - \frac{2}{S} \sum_{\mathbf{k},\mathbf{q}} \alpha_q \lambda_q \hat{b}^\dagger_{\mathbf{k}} \hat{b}_{\mathbf{k}}. \tag{3.58}$$

Averaging Eq. (3.55) over the system ground state we obtain $\langle \tilde{H} \rangle = \mathcal{E}_{\mathbf{k}}(\alpha_q) + \mathcal{E}_{ph}$, where the α_q - function gives the polaronic free energy $\mathcal{E}_{\mathbf{k}}(\alpha_q) = n_{\mathbf{k}} \epsilon_{\mathbf{k}}$, with $n_{\mathbf{k}} = \langle \hat{b}^\dagger_{\mathbf{k}} \hat{b}_{\mathbf{k}} \rangle$ and $\epsilon_{\mathbf{k}} = \frac{k^2}{2m} + \frac{1}{S} \sum_{\mathbf{q}} \left[\alpha_q^2 \frac{q^2}{2M} - 2\alpha_q \lambda_q \right] - \frac{1}{S} \sum_{\mathbf{q}} \alpha_q^2 \left[\frac{k^2}{2m} - \frac{|\mathbf{k}-\mathbf{q}|^2}{2m} \right]$.

We can symmetrize the sum to simplify such expression

$$\begin{aligned} \epsilon_{\mathbf{k}} &= \frac{k^2}{2m} + \frac{1}{S} \sum_{\mathbf{q}} \left[\alpha_q^2 \frac{q^2}{2M} - 2\alpha_q \lambda_q \right] - \frac{1}{S} \sum_{\mathbf{q}} \alpha_q^2 \left[\frac{k^2}{2m} - \frac{|\mathbf{k}-\mathbf{q}|^2}{4m} - \frac{|\mathbf{k}+\mathbf{q}|^2}{4m} \right] \\ &= \frac{k^2}{2m} + \frac{1}{S} \sum_{\mathbf{q}} \left[\alpha_q^2 \left(\frac{1}{2M} + \frac{1}{2m} \right) q^2 - 2\alpha_q \lambda_q \right], \end{aligned} \tag{3.59}$$

and then apply the minimization

$$\frac{\partial \epsilon_{\mathbf{k}}}{\partial \alpha_q} = 0 \quad \Rightarrow \quad \alpha_q = \frac{2\mu\lambda}{q}. \tag{3.60}$$

This condition gives $\alpha = 2\mu\lambda$, and a transformed Hamiltonian with an effective coupling $\lambda' = \lambda M/m$ Eq. (3.61). This variational approach brings the phonon configuration that minimizes the polaron energy. The transformed Hamiltonian describes a polaron interacting with a residual phonon background.

$$\tilde{H} = \sum_{\mathbf{q}} \frac{q^2}{2M} \, \hat{a}^\dagger_{\mathbf{q}} \, \hat{a}_{\mathbf{q}} + \sum_{\mathbf{k}} \frac{k^2}{2m} \, \hat{b}^\dagger_{\mathbf{k}} \, \hat{b}_{\mathbf{k}} + \frac{1}{\sqrt{S}} \sum_{\mathbf{k},\mathbf{q}} \lambda' \mid \mathbf{q} \mid \hat{b}^\dagger_{\mathbf{k}} \, \hat{b}_{\mathbf{k}+\mathbf{q}} \, (\hat{a}_{\mathbf{q}} + \hat{a}^\dagger_{-\mathbf{q}}). \tag{3.61}$$

Figure 10 – Self-energy insertion (a) and connect cloud diagram (b) and (c) . These second order corrections to the impurity propagator are given by the integrals in A.4.

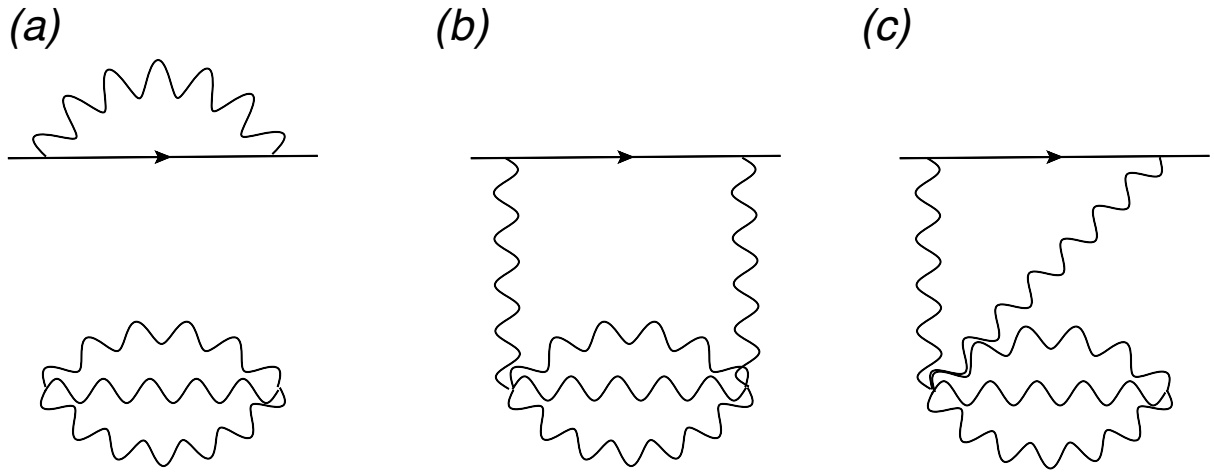

Source: elaborated by the author

When we neglect the residual interaction λ' in Eq. (3.61), we can calculate the Green's function similarly to the case of infinite mass. The difference is that now we have to use the free particle propagator $\langle \psi_B(\mathbf{r},t)\psi_B{}^{\dagger}(\mathbf{0},0)\rangle \propto\ e^{-imr^2/2t}/t$. For $M/m \ll 1$ the spectral function calculation simplifies a little and we find a power law singularity with a threshold along the impurity dispersion. The rounding may come from the decay rate of the single particle at order $(\lambda')^2$, which appears in the self-energy of ψ_B if we apply perturbation theory in λ'. In Fig. 10 we schematized a set of diagrams that give second order corrections in the impurity propagator. Note that, in this transformed scenario, the phonon background is given by an exponential field propagator, with a cloud diagram represented by the wavy lines in the bottom of Fig. 10.

Considering the residual interaction $H_r = \frac{1}{\sqrt{S}} \sum_{\mathbf{k},\mathbf{q}} \lambda'\ q\ \hat{b}^{\dagger}_{\mathbf{k}+\mathbf{q}} \hat{b}_{\mathbf{k}}\ (\hat{a}_{\mathbf{q}} + \hat{a}^{\dagger}_{-\mathbf{q}})$, we have to deal with the dressed impurity Greens function

$$G(\mathbf{r},t) = \langle T\psi_B(\mathbf{r},t)\psi_B^{\dagger}(\mathbf{0},0)e^{\alpha Y(\mathbf{r},t)}e^{-\alpha Y(\mathbf{0},0)}e^{-i\int dt_1 H_r(t_1)}\rangle.$$

Expanding Eq. (3.62) to second order in λ'

$$G(\mathbf{r},t) = -i\theta(t)\,\langle \psi_B(\mathbf{r},t)\psi_B^{\dagger}(\mathbf{0},0)\rangle\langle e^{\alpha Y(\mathbf{r},t)}e^{-\alpha Y(\mathbf{0},0)}\rangle\, +$$
$$-i(-i)^2\int dt_1 dt_2 \langle T\ \psi_B(\mathbf{r},t)\psi_B^{\dagger}(\mathbf{0},0)e^{\alpha Y(\mathbf{r},t)}e^{-\alpha Y(\mathbf{0},0)}H_r(t_1)\ H_r(t_2)\rangle. \qquad (3.62)$$

The second term in Eq. (3.62), with the time order bracket given by the operator T, provides the self-energy insertion (Fig. 10a) and connected phonon cloud (Fig. 10b and 10c) diagrams. The latter connects the impurity line to the phonon cloud propagator, but here it gives zero contribution. That can be understood from the $Y(\mathbf{r},t)$ dependence with the combination $\hat{a}_{\mathbf{q}} - \hat{a}^{\dagger}_{-\mathbf{q}}$, while the interaction is proportional to $\hat{a}_{\mathbf{q}} + \hat{a}^{\dagger}_{-\mathbf{q}}$. Making an analogy with the harmonic oscillator problem, those diagrams present contractions similar to momentum $\hat{\Pi}_{\mathbf{q}}$ $(= \hat{a}_{\mathbf{q}} - \hat{a}^{\dagger}_{-\mathbf{q}})$ and position operators $\hat{\phi}_{\mathbf{q}}$ $(= \hat{a}_{\mathbf{q}} + \hat{a}^{\dagger}_{-\mathbf{q}})$, that gives zero expected value for the ground state.

Neglecting diagrams that connect the impurity line to the phonon cloud propagator, we can move on to the Fourier transform of $G(\mathbf{r},t) = \mathcal{G}(\mathbf{r},t)\; e^{\alpha^2 I(\mathbf{r},t)}$

$$\begin{aligned} G(\mathbf{k},\omega) &= \int d^2r\, dt\, e^{-i\mathbf{k}\cdot\mathbf{r}}\, e^{i\omega t}\, G(\mathbf{r},t) \\ &= \int d^2r\, dt\, e^{-i\mathbf{k}\cdot\mathbf{r}} e^{i\omega t} \int \frac{d^2k' d\omega'}{(2\pi)^3} e^{i\mathbf{k}'\cdot\mathbf{r}} e^{-i\omega' t} \mathcal{G}(\mathbf{k}',\omega') e^{\alpha^2 I(\mathbf{r},t)}, \end{aligned} \tag{3.63}$$

where $\mathcal{G}(\mathbf{k}',\omega') = \frac{1}{\omega' - \varepsilon_{\mathbf{k}'} - \Sigma(\mathbf{k}',\omega')}$ is the impurity dressed propagator showed by Fig. 10a. The oscillation of $\mathcal{G}(\mathbf{r},t)$ suppresses the composite Green's function for $r^2 > t/m$. In the regime $m \gg M$, we can neglect the spatial dependence of $I(\mathbf{r},t)$. Physically, this means that the Tkachenko mode diffuses much faster than the impurity, thus the dominant contribution to $G(\mathbf{r},t)$ involves the long time tail of $e^{\alpha^2 I(\mathbf{r},t)}$ near the origin. Adopting $\nu = \alpha^2/4\pi$, within this approximation we obtain

$$e^{\alpha^2 I(\mathbf{r},t)} \approx \frac{\mathcal{C}}{(i\Lambda t)^{\nu}}, \tag{3.64}$$

where Λ is a UV energy cutoff and $\mathcal{C} = e^{-\gamma\nu}$. Then

$$G(\mathbf{k},\omega) = \frac{1}{2\pi} \frac{\mathcal{C}}{(i\Lambda)^{\nu}} \int dt\; d\omega'\, \frac{e^{i(\omega-\omega')t}}{t^{\nu}}\, \mathcal{G}(\mathbf{k},\omega'). \tag{3.65}$$

For $\omega' > \omega$

$$G(\mathbf{k},\omega) = 2\sin(\pi\nu) \frac{\mathcal{C}}{(i\Lambda)^{\nu}} \Gamma(1-\nu) \int_{\omega}^{\infty} \frac{d\omega'}{2\pi} \frac{\mathcal{G}(\mathbf{k},\omega')}{(\omega'-\omega)^{1-\nu}}. \tag{3.66}$$

Now we consider the self-energy that comes with the calculation of the diagram in Fig.10a. That corresponds to our previous results in section 3.1.5 but with λ' replacing λ. We found $\mathrm{Re}\left[\Sigma(\mathbf{k},\omega)\right] = \frac{\lambda'^2}{\pi}\left[|\delta\varepsilon| - \left(\delta\varepsilon + \frac{\mu k^2}{m^2}\right)\ln\left|\frac{\Lambda}{f(\mathbf{k},\omega)}\right|\right]$ and $\mathrm{Im}\left[\Sigma(\mathbf{k},\omega)\right] = -\frac{\lambda'^2}{2}\left(\delta\varepsilon + \frac{\mu k^2}{m^2}\right)\theta[\omega - \varepsilon_{min}(k)]$, with $f(\mathbf{k},\omega) = \frac{\mu k^2}{2m^2}\,\theta(\delta\varepsilon) + [\omega - \varepsilon_{min}(k)]\,\theta(-\delta\varepsilon)$, $\delta\varepsilon = \omega - \varepsilon_{\mathbf{k}}$ and the kinematic threshold $\varepsilon_{min}(k) = k^2/2(m+M)$.

Particularly, for the mass shell ($\delta\varepsilon = 0$) we have $\mathrm{Re}\left[\Sigma(\mathbf{k},\omega)\right] \to \Sigma'(\mathbf{k}) = \frac{\lambda'^2}{\pi}\left(-\frac{\mu k^2}{m^2}\ln\left|\frac{\Lambda}{f(\mathbf{k})}\right|\right)$, with $f(\mathbf{k}) \approx \frac{\mu k^2}{4m^2}$ and $\mathrm{Im}\left[\Sigma(\mathbf{k},\omega)\right] \to \Sigma''(\mathbf{k}) = -\frac{\lambda'^2}{2}\left(\frac{\mu k^2}{m^2}\right)$.

That gives, for $\nu < 1$

$$\int_{\omega}^{\infty} d\omega' \,\frac{\mathcal{G}(\mathbf{k},\omega')}{(\omega'-\omega)^{1-\nu}} = \frac{\pi\ \sin(\pi\nu)^{-1}}{\left[\omega - \varepsilon_{\mathbf{k}} - \Sigma'(\mathbf{k}) - i\Sigma''(\mathbf{k})\right]^{1-\nu}}, \tag{3.67}$$

and for the spectral function $A(\mathbf{k},\omega) = -\frac{1}{\pi}\mathrm{Im}\left[G(\mathbf{k},\omega)\right]$

$$\begin{aligned} A(\mathbf{k},\omega) &= \frac{\mathcal{C}\,\Gamma(1-\nu)}{\pi\Lambda^{\nu}}\,\mathrm{Im}\left[\left(\frac{-1}{\omega - \varepsilon_{\mathbf{k}} - \Sigma'(\mathbf{k}) - i\Sigma''(\mathbf{k})}\right)^{1-\nu}\right] \\ &= \frac{\mathcal{C}\,\Gamma(1-\nu)}{\Lambda^{\nu}}\,\frac{\sin\left(1-\nu\right)\left[\frac{\pi}{2} - \arctan\left(\frac{E_{\mathbf{k}}-\omega}{\gamma_{\mathbf{k}}}\right)\right]}{\left[(\omega - E_{\mathbf{k}})^2 + \gamma_{\mathbf{k}}^2\right]^{(1-\nu)/2}}. \end{aligned} \tag{3.68}$$

In the last line of Eq. (3.68) we associate the decay rate $\gamma_{\mathbf{k}}$ $\left(= -Z_{\mathbf{k}}^{-1}\,\Sigma''(\mathbf{k})\right)$ and we absorbed the real part of the self-energy into $E_{\mathbf{k}}$ as a renormalization of the impurity mass. This result already shows that $\gamma_{\mathbf{k}}/E_{\mathbf{k}}$ decreases as the effective impurity mass increases. Thus the peak should become more pronounced for smaller k and we recover the power-law singularity in the limit $k \to 0$, $m \to \infty$. This validity, however, is limited to the energy window where we expect the peak to be broadened, $|\,\omega - E_{\mathbf{k}}\,| \sim M\,k^2/m^2 \ll E_{\mathbf{k}}$. For the complete solution we have to consider the regions above and below the mass shell.

Calling $X(\mathbf{k},\omega) = \int_{\omega}^{\infty} d\omega' \frac{\mathcal{G}(\mathbf{k},\omega')}{(\omega'-\omega)^{1-\nu}}$, considering $\Sigma(\mathbf{k},\omega)$ above, for $\omega' > \omega > \varepsilon_{\mathbf{k}} > \varepsilon_{min}$ it

gives

$$X(\mathbf{k},\omega) = \int_{\omega}^{\infty} d\omega' \, \frac{(\omega'-\omega)^{\nu-1}}{\omega' - \varepsilon_{\mathbf{k}} - \frac{\lambda'^2}{\pi}\,(\omega'-\varepsilon_{\mathbf{k}}) + i\,\frac{\lambda'^2}{2}\,\left(\omega' - \varepsilon_{\mathbf{k}} + \frac{\mu k^2}{m^2}\right)},$$

Otherwise for $\omega' > \varepsilon_{\mathbf{k}} > \omega > \varepsilon_{min}$

$$X(\mathbf{k},\omega) = \int_{\omega}^{\varepsilon_{\mathbf{k}}} d\omega' \, \frac{(\omega'-\omega)^{\nu-1}}{\omega'-\varepsilon_{\mathbf{k}}+\frac{\lambda'^2}{\pi}\,(\omega'-\varepsilon_{\mathbf{k}})+i\,\frac{\lambda'^2}{2}\,\left(\omega'-\varepsilon_{\mathbf{k}}+\frac{\mu k^2}{m^2}\right)} + \int_{\varepsilon_{\mathbf{k}}}^{\infty} d\omega' \, \frac{(\omega'-\omega)^{\nu-1}}{\omega'-\varepsilon_{\mathbf{k}}-\frac{\lambda'^2}{\pi}\,(\omega'-\varepsilon_{\mathbf{k}})+i\,\frac{\lambda'^2}{2}\,\left(\omega'-\varepsilon_{\mathbf{k}}+\frac{\mu k^2}{m^2}\right)},$$

Finally for $\omega' > \varepsilon_{\mathbf{k}} > \varepsilon_{min} > \omega$

$$X(\mathbf{k},\omega) = \int_{\omega}^{\varepsilon_{min}} d\omega' \, \frac{(\omega'-\omega)^{\nu-1}}{\omega'-\varepsilon_{\mathbf{k}}+\frac{\lambda'^2}{\pi}\,(\omega'-\varepsilon_{\mathbf{k}})} + \int_{\varepsilon_{min}}^{\varepsilon_{\mathbf{k}}} d\omega' \, \frac{(\omega'-\omega)^{\nu-1}}{\omega'-\varepsilon_{\mathbf{k}}+\frac{\lambda'^2}{\pi}\,(\omega'-\varepsilon_{\mathbf{k}})+i\,\frac{\lambda'^2}{2}\,\left(\omega'-\varepsilon_{\mathbf{k}}+\frac{\mu k^2}{m^2}\right)}$$
$$+ \int_{\varepsilon_{\mathbf{k}}}^{\infty} d\omega' \, \frac{(\omega'-\omega)^{\nu-1}}{\omega'-\varepsilon_{\mathbf{k}}-\frac{\lambda'^2}{\pi}\,(\omega'-\varepsilon_{\mathbf{k}})+i\,\frac{\lambda'^2}{2}\,\left(\omega'-\varepsilon_{\mathbf{k}}+\frac{\mu k^2}{m^2}\right)}.$$

All these integrals have analytical expressions and will be used next to estimate the spectral function in the low energy regime. Before that, we justify the values for λ_0 and m_0 that were also applied to create the graphics in Fig. 9. First, it is easy to show that the asymptotic RG solution for λ together with the constraint $\nu < 1$ gives $\lambda_0 < \sqrt{\frac{\pi}{e}}\,M^{-1}$. Also, we must keep the initial impurity momenta below the band maxima $k < l^{-1}$, approaching the lower limit defined in section 3.1.5 (see appendix A.2), $\tilde{k} \sim l^{-1}\; e^{-1/4\nu_0}$, associated with the impurity self-localization. Inside these limits, in Fig. 11 we plot several stages of the spectra varying the width of shell integration, that is, in different regimes of energy, for the bare parameters $\lambda_0 M = 0.2$, $m_0/M = 0.5$ and $k_0\, l = 1$ in the weak coupling regime (dashed curves), followed by the low energy region (solid curves), that starts with $\lambda M = 1$, $m/M = 1$ and $k\, l = 1/\sqrt{e}$ $\;(k = k(\ell) = k_0\; e^{-\ell/2})$.

As can be seen from Fig. 11, close to low energy fixed point our result resembles the studies of optical absorption spectra in semiconductors (82), with our two-particle threshold $\varepsilon_{min}(k)$ analogous to their so called indirect threshold. Those authors analyzed the reduction of the OC characteristic exponent due to the finite lifetime of the core-hole

Figure 11 – Spectral function for the lower energy regime with normalized k $[l^{-1}]$ and ω $[l^{-2}M^{-1}]$. The black line in the (k,ω) plane indicates the free particle dispersion relation $\varepsilon_{\mathbf{k}} = k^2/2m$ and the red line indicates the lower threshold $\varepsilon_{min}(k) = k^2/2(m+M)$. Experimental parameters: we consider ^{87}Rb as the atomic species for A with atomic density $n_A = 3\ 10^{12}\ m^{-2}$, transversely trapped (harmonic trap) with frequency $\omega_0 = 2\pi \times 300\ Hz$ and characterized by the lattice vorticity $\Omega = 2\pi \times 100\ Hz$. That gives $\frac{n_A g_A}{\hbar\Omega} = 0.1$, for the quantum Hall regime. Then we can estimate $l \sim 10^{-5}\ m$ and also $M \sim 5\ m_A$.

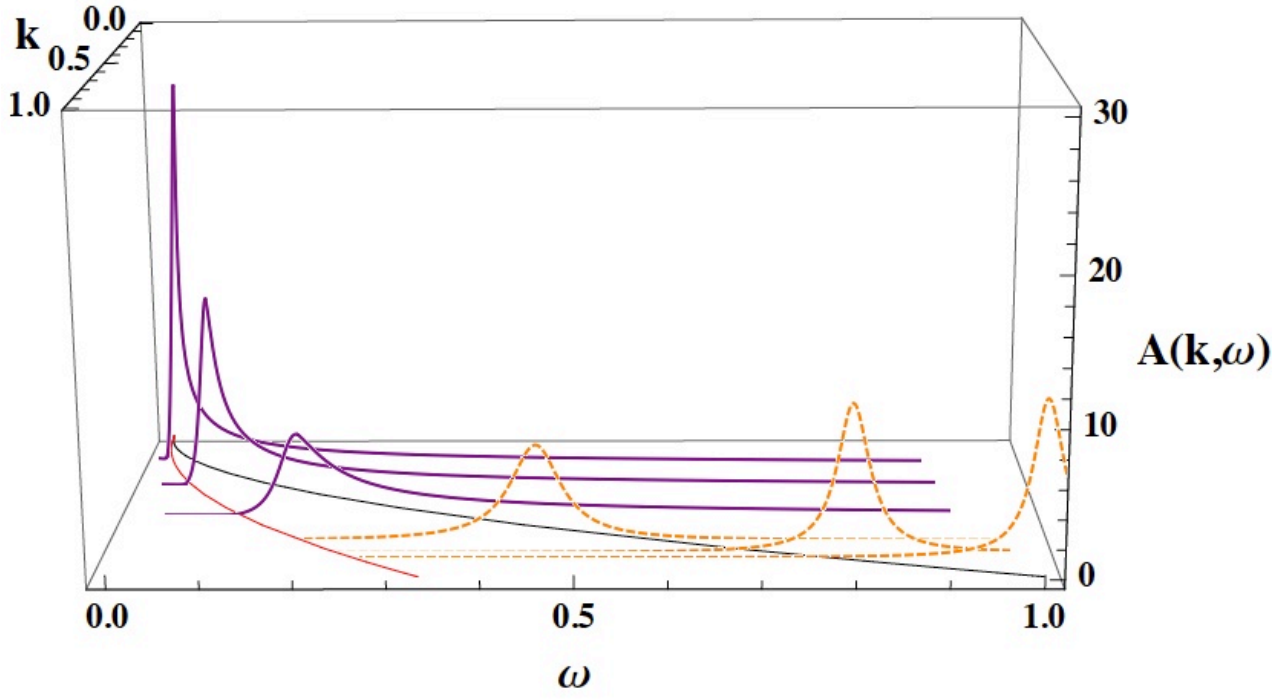

Source: elaborated by the author

(84). It is related with the particle-hole excitation recoil present in the semiconductors valence band, which has a finite dispersion instead of the flat band that gives the x-ray edge singularity in metals. When the mass of the impurity atom is much larger than the effective mass of the Tkachenko boson, one recovers the problem of a static impurity in a vortex lattice. In this limit, the quasiparticle residue Z vanishes and the spectral function exhibits a power law singularity. The reason for the breakdown of the quasiparticle picture is that the static impurity can excite an infinite number of low-energy Tkachenko excitations, causing the zero overlap between the interacting and non-interacting system ground-state, that is, the orthogonality catastrophe phenomenon (69). For a finite mass instead, it follows from momentum conservation that the impurity can generate Tkachenko excitations with recoil energy only up to $\Delta\varepsilon = \varepsilon_{\mathbf{k}} - \varepsilon_{min}(k)$, which limits the

available phase-space for scattering. Another way to verify the influence of the impurity dynamics over the bosons excitations is applying the Lee-Low-Pines transformation (91). That is based on the total momentum conservation to eliminate the impurity coordinates from the Hamiltonian. The transformed Hamiltonian shows how the dynamics of impurity is reflected in an additional correlation between the Tkachenko modes, that can not be considered with the independent boson model anymore (69).

3.2.6 Probing the excitation spectrum

Analogous to photoemission spectroscopy used to detect the excitation spectrum of interacting electrons in metals (angle resolved technique), in the cold atoms community, there is the radio-frequency spectroscopy as equivalent momentum resolved method (92). Basically, a radio-frequency (RF) light pulse transfers the impurity atoms to an hyperfine level that does not interact with the background atoms. After that, the free expansion absorption image can provide the momentum distribution of the impurity sample. Since the RF does not alter the original atomic momentum, one can recover the impurity single particle energy spectrum combining the information of the hyperfine level separation (light pulse energy) and the release energy of the free expanding impurity.

As the x-ray problem where the core-hole Greens function hold information of the single particle spectra of the Fermi-sea (69), it is possible to show that the impurity spectral function is related with the Fourier transform of the many body states superposition (Tkachenko phonon background) before and after the impurity potential perturbation (79, 81). We finalize this section analyzing the power law dependence expected for long time of this overlap function, that is, for the low energy regime of our system. Considering the overlap between initial (non interacting) and final (interacting) states of the system as given by the response function $\mathcal{S}(t) = \langle 0_k | e^{i(H_A+H_B)t}\ e^{-i(H_A+H_B+H_{int})t} | 0_k \rangle$, with the brackets being the phonon vacuum and the impurity with the initial momentum k. The function $\mathcal{S}(t)$ is basically the overlap between the system background evolved to the time t, with and without the impurity interaction. The dynamic OC theory of Nozières (83)

allows to relate this function with the impurity propagator, for infinity impurity lifetime. We define the intermediate (large impurity $k_>$) and the long times (small impurity $k_<$) regimes inside the interval $\omega_0^{-1} < t < \gamma_k^{-1}$, limited by the polaron lifetime γ_k^{-1} and by the higher characteristic energy of our system ω_0. For initial times, the overlap function $\mathcal{S}(t) \propto e^{-\gamma_k t}$ has exponential decay with a Lorentzian $A(k_>, \omega) \propto \mathrm{Im}[\omega + i\gamma_k]^{-1}$. Otherwise, for long times, we can probe the orthogonality catastrophe from the power law decay of $\mathcal{S}(t) \propto t^{-\nu}$, that translates into a singular long tail spectral function $A(k_<, \omega) \propto \omega^{\nu-1}$.

To probe each regime of the spectrum, that is, to detect the spectral function at different times until the impurity localization, we should start with an external force that acts selectively on impurity atoms (e.g. through a magnetic field gradient) to impart a finite initial momentum. Then a RF pulse can be applied after an appropriate time interval to transfer the initially interacting impurities to non interacting final state. The release energy of the dilute impurity cloud can be measured trough the time of flight state-selective absorption image realized with different hold times.

3.3 Summary

We analyzed the properties of impurities immersed in a vortex lattice formed by ultracold bosons in the mean field quantum Hall regime. Besides the effects of a periodic lattice potential, the impurity is dressed by collective modes with parabolic dispersion (Tkachenko modes). We derived the effective impurity-phonon model, which at weak coupling is equivalent to a renormalizable quantum field theory with a marginally relevant interaction. Using the RG formalism, we tracked the impurity excitation spectra as function of the background coupling interaction toward the low energy fixed point, where we show that it acquires the power law signature of the orthogonality catastrophe. These impurity spectral function properties can be detected experimentally using momentum-resolved spectroscopy.

4 Double Superfluid System

4.1 Introduction

Two component condensate systems have had an enormous impact in the field of ultracold atoms, in special since the experimental production of Bose-Einstein condensate (BEC) of fermions. That consist of effective bosonic molecules, the tightly bound Cooper pairs, formed after the fermions be combined cooling with bosonic atoms (13). The experimental observation of the BEC-BCS transition with this molecular BEC made the ultracold atoms a powerful tool to test condensate matter models, which can be studied in a highly controllable environment. The two-species BEC of atomic bosons also has rich new physics to be explored. There are important experiments in this field, including that of Cornell's group, with different ^{87}Rb hyperfine states (93), where the static proprieties of binary mixtures, their relative phase coherence and dynamics (94–97) were investigated. The same group was able to nucleate vortex with this system (98), and most recently, to produce the superposition of two array of vortices (99).

The possibility of tuning the scattering length is also fundamental tool in the two component BEC scenario. In the experiments of the Inguscio's group (100), they use different atomic species, more specifically the ^{87}Rb and ^{41}K, to produce a two component BEC via sympathetic cooling technique. In spite of the different traps seen by each species (different mass involved), even a small superposition of the BEC clouds brings observable effects of the interaction between them. Important results obtained by this group (100–102) relies on the high control of the intra and inter-species scattering length via Feshbach resonance technique (103).

Based on these experiments and related theory, here we considered a mixture of two superfluids and explored the possibility of trapping one very dilute superfluid species in the vortex core of the second species, with much higher density. Basically we have an array of vortices in a BEC that overlaps with another interacting superfluid component.

We studied the properties of the resulting lattice system through the Bose-Hubbard model, proposing an experiment to characterize the trapped species quantum phase transition, by scattering length tuning. A particularity of our lattice will be the presence of its own dynamics giving by the Tkachenko phonons. The effects of the lattice dynamics over the dilute species were also explored here, with the polaronic transformation of the impurity's Hamiltonian.

4.2 Phase transition in a filled Vortex Lattice

Again we consider a two component superfluid mixture, one with an Abrikosov vortex array with vorticity Ω. This quasi-$2D$ system, strong confined along the rotation axes with harmonic trap frequency ω_0 and respective oscillator length $l_0 = \sqrt{\frac{\hbar}{m\omega_0}}$, is described by the Hamiltonian $H = H_A + H_B + H_{AB}$ in Eq. (3.1). We have also a harmonic confinement in the plane of rotation $V_{ext}(\mathrm{r})$, characterized here by the frequency $\omega_\perp$.

The set of lowest Landau level states (LLL) provides a convenient description of an equilibrium rapidly rotating condensate (5). It also describes an analogous situation that is our BEC A subjected to the artificial Gauge field, as detailed in section 3.1.4. Coriolis effect provided by Ω changes the nonrotating spectrum of the original harmonic confinement. In the extreme situation $\Omega \to \omega_\perp$, those states become nearly degenerate, forming horizontal rows that originates the Landau levels. In particular, there is an energy gap $2\hbar\Omega$ between the nearly degenerate LLL and the first excited Landau level. Additionally, as Ω increases, the condensate expands radially, decreasing both the central particle density and the mean interaction energy $n_A g_A$, which thus becomes smaller than the energy gap. Since the relevant energies for BEC A particles are the gap ($2\hbar\Omega$) between adjacent Landau levels and the mean interaction energy ($n_A g_A$), we conclude that, inside the mean quantum Hall regime ($g_A n_A \ll \hbar\Omega$), the vortex array in species A is the rotational GPE solution given by a linear combination of LLL (64). That corresponds to an Abrikosov vortex Lattice described by $\psi_A(z) = \sqrt{n_A}\varphi_A(z)$, with the normalized function $\varphi_A(z) = (2\varsigma)^{1/4}\ \vartheta_1(\sqrt{\pi\varsigma}z, \rho)\ e^{z^2/2}\ e^{-|z|^2/2}$ (see section 3.1.4) that gives the triangular

configuration for the vortex singularities.

For the dilute species B ($N_B \ll N_A$), the repulsive interaction with A will promote the localization inside the vortex core position ($\mathbf{R}_i$). Adding this mean field vortex lattice trap for species B allow us to rewrite the impurity Hamiltonian in a Bose-Hubbard type model (BH) (104,105). To guarantee commensurable, unity filling of the lattice sites, we consider $N_B = N_V \ll N_A$. The small number of impurities, however, allow us to disregard the interaction effects of the dilute species over stability properties of the background vortex lattice species, kept at $T = 0$.

Now we repeat the steps of section 3.1.4 that brought us to Eq. (3.3), starting with the Bogoliubov transformation $\hat{\psi}_A = \psi_A + \delta\hat{\psi}_A$, followed by the grouping of the Hamiltonian terms in powers of $\delta\hat{\psi}_A$, as showed by Eq. (3.4). In the zero order term K_B, the density-density mean field interaction $H_{int}^{(0)} = \int d^2r\, V(\mathbf{r})\hat{\psi}_B^\dagger(\mathbf{r})\hat{\psi}_B(\mathbf{r})$ has the BEC A as an effective potential $V(\mathbf{r}) = n_A g_{AB}|\varphi_A(\mathbf{r})|^2$ without the quantum fluctuation. That potential accounts for the static lattice potential seen by the impurity species B, that is analogous to the periodic potential produced by laser beams in optical lattices (4).

Previously, when we compare the recoil energy E_r of an atom B localized in the vortex core size $\xi = \frac{\hbar}{\sqrt{2m_A g_A n_A}}$ with the lattice potential depth $V_0 = n_A g_{AB}$, we conclude that shallow lattice limit $E_r \gg V_0$ is more natural if $m_A \sim m_B$ and $g_{AB} \sim g_A$ inside the mean field quantum Hall regime. Here, however, we will establish the deep lattice limit imposing $m_B \gg m_A$. This condition gives the reduced mass $\mu \sim m_A$ and, as $a_A \sim a_B \sim a_{AB}$, that keeps the two species inside the immiscible regime $g_{AB}^2 > g_A g_B$.

Assuming the tight binding regime, we can expand the field operator of species B in terms of the Bloch wave function

$$\hat{\psi}_B(\mathbf{r}) = \sum_{\mathbf{k}} \Phi_{\mathbf{k}}(\mathbf{r})\, \hat{b}_{\mathbf{k}}, \tag{4.1}$$

where $\hat{b}_{\mathbf{k}}$ destroys a particle in a quasi-momentum state $\mathbf{k}$ and the Bloch wave function $\Phi_{\mathbf{k}}$ is the Fourier transform of the Wannier function $\Phi_{\mathbf{k}}(\mathbf{r}) = \sum_i \varphi_B(r_i)\, e^{i\mathbf{k}.\mathbf{R}_i}$ ($r_i = |\mathbf{r} - \mathbf{R}_i|$). The latter is localized in the core sites and normalized to one. Expanding the field operator as a sum of the Wannier functions in each lattice site, considering just the nearest neighbor

hopping and on-site interaction, we rewrite K_B as the Bose-Hubbard (BH) Hamiltonian (105)

$$K_B = -J \sum_{\langle i,j \rangle} \hat{b}_i^\dagger \hat{b}_j + \frac{1}{2} U \sum_i \hat{n}_i(\hat{n}_i - 1) - \mu_B \sum_i \hat{n}_i, \tag{4.2}$$

with the occupation of the site i given by the operator $\hat{n}_i = \hat{b}_i^\dagger \hat{b}_i$ ($\hat{b}_i = \sum_{\mathbf{k}} e^{i\mathbf{k}.\mathbf{R}_i} \hat{b}_{\mathbf{k}}$), while the tunneling and interaction energy constants are given, respectively, by

$$\begin{aligned} J &= \int d^2r \, \overline{\varphi}_B(r_i) \, [-\frac{\hbar^2 \nabla^2}{2m_B} + g_{AB} \, n_A \, |\varphi_A(\mathbf{r})|^2] \, \varphi_B(r_j) \\ U &= g_B \int d^2r \, |\varphi_B(r)|^4. \end{aligned} \tag{4.3}$$

According to (4), we can easily calculate U assuming a gaussian function for $\varphi_B(r)$ ($= \frac{1}{(\pi\xi^2)^{1/2}} e^{-r^2/2\xi^2}$), with width given by the site core dimension and normalization $\int d^2r \, |\varphi_B(r)|^2 = 1$. Contrary to U ($= \frac{g_B}{2} \frac{1}{\pi\xi^2}$), the expression for J can not be well defined with the gaussian ansatz for B. Instead, we should based on the solution of $1D$ Mathieu equation (106) to better characterize the tail of the Wannier function. The appropriate equation for J can be easily determined based on the results for atoms confined in a strong optical lattice, where it is given by

$$J = \frac{4}{\sqrt{\pi}} E_r \left(\frac{V_0}{E_r}\right)^{\frac{3}{4}} e^{-2\sqrt{\frac{V_0}{E_r}}}, \tag{4.4}$$

with V_0 an adjustable potential barrier controlled by the laser intensity, and the quantity $E_r = \hbar^2 k^2 / 2m$ the recoil rate fixed by laser frequency. Mapping the recoil energy and the lattice potential depth as $E_r \to \hbar^2 / 2m_B \xi^2$ and $V_0 \to n_A g_{AB}$, thus $V_0/E_r \to (m_B/m_A)(g_{AB}/g_A) = \Gamma$, and we can write Eq. (4.4) as

$$J = \frac{4}{\sqrt{\pi}} n_A g_A \frac{m_A}{m_B} \Gamma^{\frac{3}{4}} e^{-2\sqrt{\Gamma}}. \tag{4.5}$$

Also, we can determine the ratio

$$\frac{U}{J} = \frac{\sqrt{\pi}}{8} \frac{1}{\upsilon} \left(\frac{l}{\xi}\right)^2 \frac{g_B}{g_A} \frac{m_B}{m_A} \Gamma^{-\frac{3}{4}} e^{2\sqrt{\Gamma}}. \tag{4.6}$$

While in the optical lattice the ratio U/J can be modified by the laser intensity V_0, in the vortex lattice that can be tuned through the atomic scattering length a_s. An important remark is the flexibility of this vortex trap, that allow us to scan the ratio in Eq. (4.6),

independently by U or J, with intra or inter-species scattering length tuning. In the optical lattice, otherwise, we have the variation of U constrained with that of J, since we usually change the laser intensity only.

Equation (4.6) can be used to estimate the value for the Mott insulator - superfluid transition (MI-SF), that can be reached varying the scattering length. According to mean field calculation (4), the MI-SF transition for a $2D$ system is given by $(U/J)_{crit} \sim 5.8\, z_j$. Considering an Abrikosov vortex lattice, the number of nearest neighbors for this two dimensional triangular lattice configuration is $z_j = 6$. In the following we applied reasonable experimental parameters to predict the critical scattering length (a_B^{crit}) of the transition. We assumed fixed parameters g_A and g_{AB} in order to keep the lattice properties, and vary g_B to cross the critical point inside the appropriate regime. That is the simplest theoretical proposal, in spite of not be the unique experimental possibility.

For the vortex lattice we have the mean distance between the sites $l = \sqrt{\frac{\hbar}{m_A \Omega}}$ and we characterized the lattice site confinement with a core site frequency $\omega \sim \frac{\hbar}{m_B \xi^2}$, so that, in the mean field approximation (105) we have to constrain $a_B < \xi < l$ and $g_B/\xi^2 < \hbar\omega$. Both conditions guarantee that the energy scales of our system, given by the mean field interaction between the particles of B, do not overcome the Bloch bands separation, which is defined from the lattice scales of BEC A.

We assume $\Gamma \sim m_B/m_A = 20$, unit occupancy of the sites ($N_B = N_V \sim 100$) and the filling factor $\upsilon \sim 1000$. For species A we adopt the experimental parameters for ^{87}Rb clouds ($n_A = 3\ 10^8\ cm^{-2}$, $a_A = 100 a_0$ and $m_A = 1.443\, 10^{-25}$ kg), the array vorticity $\Omega = 2\pi \times 100 Hz$ and the axial confinement $\omega_0 = 2\pi \times 300 Hz$. Then, we obtain the critical atomic cross section

$$\begin{aligned} a_B^{crit(1)} &= (5.8\, z_j)\, \frac{4}{\sqrt{\pi}} \upsilon \left(\frac{\hbar\Omega}{n_A g_A}\right) \Gamma^{\frac{3}{4}}\, e^{-2\sqrt{\Gamma}}\, a_A \\ &\sim 100\, a_A. \end{aligned} \tag{4.7}$$

Let us consider now a non-adiabatic fast loading of the optical lattice. The non adiabaticity comes when the potential barrier increases faster than the particle tunneling rate in the lattice. This process generates the heating of the trapped particles (107),

since it is also fast in comparison to the interval of particles collision, do not allowing their thermal equilibration, that is, the redistribution of those particles between the final energy states of the potential. In our atomic lattice, otherwise, the dominant mechanism of particles loss is the inelastic three body collisions that occur when interaction is tuned near a Feshbach resonance (108). The advantage of varying the interaction parameter g_B, instead of the lattice properties though the inter-species or g_A interaction, is to control the particle losses, since we change the atomic properties of the low density species.

The tunability of the vortex lattice, otherwise, allows one to access a wide range of Hubbard parameters. Compared with optical lattices, for example, a small scale lattice yields significantly enhanced hopping amplitudes, which set the relevant energy scale for our Hubbard model to realize strongly correlated quantum phases. Another particularity of the vortex lattice is the intrinsic dynamic given by its normal modes, as the lowest Tkachenko modes. Hopping amplitudes and interactions can be modified by coupling the trapped atoms with the lattice phonons. This scenario will be explored next.

4.3 Vortex Lattice dynamics

Additionally to the trap mechanism, we can consider the scattering between the atoms B and the phonon excitation (Tkachenko modes) of the atomic reservoir, given by the vortex array species A. In the following, we derive the effective *polaronic* Hamiltonian that comes with the impurity-phonon interaction (109). After substituting the Bogoliubov transform for the field operator $\hat{\psi}_A$ in the system Hamiltonian, according with Eq. (3.4), the first order term in the field fluctuation $\delta\hat{\psi}_A$ gives the interaction Hamiltonian

$$H_{int}^{(1)} = g_{AB} \int d^2r \left[\delta\hat{\psi}_A^\dagger \hat{\psi}_B^\dagger \hat{\psi}_B \psi_A + \overline{\psi}_A \hat{\psi}_B^\dagger \hat{\psi}_B \delta\hat{\psi}_A\right]. \tag{4.8}$$

That can be simplified applying the solution for $\delta\hat{\psi}_A(\mathbf{r}) = \frac{1}{\sqrt{S}} \sum_{\mathbf{q}\in \mathrm{BZ}} \left[u_{\mathbf{q}}(\mathbf{r})\hat{a}_{\mathbf{q}} - v_{\mathbf{q}}(\mathbf{r})\hat{a}_{\mathbf{q}}^\dagger\right]$ that diagonalize H_A; together the expansion of $\hat{\psi}_B$ with localized Wannier functions, we

transformed Eq. (3.4) as

$$K = \sum_{\mathbf{q}} \omega_q \hat{a}^\dagger_{\mathbf{q}} \hat{a}_{\mathbf{q}} - J \sum_{\langle i,j \rangle} \hat{b}^\dagger_i \hat{b}_j + \frac{1}{2} U \sum_i \hat{n}_i(\hat{n}_i - 1)$$
$$-\mu_B \sum_i \hat{n}_i + \sqrt{n_A} g_{AB} \frac{1}{\sqrt{S}} \sum_{\mathbf{q},j} \left[\Lambda_{\mathbf{q},j} \hat{a}_{\mathbf{q}} + \Lambda^*_{\mathbf{q},j} \hat{a}^\dagger_{\mathbf{q}} \right] \hat{n}_j, \tag{4.9}$$

with J and U given by Eq. (4.3), and the last term coefficient

$$\Lambda_{\mathbf{q},j} = \int d^2 r \left[\varphi^*_A(\mathbf{r}) u_{\mathbf{q}}(\mathbf{r}) - \varphi_A(\mathbf{r}) v^*_{\mathbf{q}}(\mathbf{r}) \right] |\varphi_B(r_j)|^2. \tag{4.10}$$

Our next step will be apply an unitary transformation (46, 69, 109) in Eq. (4.9) to cancel the impurity-phonon interaction term. The latter will be incorporated in the interaction and kinetic terms of the impurity Hamiltonian, providing an effective polaronic model. We consider the unitary transformation $\tilde{K} = e^{-S} K e^{S}$, with

$$S = \frac{1}{\sqrt{S}} \sum_{\mathbf{q},j} \left[\alpha^*_{\mathbf{q},j} \, \hat{a}^\dagger_{\mathbf{q}} - \alpha_{\mathbf{q},j} \, \hat{a}_{\mathbf{q}} \right] \hat{n}_j. \tag{4.11}$$

An easily way to calculated the transformed Hamiltonian is apply the transformation separately in the impurities and phonon operators, and them replace the original operators of K. For the real space impurity operator we have

$$e^{-S} \hat{b}_i e^{S} = \hat{b}_i \hat{X}_i \rightarrow \hat{X}_i = e^{\hat{Y}_i},$$
$$e^{-S} \hat{b}^\dagger_i e^{S} = \hat{b}^\dagger_i \hat{X}^\dagger_i \rightarrow \hat{X}^\dagger_i = e^{-\hat{Y}_i}, \tag{4.12}$$

with $\hat{Y}_i = \frac{1}{\sqrt{S}} \sum_{\mathbf{q}} \left(\alpha_{\mathbf{q},i} \, \hat{a}_{\mathbf{q}} - \alpha^*_{\mathbf{q},i} \, \hat{a}^\dagger_{\mathbf{q}} \right)$. Otherwise, for the phonon operator in the momentum space we have

$$e^{-S} \hat{a}_{\mathbf{q}} e^{S} = \hat{a}_{\mathbf{q}} - \frac{1}{\sqrt{S}} \sum_i \alpha^*_{\mathbf{q},i} \, \hat{n}_i$$
$$e^{-S} \hat{a}^\dagger_{\mathbf{q}} e^{S} = \hat{a}^\dagger_{\mathbf{q}} - \frac{1}{\sqrt{S}} \sum_i \alpha_{\mathbf{q},i} \, \hat{n}_i \tag{4.13}$$

To derive the effective Bose-Hubbard model we consider $\alpha_{\mathbf{q},j} = \frac{\sqrt{n_A} g_{AB}}{\omega_q} \Lambda_{\mathbf{q},j}$ to cancel the impurity-phonon interaction in Eq. (4.9). That results in the transformed Hamiltonian

$$\tilde{K} = \sum_{\mathbf{q}} \omega_q \, \hat{a}^\dagger_{\mathbf{q}} \, \hat{a}_{\mathbf{q}} - J \sum_{\langle i,j \rangle} \hat{b}^\dagger_i \hat{X}^\dagger_i \, \hat{b}_j \hat{X}_j + \frac{1}{2} \, U \sum_i \hat{n}_i(\hat{n}_i - 1)$$
$$-\frac{1}{2} \sum_{\langle i,j \rangle} V_{i,j} \, \hat{n}_i \hat{n}_j, \tag{4.14}$$

with a non local interaction given by

$$V_{i,j} = \frac{2n_A g_{AB}^2}{S} \sum_{\mathbf{q}} \frac{\Lambda_{\mathbf{q},i}\, \Lambda^*_{\mathbf{q},j}}{\omega_q}. \tag{4.15}$$

Taking the projection of Eq. (4.14) over the phonon vacuum state we obtain the extended Bose-Hubbard model (EBH)

$$\begin{aligned} K_{eBH} = &-\tilde{J} \sum_{i,j} \hat{b}_i^\dagger\, \hat{b}_j + \frac{1}{2}\, \tilde{U} \sum_i \hat{n}_i(\hat{n}_i - 1) \\ &-\frac{1}{2} \sum_{i,j(i\neq j)} V_{i,j}\, \hat{n}_i\, \hat{n}_j - \mu_B \sum_i \hat{n}_i. \end{aligned} \tag{4.16}$$

That comes with the inclusion of the vortex array dynamics in the BH model given by Eq. (4.2). In Eq. (4.16) the renormalized values of $\tilde{U}$ and $\tilde{J}$, that is, for the interaction and tunneling parameters of species B in the presence of the phonons will be (69)

$$\begin{aligned} \tilde{J} &= J\ \langle \hat{X}_i^\dagger \hat{X}_j \rangle_{ph} = J\ \mathrm{e}^{\left[-\frac{1}{S}\sum_{\mathbf{q}} |\alpha_{\mathbf{q},0}|^2 (1 - e^{i\mathbf{q}\cdot\mathbf{l}})\right]}, \\ \tilde{U} &= U - \frac{2n_A g_{AB}^2}{S} \sum_{\mathbf{q},j} \frac{|\Lambda_{\mathbf{q},j}|^2}{\omega_q}. \end{aligned} \tag{4.17}$$

Besides that, in the last line of Eq. (4.16) we have a long range attractive potential between the impurities mediated by lattice phonons. This combination brings new aspects to the ordinary phase transition of the static lattice. In the next section, we start to analyze the expected modifications in the system phase diagram through a simple mean field approach. Further consideration for the small q regime were also made to provide analytical results.

4.4 Mean field approach to the phase diagram

Now we briefly describe a mean field approximation (110,111) that can be applied to construct the phase diagram of the EBH system ruled by Eq. (4.16). We start with the mean field approach $\hat{b}_i^\dagger\, \hat{b}_j = \langle \hat{b}_i^\dagger \rangle \hat{b}_j + \hat{b}_i^\dagger\, \langle \hat{b}_j \rangle - \langle \hat{b}_i^\dagger \rangle \langle \hat{b}_j \rangle$, where we replace the expected value of the operator by the order parameter $\langle \hat{b}_i \rangle \sim \Psi$. This procedure decouples the kinetic

term in Eq. (4.16), that is

$$K_{EBH} = -\tilde{J}z\Psi\sum_i(\hat{b}_i^\dagger + \hat{b}_i) + \tilde{J}\Psi^2 z N_V + \frac{1}{2}\tilde{U}\sum_i \hat{n}_i(\hat{n}_i - 1) - \frac{1}{2}\sum_i\left[\sum_j V_{i,j}\hat{n}_j\right]\hat{n}_i - \mu_B\sum_i \hat{n}_i. \tag{4.18}$$

We can treat the kinetic term perturbatively assuming $\tilde{J}z \ll \tilde{U}, V_{i,j}$. Then, for a particular site i we have the non perturbed Hamiltonian $H_0 = \tilde{J}\Psi^2 z + \frac{1}{2}\tilde{U}\hat{n}_i(\hat{n}_i - 1) - \frac{1}{2}\Omega_i\hat{n}_i - \mu_B\,\hat{n}_i$, with the long range interaction $\Omega_i = \sum_j V_{i,j}\hat{n}_j$ (sum take over the first neighbors j of the site i), and the perturbation $\hat{V} = -\tilde{J}z\Psi(\hat{b}_i^\dagger + \hat{b}_i)$. According with H_0, for $\tilde{U}\,(g-1) - \frac{1}{2}\Omega_i < \mu_B < \tilde{U}\,g - \frac{1}{2}\Omega_i$, the ground state energy corresponds to $E_g^{(0)} = \tilde{J}\Psi^2 z + \frac{1}{2}\tilde{U}g(g-1) - \frac{1}{2}\Omega_i g - \mu_B g$. The low energy correction (second order in Ψ) to the site energy is given by $E_g = E_g^{(0)} + E_g^{(2)}$, with $E_g^{(2)} = \sum_{n\neq g}\frac{|\langle n|\hat{V}|g\rangle|^2}{E_g^{(0)} - E_n^{(0)}}$. That gives

$$E_g(\Psi) = a_0(\tilde{U},\mu) + a_2(\tilde{U},\mu)\; z\tilde{J}\Psi^2 + \mathcal{O}(\Psi^4), \tag{4.19}$$

with $a_0 = \frac{1}{2}\tilde{U}g(g-1) - \frac{1}{2}\Omega_i g - \mu g$ and $a_2 = 1 + \frac{g}{\tilde{U}(g-1) - \frac{1}{2}\Omega_i - \mu} - \frac{g+1}{\tilde{U}g - \frac{1}{2}\Omega_i - \mu}$. Then we can apply the Landau phase transition criteria in Eq. (4.19) to determine the boundary between the superfluid $\Psi \neq 0$ and Mott insulator $\Psi = 0$ phases. Basically it is given by the μ solution that comes from the condition $a_2 = 0$. This constrain for a_2 separates the trivial ($a_2 > 0$ - Mot insulator) from the non trivial solution ($a_2 < 0$ - superfluid) for the order parameter Ψ. We obtain the limit extension for the insulate phase, that is, the Mott lobe boundaries

$$\mu_\pm = \mu_\pm^0 - \frac{1}{2}\Omega_i \tag{4.20}$$

where

$$\mu_\pm^0 = \frac{1}{2}[\tilde{U}(2n-1) - \tilde{J}z] \pm \frac{1}{2}\sqrt{\tilde{U}^2 - 2z\tilde{J}\tilde{U}(2n+1) + z^2\tilde{J}^2}. \tag{4.21}$$

That can be normalized by $\tilde{U}$ to give the phase diagram $\tilde{J}z/\tilde{U} \times \mu/\tilde{U}$. For $V_{i,j} = 0$, equation (4.20) gives the well known result for the on-site BH model. Its long range potential modifies only the Mott lobes separation, keeping their original shapes.

4.5 Analytical results for small q

As studied in section 3.1.4, for $q \ll l^{-1}$, the gapless Tkachenko modes have dispersion relation $\hbar\omega_{\mathbf{q}} \approx \hbar^2 q^2/2M$, with $M = \frac{1}{2\kappa\sqrt{\eta}}\frac{\hbar\Omega}{n_A g_A} m_A$. In this low-momentum limit we have $u_{\mathbf{q}}(\mathbf{r}) \approx \varphi_A(\mathbf{r})\, c_{1\mathbf{q}}\, e^{i\mathbf{q}\cdot\mathbf{r}}$ and $v_{\mathbf{q}}(\mathbf{r}) \approx \varphi_A(\mathbf{r})\, c_{2\mathbf{q}}\, e^{-i\mathbf{q}\cdot\mathbf{r}}$ (65), that allow us to derive explicitly coefficients for H_{int} in Eq. (4.9). Expressing the operators $\hat{b}_j$ in terms of its the fourier transform, associated with the coordinates changing $\mathbf{r} = \mathbf{r}' + \mathbf{R}_i$, remembering that $\varphi_A(\mathbf{r} + \mathbf{R}_i) = \varphi_A(\mathbf{r})$, we easily obtain

$$H_{int} = \sqrt{n_A} g_{AB} \frac{1}{\sqrt{S}} \sum_{\mathbf{q},\mathbf{k}} \Lambda_{\mathbf{q},0}\, (\hat{a}_{\mathbf{q}} + \hat{a}^{\dagger}_{-\mathbf{q}})\, \hat{b}^{\dagger}_{\mathbf{k}+\mathbf{q}} \hat{b}_{\mathbf{k}}, \tag{4.22}$$

with coefficient given by

$$\Lambda_{\mathbf{q},0} = (c_{1\mathbf{q}} - c_{2\mathbf{q}}) \int d^2 r |\varphi_A(\mathbf{r})|^2 |\varphi_B(\mathbf{r})|^2\, e^{i\mathbf{q}.\mathbf{r}}. \tag{4.23}$$

Again, the small values of $\mathbf{q}$ allow us to adopt $(c_{1q} - c_{2q}) \approx \frac{1}{\sqrt{2}}\, \eta^{1/4}\, (q\, l)$ and also $\mathcal{I}_{\mathbf{q}} = \int d^2 r |\varphi_A(\mathbf{r})|^2 |\varphi_B(\mathbf{r})|^2\, e^{i\mathbf{q}.\mathbf{r}} \sim \mathcal{I}$. In this limit, the interaction Hamiltonian can be expressed as

$$H_{int} = \frac{1}{\sqrt{S}} \sum_{\mathbf{q},\mathbf{k}} \lambda_{\mathbf{q}}\, (a_{\mathbf{q}} + a^{\dagger}_{-\mathbf{q}})\, \hat{b}^{\dagger}_{\mathbf{k}-\mathbf{q}} \hat{b}_{\mathbf{k}}, \tag{4.24}$$

where we recovered the linear momentum coupling

$$\lambda_{\mathbf{q}} = \frac{1}{\sqrt{2\pi}}\, \eta^{1/4}\, \mathcal{I}\, g_{AB}\, \upsilon^{1/2}\, q. \tag{4.25}$$

As before, applying the Lang Firsov unitary transformation (69), the new values for the interaction and tunneling parameters of the trapped species B in the presence of the phonons will be $\tilde{U} = U - 2\Delta$ and $\tilde{J} = J\, e^{-S_T}$, with $\Delta = \frac{1}{S}\sum_{\mathbf{q}} \frac{|\lambda_{\mathbf{q}}|^2}{\omega_q}$ and $S_T = \frac{1}{S}\sum_{\mathbf{q}} \frac{|\lambda_{\mathbf{q}}|^2}{\omega_q^2}[1 - cos(\mathbf{q}.\mathrm{l})]$. We can rewrite the discrete momentum sum in terms of the integration restrict to the first Brillouin zone, $\Lambda = \pi/l$. We obtain $\Delta = \frac{\pi^2}{8}\, \frac{\mathcal{I}^2}{\kappa\, \upsilon}\, n_A \left(\frac{{g_{AB}}^2}{g_A}\right)$ and, with $\cos(\mathbf{k}.\mathbf{l}) \sim 1 - (q\, l\, cos\phi)^2/2$, $S_T = \frac{\pi^2}{32}\, \frac{\mathcal{I}^2}{\sqrt{\eta}\, \kappa^2\, \upsilon} \left(\frac{g_{AB}}{g_A}\right)^2$.

Assuming the same experimental parameters of the previous section, we found a small correction in the value for critical scattering length, that is now given by

$$a_B^{crit(2)} \sim 90\, a_A. \tag{4.26}$$

In the previous section we classified the possible phases of our system imposing the appropriate restriction to the order parameter (111), which gave Eq. (4.20) with $\Omega_i \sim z\Delta$ (the interaction in Eq. (4.15) should be of the order of Δ). Many works suggest adding long range interaction between particles in the optical lattice by trapping strong magnetic dipolar condensates, or even with the electric dipole-dipole interaction of a degenerated gas of polar molecules (112–114) . There is a recent proposal (115), however, that is closer related to the EBH scenario constructed here. It consists of a system of boson in an optical lattice immersed in a non trapped, degenerate Fermi gas. The particle-hole pair excitations of the fermion background mediate the long range interaction between the trapped bosons. Compared to the dipole-dipole interaction proposals, either in the Spielman's experimental apparatus (115) as in our system, we have a higher control of the long range interaction due to the Feshbach resonance technique.

We can separately tuning the intra or the inter-species scattering length and try to increase the magnitude of the long range interaction in comparison to the intra-species interaction potential U, for example, to experimentally detect the manifestation of the first in the system phase diagram. As showed by (116), with the $2D$ layer lattice of aligned dipoles, the repulsive long range interaction provides a rich phase diagram for the trapped system, with the appearance of the supersolid and density wave phases (111). The repulsive long range interaction can be created in (115) with different hyperfine states of the atomic sample. Even with an attractive long range interaction, however, our system is still a promising candidate to observe new quantum phases (116).

4.6 Conclusion

Important aspects of our investigation here is that it follows a new trend in cold atoms field, that is introduce artificially dynamics in the static optical lattice to better simulate condensate matter models (46,47,67,117). With our system we give an alternative solution for this task, where the dynamic comes naturally with the system excitation modes. The main result here is the polaronic Bose-Hubbard effective Hamiltonian, that

predicted new transport and interaction properties for the lattice impurities, including the long range phonon mediated interaction. That provides rich quantum phase diagram for the trapped species (61, 112, 113). Again, to attain these phases, the ultracold atoms in optical lattice have been intensively explored, with many proposals for finite range interaction to create extended Bose-Hubbard models (112, 116, 118). Our new system is still a promising candidate to realize these observations, with the high control of the system properties to reach the necessary conditions and the noise correlation techniques available to guarantee experimental observability of the quantum phases (119).

5 Conclusions

5.1 Turbulent superfluid

We presented a simple model that seems to capture the main physical mechanism behind the intriguing anomalous free expansion of the turbulent cloud. Our model shows that the behavior of the expansion depends intrinsically on the amount and distribution of vorticity present in the sample. Although very phenomenological in nature, this model already gives a clear indication that a disordered volumetric distribution of vortex lines can greatly affect the dynamics of the density profile in time-of-flight.

It is clear that an elaborate numerical simulation of the turbulent regime, including the vortex dynamics and possibly reconnection effects, will be needed to complement our results and fully account for the experimental observations. We do not believe, however, that these considerations greatly affect the behavior of the expanding cloud, which is a very diluted atomic sample with slowed down vortex line dynamics. Our prediction for the collective modes frequency of a cloud plenty of vortices, otherwise, has to be enforced by the numerical simulations, an important step to validate our hydrodynamic model description for a non equilibrium superfluid state. These modes properties should bring an additional signature of turbulence in the atomic cloud.

5.2 Polaron physics

We derived an effective impurity-phonon model to treat an impurity moving in a vortex lattice. At weak coupling, the dressed impurity, that is, the Tkachenko polaron, presented an unconventional quasiparticle decay rate at small wave vectors. That comes from our renormalizable theory with a marginally relevant interaction. In conclusion, we have shown that impurities are strongly damped due to coupling with parabolic dispersion vortex lattice collective modes. Different from the case of acoustic phonons in a homoge-

neous BEC, this quadratic dispersion of the Tkachenko modes allows one to circumvent the kinematic constraints that hinder cooling (47).

We tracked the impurity spectral function as function of the background coupling interaction toward the low energy fixed point, where it acquires the power law signature of the orthogonality catastrophe. That is a remarkable property long time predicted for degenerate fermionic systems (pair hole excitations of the Fermi sea background), that is now extended to our bosonic, Tkachenko phonons background. Interesting features of our system include the impurity dynamics, that smooth the OC singularity exponent. It makes it possible to study the spectral function evolution as the polaron properties approach the static impurity physics, with increasing ratio m/M. With our apparatus, we can also realize some experimental proposal not possible with an optical lattice due to the intrinsic heating coming from the recoil energy of the trapped atom (classical magnetism frustration in triangular lattice (120), short range magnetic correlations (121, 122)). The deep understanding of the effects of a single neutral impurity in a vortex lattice background open the way to analyze interesting physics of the multiple impurities interacting with this same background (109, 123), as we started exploring in section 4.

5.3 Prospects

In the last year our group reproduced the quantum turbulent BEC experiments of the 2009 and obtained new absorption images for the excited cloud expansion, varying the amplitude and time of the excitation potential inside the trap. They showed how the aspect-ratio inversion starts to decelerate until its complete inhibition, even prior to the appearance of the vortex line configuration, already with the excitation of the BEC collective modes. That sounds reasonable, according with the generalized hydrodynamic results, since the transference of angular momentum to the BEC cloud (already with the excitation of the collective modes), increases the rotational kinetic energy of the system. The tangle vortices configuration, final state resulting from this excitation, being the limit case that brings the aspect-ratio asymptotic value lower than one. The relation between

the excited BEC system and its aspect-ratio evolution during the free expansion allow us to characterize the amplitude and time of the excitation with the number of vortices imprinted in the BEC cloud. These analyses could improve the phase diagram constructed in (124), that was based on the absorption image density profile only.
Since we are dealing with a finite trapped BEC system, those analyses help us to predict the maxima vortex line density possible to be establish in the cloud before the turbulent regime appears. Recently, we are working on our experimental data to understand how the appearance of the first vortex lines affect the collective mode frequencies, comparing this observations with the results predicted by our linearized hydrodynamic equations.

About the project of the two superfluids species, we will keep on exploring a dilute sample of ultracold neutral atoms trapped in a vortex array condensate. We started showing here that impurity properties resulted from the interplay of Bose-Hubbard dynamics and the lattice phonons coupling. In addition, using a mean field approach to perturbatively treat the kinetic term, in accordance with the usual strength of the atomic interactions, we determined the ground state phase diagram of the system in the presence of the long range phonon mediated interaction. A more rigorous analyses including the Monte Carlo calculation (109, 125) will be needed to determine the system phase diagram, for the theory parameters inside the management window of the experiments. As described in the last section, new quantum phases are expected for the particles trapped in our dynamic vortex lattice due to the induced long range attractive interaction, besides the superfluid and Mott-insulate states.
Finally, the possibility of tuning the inter-species scattering length to induce quantum phase transition in the confined cloud, as it is done in the optical lattice by light intensity, it will be further explored in a next work, followed by a criteriously analyze of the associated particle loss mechanism.

References

1 KAPTIZA, P. Viscosity of liquid Helium below the λ-point. *Nature*, v. 141, p. 74, 1938.

2 TILLEY, D. R.; TILLEY, J. *Superfluidity and superconductivity*, 3rd ed. New York: IOP Publishing Ltd., 1990.

3 DALFOVO, F. et al. Theory of Bose-Einstein condensation in trapped gases. *Reviews of Modern Physics*, v. 71, p. 463–512, 1999.

4 BLOCH, I.; DALIBARD, J.; ZWERGER, W. Many-body physics with ultracold gases. *Reviews of Modern Physics*, v. 80, p. 885–964, 2008.

5 FETTER, A. L. Rotating trapped Bose-Einstein condensates. *Reviews of Modern Physics*, v. 81, p. 647–691, 2009.

6 PITAEVSKII, L.; STRINGARI, S. *Bose-Einstein condensation*, Oxford: Oxford University Press, 2003.

7 PETHICK, C.; SMITH, H. *Bose-Einstein condensation in dilute gases*, 2nd ed. Cambridge: Cambridge University Press, 2008.

8 PROUKAKIS, N. P.; JACKSON, B. Finite-temperature models of Bose-Einstein condensation. *Journal of Physics B: atomic, molecular and optical physics*, v. 41, p. 203002, 2008.

9 BERLOFF, N. G.; SVISTUNOV, B. V. Scenario of strongly nonequilibrated Bose-Einstein condensation. *Physical Review A*, v. 66, p. 013603, 2002.

10 KOBAYASHI, M.; TSUBOTA, M. Quantum turbulence in a trapped Bose-Einstein condensate. *Physical Review A*, v. 76, p. 045603, 2007.

11 DALIBARD, J. et al. Artificial gauge potentials for neutral atoms. *Reviews of Modern Physics*, v. 83, p. 1523–1543, 2011.

12 BAGNATO, V.; PRITCHARD, D. E.; KLEPPNER, D. Bose-Einstein condensation in an external potential. *Physical Review A*, v. 35, p. 4354–4358, 1987.

13 LEGGETT, A. J. *Quantum liquids: Bose condensation and Cooper pairing in condensed matter systems*, Oxford: Oxford University Press, 2006.

14 NOZIERES, P.; PINES, D. *Theory of quantum liquids: superfluid Bose liquids*, New York: Westview Press, 1994.

15 PITAEVSKII, L. P. Vortex lines in an imperfect Bose gas. *Journal of Experimental and Theoretical Physics*, v. 40, p. 646, 1961.

16 GROSS, E. P. Hydrodynamics of a superfluid condensate. *Journal of Mathematical Physics*, v. 4, p. 195, 1963.

17 ALTLAND, A.; SIMONS, B. *Condensed matter field theory*, 2nd ed. Cambridge: Cambridge University Press, 2010.

18 VINEN, W. F. Mutual friction in a heat current in liquid Helium II. *Proceedings of the Royal Society of London A.*, v. 243, p. 400–413, 1958.

19 FEYNMAN, R. Application of quantum mechanics to liquid Helium. *Progress in Low Temperature Physics*, v. 1, p. 17–53, 1955.

20 HENN, E. A. L. et al. Observation of vortex formation in an oscillating trapped Bose–Einstein condensate. *Physical Review A*, v. 79, p. 043618, 2009.

21 HENN, E. A. L. et al. Emergence of turbulence in an oscillating Bose–Einstein Condensate. *Physical Review Letters*, v. 103, p. 045301, 2009.

22 WHITE, A. C.; ANDERSON, B. P.; BAGNATO, V. S. Vortices and turbulence in trapped atomic condensates. *Proceedings of the National Academy of Sciences*, v. 111, p. 4719–4726, 2014.

23 ZUCCHER, S. et al. Quantum vortex reconnections. *Physics of fluids*, v. 24, p. 125108, 2012.

24 NOWAK, B.; SEXTY, D.; GASENZER, T. Superfluid turbulence: nonthermal fixed point in an ultracold Bose gas. *Physical Review B*, v. 84, p. 020506, 2011.

25 BAGGALEY, A. W.; BARENGHI, C. F. Quantum turbulent velocity statistics and quasiclassical limit. *Physical Review E*, v. 84, p. 067301, 2011.

26 BRADLEY, A. S.; ANDERSON, B. P. Energy spectra of vortex distributions in two-dimensional quantum turbulence. *Physical Review X*, v. 2, p. 041001, 2012.

27 WHITE, A. C. et al. Nonclassical velocity statistics in a turbulent atomic Bose-Einstein condensate. *Physical Review Letters*, v. 104, p. 075301, 2010.

28 HENN, E. A. L. et al. Bose-Einstein condensation in ^{87}Rb: characterization of the Brazilian experiment. *Brazilian Journal of Physics*, v. 38, p. 279–286, 2008.

29 CARACANHAS, M. et al. Self-similar expansion of the density profile in a turbulent Bose-Einstein condensate. *Journal of Low Temperature Physics*, v. 166, p. 49–58, 2012.

30 CARACANHAS, M. et al. Self-similar expansion of a turbulent Bose-Einstein condensate: a generalized hydrodynamic model. *Journal of Low Temperature Physics*, v. 170, p. 133–142, 2013.

31 COZZINI, M.; STRINGARI, S. Macroscopic dynamics of a Bose-Einstein condensate containing a vortex lattice. *Physical Review A*, v. 67, p. 041602, 2003.

32 STRINGARI, S. Collective excitations of a trapped Bose-condensed gas. *Physical Review Letters*, v. 77, p. 2360–2363, 1996.

33 PEREZ-GARCIA, V. M. et al. Low energy excitations of a Bose-Einstein condensate: a time-dependent variational analysis. *Physical Review Letters*, v. 77, p. 5320–5323, 1996.

34 ALEXANDROV, A. S.; DEVREESE, J. T. *Advances in polaron physics*, New York: Springer, 2010. (Springer Series in Solid–State Sciences, v. 159).

35 MANNELLA, N. et al. Nodal quasiparticle in pseudogapped colossal magnetoresistive manganites. *Nature*, v. 438, p. 474–478, 2005.

36 LEE PATRICK A.; NAGAOSA, N.; WEN, X.-G. Doping a Mott insulator: physics of high-temperature superconductivity. *Reviews of Modern Physics*, v. 78, p. 17–85, 2006.

37 KONDO, J. Resistance minimum in dilute magnetic alloys. *Progress of Theoretical Physics*, v. 32, p. 37, 1964.

38 LANDAU, L. Electron motion in crystal lattices. *Physikalische Zeitschrift der Sowjetunion*, v. 3, p. 664, 1933.

39 PEKAR, S. Local quantum states of an electron in an ideal ionic crystal. *Journal of Experimental and Theoretical Physics*, v. 16, p. 341, 1946.

40 WHITFIELD, G. D.; KUPER, C. G. *Polarons and excitons : Scottish universities' summer school 1962*, London: London Academic Press, 1963.

41 FEYNMAN, R. P.; COHEN, M. Energy spectrum of the excitations in liquid Helium. *Physical Review*, v. 102, p. 1189–1204, 1956.

42 SCHIROTZEK, A. et al. Observation of Fermi polarons in a tunable Fermi liquid of ultracold atoms. *Physical Review Letters*, v. 102, p. 230402, 2009.

43 KOHSTALL, C. et al. Metastability and coherence of repulsive polarons in a strongly interacting Fermi mixture. *Nature*, v. 485, p. 615–618, 2012.

44 MASSIGNAN, P.; ZACCANTI, M.; BRUUN, G. M. Polarons, dressed molecules and itinerant ferromagnetism in ultracold Fermi gases. *Reports on Progress in Physics*, v. 77, p. 034401, 2014.

45 SHASHI, A. et al. *Radio frequency spectroscopy of polarons in ultracold Bose gases. Disponível em: < http://arxiv.org/pdf/1401.0952v1.pdf > - Acesso em: 15 abr. 2014.*

46 BRUDERER, M. et al. Polaron physics in optical lattices. *Physical Review A*, v. 76, p. 011605, 2007.

47 GRIESSNER, A. et al. Dissipative dynamics of atomic Hubbard models coupled to a phonon bath. *New Journal of Physics*, v. 9, p. 44, 2007.

48 ABO-SHAEER, J. R. et al. Observation of vortex lattices in Bose-Einstein condensates. *Science*, v. 292, p. 476–479, 2001.

49 CODDINGTON, I. et al. Observation of Tkachenko oscillations in rapidly rotating Bose-Einstein condensates. *Physical Review Letters*, v. 91, p. 100402, 2003.

50 SONIN, E. B. Vortex oscillations and hydrodynamics of rotating superfluids. *Reviews of Modern Physics*, v. 59, p. 87–155, 1987.

51 BAYM, G. Tkachenko modes of vortex lattices in rapidly rotating Bose-Einstein condensates. *Physical Review Letters*, v. 91, p. 110402, 2003.

52 SONIN, E. B. Continuum theory of Tkachenko modes in rotating Bose-Einstein condensate. *Physical Review A*, v. 71, p. 011603, 2005.

53 SCHWEIKHARD, V. et al. Rapidly rotating Bose-Einstein condensates in and near the lowest Landau level. *Physical Review Letters*, v. 92, p. 040404, 2004.

54 BRETIN V.; STOCK, S. S. Y.; DALIBARD, J. *Fast rotation of an ultracold Bose gas. Disponível em: < http://arxiv.org/abs/cond-mat/0307464 >. Acesso em: 15 abr. 2014.*

55 TKACHENKO, V. K. Stability of vortex lattices. *Journal of Experimental and Theoretical Physics*, v. 50, p. 1573–1585, 1966.

56 TKACHENKO, V. K. Elasticity of vortex lattices. *Journal of Experimental and Theoretical Physics*, v. 56, p. 1763–1765, 1969.

57 SINOVA, J.; HANNA, C. B.; MACDONALD, A. H. Quantum melting and absence of Bose-Einstein condensation in two-dimensional vortex matter. *Physical Review Letters*, v. 89, p. 030403, 2002.

58 BAYM, G. Vortex lattices in rapidly rotating Bose-Einstein condensates: modes and correlation functions. *Physical Review A*, v. 69, p. 043618, 2004.

59 NIELSEN, H.; CHADHA, S. On how to count Goldstone bosons. *Nuclear Physics B*, v. 105, p. 445 – 453, 1976.

60 LIN, Y. et al. Synthetic magnetic fields for ultracold neutral atoms. *Nature*, v. 462, p. 628–632, 2009.

61 SPIELMAN, I. B. Raman processes and effective gauge potentials. *Physical Review A*, v. 79, p. 063613, 2009.

62 HO, T.-L. Bose-Einstein condensates with large number of vortices. *Physical Review Letters*, v. 87, p. 060403, 2001.

63 MUELLER, E. J.; HO, T.-L. Two-component Bose-Einstein condensates with a large number of vortices. *Physical Review Letters*, v. 88, p. 180403, 2002.

64 MATVEENKO, S. I. et al. Vortex structures in rotating Bose-Einstein condensates. *Physical Review A*, v. 80, p. 063621, 2009.

65 MATVEENKO, S. I.; SHLYAPNIKOV, G. V. Tkachenko modes and their damping in the vortex lattice regime of rapidly rotating bosons. *Physical Review A*, v. 83, p. 033604, 2011.

66 DEVREESE, J. T.; ALEXANDROV, A. S. Frohlich polaron and bipolaron: recent developments. *Reports on Progress in Physics*, v. 72, p. 066501, 2009.

67 HERRERA, F. et al. Investigating polaron transitions with polar molecules. *Physical Review Letters*, v. 110, p. 223002, 2013.

68 CARACANHAS, M. A.; BAGNATO, V. S.; PEREIRA, R. G. Tkachenko polarons in vortex lattices. *Physical Review Letters*, v. 111, p. 115304, 2013.

69 MAHAN, G. D. *Many-particle physics*, 3rd ed. New York: Plenum, 2000.

70 LANDAU, L. Theory of Fermi-liquids. *Journal of Experimental and Theoretical Physics*, v. 30, p. 1058, 1956.

71 SHANKAR, R. Renormalization-group approach to interacting fermions. *Reviews of Modern Physics*, v. 66, p. 129–192, 1994.

72 FRADKIN, E. *Field theories of condensed matter physics*, 2nd ed. Cambridge: Cambridge University Press, 2013.

73 GONZÁLEZ, J.; GUINEA, F.; VOZMEDIANO, M. A. H. Unconventional quasiparticle lifetime in graphite. *Physical Review Letters*, v. 77, p. 3589–3592, 1996.

74 LI, Z.; CHANDLER, C. J.; MARSIGLIO, F. Perturbation theory of the mass enhancement for a polaron coupled to acoustic phonons. *Physical Review B*, v. 83, p. 045104, 2011.

75 LANDAU, L. Oscillations in a Fermi-liquid. *Journal of Experimental and Theoretical Physics*, v. 32, p. 59, 1957.

76 ANDERSON, P. W. Infrared catastrophe in fermi gases with local scattering potentials. *Physical Review Letters*, v. 18, p. 1049–1051, 1967.

77 MAHAN, G. D. Excitons in metals: infinite hole mass. *Physical Review*, v. 163, p. 612–617, 1967.

78 VARMA, C.; NUSSINOV, Z.; SAARLOOS, W. van. Singular or non-Fermi liquids. *Physics Reports*, v. 361, p. 267 – 417, 2002.

79 KNAP, M. et al. Time-dependent impurity in ultracold fermions: orthogonality catastrophe and beyond. *Physical Review X*, v. 2, p. 041020, 2012.

80 REFAEL, G.; DEMLER, E. Superfluid-insulator transition in Fermi-Bose mixtures and the orthogonality catastrophe. *Physical Review B*, v. 77, p. 144511, 2008.

81 GOOLD, J. et al. Orthogonality catastrophe as a consequence of qubit embedding in an ultracold Fermi gas. *Physical Review A*, v. 84, p. 063632, 2011.

82 GAVORET, J. et al. Optical absorption in degenerate semiconductors. *Le Journal de Physique*, v. 30, p. 987–997, 1969.

83 NOZIÈRES, P.; DOMINICIS, C. T. D. Singularities in the x-ray absorption and emission of metals III. one-body theory exact solution. *Physical Review*, v. 178, p. 1097–1107, 1969.

84 NOZIERES, P. The effect of recoil on edge singularities. *Journal de Physique I*, v. 4, p. 1275, 1994.

85 GOGOLIN, A. O.; NERSESYAN, A. A.; TSVELIK, A. M. *Bosonization and strongly correlated system*, Cambridge: Cambridge University Press, 1998.

86 KOSTERLITZ, J.; THOULESS, D. Ordering, metastability and phase transitions in two-dimensional systems. *Journal of Physics C*, v. 6, p. 1181, 1973.

87 ANDERSON, P. A poor man's derivation of scaling laws for the Kondo problem. *Journal of Physics C*, v. 3, p. 2436, 1970.

88 GIAMARCHI, T. et al. Singular low energy properties of an impurity model with finite range interactions. *Physical Review Letters*, v. 70, p. 3967–3970, 1993.

89 CUCCHIETTI, F. M.; TIMMERMANS, E. Strong-coupling polarons in dilute gas Bose-Einstein condensates. *Physical Review Letters*, v. 96, p. 210401, 2006.

90 AGARWAL, K. et al. Polaronic model of two-level systems in amorphous solids. *Physical Review B*, v. 87, p. 144201, 2013.

91 LEE, T. D.; LOW, F. E.; PINES, D. The motion of slow electrons in a polar crystal. *Physical Review*, v. 90, p. 297, 1953.

92 STEWART, J. T.; GAEBLER, J. P.; JIN, D. S. Using photoemission spectroscopy to probe a strongly interacting Fermi gas. *Nature*, v. 454, p. 744–747, 2008.

93 MYATT, C. J. et al. Production of two overlapping Bose-Einstein condensates by sympathetic cooling. *Physical Review Letters*, v. 78, p. 586–589, 1997.

94 MATTHEWS, M. R. et al. Dynamical response of a Bose-Einstein condensate to a discontinuous change in internal state. *Physical Review Letters*, v. 81, p. 243–247, 1998.

95 HALL, D. S. et al. Dynamics of component separation in a binary mixture of Bose-Einstein condensates. *Physical Review Letters*, v. 81, p. 1539–1542, 1998.

96 HALL, D. S. et al. Measurements of relative phase in two-component Bose-Einstein condensates. *Physical Review Letters*, v. 81, p. 1543–1546, 1998.

97 MATTHEWS, M. R. et al. Watching a superfluid untwist Itself: recurrence of Rabi oscillations in a Bose - Einstein condensate. *Physical Review Letters*, v. 83, p. 3358–3361, 1999.

98 MATTHEWS, M. R. et al. Vortices in a Bose-Einstein condensate. *Physical Review Letters*, v. 83, p. 2498–2501, 1999.

99 SCHWEIKHARD, V. et al. Vortex-lattice dynamics in rotating spinor Bose-Einstein condensates. *Physical Review Letters*, v. 93, p. 210403, 2004.

100 MODUGNO, G. et al. Two atomic species superfluid. *Physical Review Letters*, v. 89, p. 190404, 2002.

101 CATANI, J. et al. Degenerate Bose-Bose mixture in a three-dimensional optical lattice. *Physical Review A*, v. 77, p. 011603, 2008.

102 CATANI, J. et al. Entropy exchange in a mixture of ultracold atoms. *Physical Review Letters*, v. 103, p. 140401, 2009.

103 THALHAMMER, G. et al. Double species Bose-Einstein condensate with tunable interspecies interactions. *Physical Review Letters*, v. 100, p. 210402, 2008.

104 FISHER, M. P. A. et al. Boson localization and the superfluid-insulator transition. *Physical Review B*, v. 40, p. 546–570, 1989.

105 JAKSCH, D. et al. Cold bosonic atoms in optical lattices. *Physical Review Letters*, v. 81, p. 3108–3111, 1998.

106 ZWERGER, W. Mott–Hubbard transition of cold atoms in optical lattices. *Journal of Optics B: quantum and semiclassical optics*, v. 5, p. S9, 2003.

107 BLAKIE, P. B.; PORTO, J. V. Adiabatic loading of bosons into optical lattices. *Physical Review A*, v. 69, p. 013603, 2004.

108 STENGER, J. et al. Strongly enhanced inelastic collisions in a Bose-Einstein condensate near Feshbach resonances. *Physical Review Letters*, v. 82, p. 2422–2425, 1999.

109 BENJAMIN, D.; DEMLER, E. *Variational polaron method for Bose-Bose mixtures. Disponível em: < http://arxiv.org/pdf/1401.0311v1.pdf> - Acesso em: 02 jul. 2014.*

110 OOSTEN, D. van; STRATEN, P. van der; STOOF, H. T. C. Quantum phases in an optical lattice. *Physical Review A*, v. 63, p. 053601, 2001.

111 ISKIN, M.; FREERICKS, J. K. Strong-coupling perturbation theory for the extended Bose-Hubbard model. *Physical Review A*, v. 79, p. 053634, 2009.

112 GÓRAL, K.; SANTOS, L.; LEWENSTEIN, M. Quantum phases of dipolar bosons in optical lattices. *Physical Review Letters*, v. 88, p. 170406, 2002.

113 YI, S.; LI, T.; SUN, C. P. Novel quantum phases of dipolar Bose gases in optical lattices. *Physical Review Letters*, v. 98, p. 260405, 2007.

114 PUPILLO, G. et al. Cold atoms and molecules in self-assembled dipolar lattices. *Physical Review Letters*, v. 100, p. 050402, 2008.

115 DE, S.; SPIELMAN, I. Fermion-mediated long-range interactions between bosons stored in an optical lattice. *Applied Physics B*, v. 114, p. 527–536, 2014.

116 TREFZGER, C.; MENOTTI, C.; LEWENSTEIN, M. Pair-supersolid phase in a bilayer system of dipolar lattice bosons. *Physical Review Letters*, v. 103, p. 035304, 2009.

117 GRIESSNER, A. et al. Dark-state cooling of atoms by superfluid immersion. *Physical Review Letters*, v. 97, p. 220403, 2006.

118 SCAROLA, V. W.; SARMA, S. D. Quantum phases of the extended Bose-Hubbard Hamiltonian: possibility of a supersolid state of cold atoms in optical lattices. *Physical Review Letters*, v. 95, p. 033003, 2005.

119 SCAROLA, V. W.; DEMLER, E.; SARMA, S. D. Searching for a supersolid in cold-atom optical lattices. *Physical Review A*, v. 73, p. 051601, 2006.

120 STRUCK, J. et al. Quantum simulation of frustrated classical magnetism in triangular optical lattices. *Science*, v. 333, p. 996–999, 2011.

121 TROTZKY, S. et al. Time-resolved observation and control of superexchange interactions with ultracold atoms in optical lattices. *Science*, v. 319, p. 295–299, 2008.

122 GREIF, D. et al. Short-range quantum magnetism of ultracold fermions in an optical lattice. *Science*, v. 340, p. 1307–1310, 2013.

123 CASTEELS, W.; TEMPERE, J.; DEVREESE, J. T. Many-polaron description of impurities in a Bose-Einstein condensate in the weak-coupling regime. *Physical Review A*, v. 84, p. 063612, 2011.

124 SEMAN, J. A. et al. Route to turbulence in a trapped Bose-Einstein condensate. *Laser Physics Letters*, v. 8, p. 691, 2011.

125 GUGLIELMINO, M.; PENNA, V.; CAPOGROSSO-SANSONE, B. Mott-insulator–to–superfluid transition in Bose-Bose mixtures in a two-dimensional lattice. *Physical Review A*, v. 82, p. 021601, 2010.

Appendix

APPENDIX A –

A.1 Impurity-phonon interaction for shallow lattice potential

In the following we set $\hbar = 1$. When we substitute the expansion for the field operator $\hat{\psi}_A(\mathbf{r}) \approx \sqrt{n_A}\varphi_A(\mathbf{r}) + \delta\hat{\psi}_A(\mathbf{r})$ in H_{int} in Eq. (3.1) of the main text, the first-order term in the fluctuation $\delta\hat{\psi}_A$ gives the impurity-phonon interaction

$$H_{imp-ph} = \sqrt{n_A} g_{AB} \int d^2r \left(\varphi_A \delta\hat{\psi}_A^\dagger \hat{\psi}_B^\dagger \hat{\psi}_B + \varphi_A^* \delta\hat{\psi}_A \hat{\psi}_B^\dagger \hat{\psi}_B \right). \tag{A.1}$$

For $\delta\hat{\psi}_A$, we utilize the mode expansion in Eq. (3.2) of the main text. The functions $u_{\mathbf{q}}(\mathbf{r})$ and $v_{\mathbf{q}}(\mathbf{r})$ are obtained following the derivation by Matveenko and Shlyapnikov (65). We take the continuum limit $ql \ll 1$ in Eqs. (22), (23) and (27) of Ref. (65), which leads to the simplified spatial dependence $u_{\mathbf{q}}(\mathbf{r}), v_{\mathbf{q}}(\mathbf{r}) \propto \varphi_A(\mathbf{r})$. In addition, we rescale the momentum $\mathbf{q} \to 2\mathbf{q}$ in the definition of the annihilation operators $a_{\mathbf{q}} = \tilde{a}_{2\mathbf{q}}$. We then obtain

$$H_{imp-ph} = \frac{g_{AB}\sqrt{n_A}}{\sqrt{\mathcal{S}}} \sum_{\mathbf{q}} \int d^2r \, |\varphi_A(\mathbf{r})|^2 \, e^{i\,\mathbf{q}.\mathbf{r}} \, (c_{1\mathbf{q}} - c_{2\mathbf{q}}) \, (a_{\mathbf{q}} + a_{-\mathbf{q}}^\dagger) \, \hat{\psi}_B^\dagger(\mathbf{r}) \, \hat{\psi}_B(\mathbf{r}). \tag{A.2}$$

We expand the field operator $\hat{\psi}_B$ in terms of the lowest band Bloch function $\Phi_{\mathbf{k}}(\mathbf{r})$, which obeys $\Phi_{\mathbf{k}}(\mathbf{r}+\mathbf{R}) = \Phi_{\mathbf{k}}(\mathbf{r}) e^{i\mathbf{k}\cdot\mathbf{R}}$. Thus

$$H_{imp-ph} = \frac{g_{AB}\sqrt{n_A}}{\mathcal{S}^{3/2}} \sum_{\mathbf{q},\mathbf{k},\mathbf{k}'} (c_{1\mathbf{q}} - c_{2\mathbf{q}}) \, (a_{\mathbf{q}} + a_{-\mathbf{q}}^\dagger) \int d^2r \, |\varphi_A(\mathbf{r})|^2 \, e^{i\mathbf{q}\cdot\mathbf{r}} \Phi_{\mathbf{k}'}^*(\mathbf{r}) \Phi_{\mathbf{k}}(\mathbf{r}). \tag{A.3}$$

Next, we use the facts that the local density of majority atoms $|\varphi_A(\mathbf{r})|^2$ is periodic under lattice translations and that $\Phi_{\mathbf{k}}(\mathbf{r})$ is a Bloch function in order to reduce the integral over the entire system to the integral over a single unit cell s_V

$$\begin{aligned}
&\int d^2r \, |\varphi_A(\mathbf{r})|^2 \, e^{i(\mathbf{k}+\mathbf{q}-\mathbf{k}')\cdot\mathbf{r}} \Phi_{\mathbf{k}'}^*(\mathbf{r}) \Phi_{\mathbf{k}}(\mathbf{r}) = \\
&= \sum_j \int_{s_V} d^2r' \, |\varphi_A(\mathbf{r}' + \mathbf{R}_j)|^2 \, e^{i\mathbf{q}\cdot(\mathbf{r}'+\mathbf{R}_j)} \Phi_{\mathbf{k}'}^*(\mathbf{r}' + \mathbf{R}_j) \Phi_{\mathbf{k}}(\mathbf{r}' + \mathbf{R}_j) \\
&= \int_{s_V} d^2r' \, |\varphi_A(\mathbf{r}')|^2 \, e^{i\mathbf{q}\cdot\mathbf{r}'} \Phi_{\mathbf{k}'}^*(\mathbf{r}') \Phi_{\mathbf{k}}(\mathbf{r}') \sum_j e^{i(\mathbf{k}+\mathbf{q}-\mathbf{k}')\cdot\mathbf{R}_j} \\
&= N_V \delta_{\mathbf{k}',\mathbf{k}+\mathbf{q}} \int_{s_V} d^2r' \, |\varphi_A(\mathbf{r}')|^2 e^{i\mathbf{q}\cdot\mathbf{r}'} \Phi_{\mathbf{k}+\mathbf{q}}^*(\mathbf{r}') \Phi_{\mathbf{k}}(\mathbf{r}').
\end{aligned} \tag{A.4}$$

Thus we can rewrite Eq. (A.3) as

$$H_{imp-ph} = \frac{g_{AB}\sqrt{n_A}}{\sqrt{\mathcal{S}}} \sum_{\mathbf{k},\mathbf{q}} \mathcal{I}_{\mathbf{k},\mathbf{q}} \left(c_{1\mathbf{q}} - c_{2\mathbf{q}}\right) \left(a_{\mathbf{q}} + a^{\dagger}_{-\mathbf{q}}\right) b^{\dagger}_{\mathbf{k}+\mathbf{q}}\, b_{\mathbf{k}}, \tag{A.5}$$

where (using $N_V/\mathcal{S} = 1/\pi l^2$)

$$\mathcal{I}_{\mathbf{k},\mathbf{q}} = \int_{s_V} \frac{d^2 r'}{\pi l^2} \left|\varphi_A(\mathbf{r}')\right|^2 e^{i\mathbf{q}\cdot\mathbf{r}'} \Phi^{*}_{\mathbf{k}+\mathbf{q}}(\mathbf{r}') \Phi_{\mathbf{k}}(\mathbf{r}'). \tag{A.6}$$

In the regime of weak interactions and shallow lattice potential, we approximate the Bloch functions for small $\mathbf{k}$ by plane waves (nearly free impurities), $\Phi_k(\mathbf{r}) \approx e^{i\mathbf{k}\cdot\mathbf{r}}$. In this case,

$$\mathcal{I}_{\mathbf{k},\mathbf{q}} \approx \int_{s_V} \frac{d^2 r'}{\pi l^2} \left|\varphi_A(\mathbf{r}')\right|^2 = 1, \tag{A.7}$$

where we used the normalization of the ground state wave function $n_A \int d^2 r \left|\varphi_A(\mathbf{r})\right|^2 = N_A$. Therefore the dependence on impurity momentum $\mathbf{k}$ disappears in the continuum limit. Corrections to Eq. (A.7) are higher order in momentum or interaction strength.

Finally, the expansion $c_{1\mathbf{q}} - c_{2\mathbf{q}} \approx \frac{1}{\sqrt{2}}\, \eta^{1/4}\, (q\, l)$ for $ql \ll 1$ provides the final expression

$$H_{imp-ph} = \frac{1}{\sqrt{\mathcal{S}}} \frac{\eta^{1/4} g_{AB} \sqrt{n_A} l}{\sqrt{2}} \sum_{\mathbf{k},\mathbf{q}} q (a_{\mathbf{q}} + a^{\dagger}_{-\mathbf{q}})\, b^{\dagger}_{\mathbf{k}+\mathbf{q}}\, b_{\mathbf{k}}, \tag{A.8}$$

Comparing with Eq. (4) of the main text and substituting $n_A l^2 = \upsilon/\pi$, we identify the impurity-phonon coupling in the "large polaron" regime

$$g_{\mathbf{q}} = \frac{1}{\sqrt{2\pi}}\, \eta^{1/4} g_{AB}\, \upsilon^{1/2}\, q.$$

A.2 Perturbative renormalization group

In order to derive perturbative RG equations (*Shankar, R.; RMP.*1994), we will need the noninteracting Green's functions for impurity and phonon operators:

$$\begin{aligned} G(\mathbf{k}, i\omega) &= -\int d\tau\, e^{i\omega\tau} \langle T_\tau b_{\mathbf{k}}(\tau) b^\dagger_{\mathbf{k}}(0)\rangle_0 \\ &= \frac{1}{i\omega - \varepsilon_{\mathbf{k}}}, \end{aligned} \tag{A.9}$$

$$\begin{aligned} D(\mathbf{q}, i\nu) &= -\int d\tau\, e^{i\nu\tau} \langle T_\tau [a_{\mathbf{q}}(\tau) + a^\dagger_{-\mathbf{q}}(\tau)][a^\dagger_{\mathbf{q}}(0) + a_{-\mathbf{q}}(0)]\rangle_0 \\ &= -\frac{2\omega_{\mathbf{q}}}{\nu^2 + \omega_{\mathbf{q}^2}}. \end{aligned} \tag{A.10}$$

A.2.1 Interaction vertex

We define the effective coupling constant λ_{eff} from the three-point function as follows:

$$\begin{aligned} &\Gamma(\mathbf{k}, \mathbf{k}', \mathbf{q}; \omega, \omega', \nu) = \\ &= \int d\tau d\tau' d\tau''\, e^{i\omega\tau} e^{i\omega'\tau'} e^{i\nu\tau''} \langle b^\dagger_{\mathbf{k}}(\tau) b_{\mathbf{k}'}(\tau') [a^\dagger_{\mathbf{q}}(\tau'') + a_{-\mathbf{q}}(\tau'')] e^{-\int d\tau\, H_{imp-ph}(\tau)}\rangle_0 \\ &= \frac{1}{\sqrt{\mathcal{S}}}\, \lambda_{eff} q \delta_{\mathbf{k}', \mathbf{k}+\mathbf{q}} 2\pi\delta(\omega' - \omega - \nu) G(\mathbf{k}, i\omega) G(\mathbf{k}', i\omega') D(\mathbf{q}, i\nu). \end{aligned} \tag{A.11}$$

To first order in the interaction, we obtain

$$\begin{aligned} \Gamma^{(1)} &= -\frac{\lambda}{\sqrt{\mathcal{S}}} \sum_{\mathbf{p}_1, \mathbf{q}_1} q_1 \int d\tau_1 d\tau d\tau' d\tau''\, e^{i\omega\tau} e^{i\omega'\tau'} e^{i\nu\tau''} \langle b^\dagger_{\mathbf{k}}(\tau) b_{\mathbf{k}'}(\tau') b^\dagger_{\mathbf{p}_1+\mathbf{q}_1}(\tau_1) b_{\mathbf{p}}(\tau_1)\rangle_0 \\ &\quad \times \langle [a^\dagger_{\mathbf{q}}(\tau'') + a_{-\mathbf{q}}(\tau'')][a_{\mathbf{q}_1}(\tau_1) + a^\dagger_{-\mathbf{q}_1}(\tau_1)]\rangle_0 \\ &= \frac{1}{\sqrt{\mathcal{S}}}\, \lambda q \delta_{\mathbf{k}', \mathbf{k}+\mathbf{q}} \int d\tau_1 d\tau d\tau' d\tau''\, e^{i\omega\tau} e^{i\omega'\tau'} e^{i\nu\tau''} G(\mathbf{k}, \tau_1 - \tau) G(\mathbf{k}', \tau' - \tau_1) D(\mathbf{q}, \tau_1 - \tau'') \\ &= \frac{1}{\sqrt{\mathcal{S}}}\, \lambda q \delta_{\mathbf{k}', \mathbf{k}+\mathbf{q}} 2\pi\delta(\omega' - \omega - \nu) G(\mathbf{k}, i\omega) G(\mathbf{k}', i\omega') D(\mathbf{q}, i\nu). \end{aligned} \tag{A.12}$$

Therefore, to first order $\lambda_{eff} = \lambda$. We are interested in the logarithmic correction to λ_{eff} when we integrate out high-energy modes. At third order (see diagram in Fig. 1 of the

main text), we obtain

$$\begin{aligned}\Gamma^{(3)} &= -\frac{\lambda^3}{3!\mathcal{S}^{3/2}}\sum_{\mathbf{p}_1,\mathbf{q}_1} q_1 \sum_{\mathbf{p}_2,\mathbf{q}_2} q_2 \sum_{\mathbf{p}_3,\mathbf{q}_3} q_3 \int d\tau_1 d\tau_2 d\tau_3 d\tau d\tau' d\tau'' \times \\ &\times \langle b^\dagger_{\mathbf{k}}(\tau) b_{\mathbf{k}'}(\tau') b^\dagger_{\mathbf{p}_1+\mathbf{q}_1}(\tau_1) b_{\mathbf{p}_1}(\tau_1) b^\dagger_{\mathbf{p}_2+\mathbf{q}_2}(\tau_2) b_{\mathbf{p}_2}(\tau_2) b^\dagger_{\mathbf{p}_3+\mathbf{q}_3}(\tau_3) b_{\mathbf{p}_3}(\tau_3)\rangle_0 \\ &\times \langle [a^\dagger_{\mathbf{q}}(\tau'') + a_{-\mathbf{q}}(\tau'')][a_{\mathbf{q}_1}(\tau_1) + a^\dagger_{-\mathbf{q}_1}(\tau_1)][a_{\mathbf{q}_2}(\tau_2) + a^\dagger_{-\mathbf{q}_2}(\tau_2)][a_{\mathbf{q}_3}(\tau_3) + a^\dagger_{-\mathbf{q}_3}(\tau_3)]\rangle_0 \\ &= -\frac{\lambda^3}{\mathcal{S}^{3/2}}\, q \delta_{\mathbf{k}',\mathbf{k}+\mathbf{q}} 2\pi\delta(\omega' - \omega - \nu) G(\mathbf{k}, i\omega) G(\mathbf{k}', i\omega') D(\mathbf{q}, i\nu) \\ &\times \sum_{\mathbf{q}_1} q_1^2 \int \frac{d\nu_1}{2\pi}\, G(\mathbf{k}+\mathbf{q}_1, i\omega + i\nu_1) G(\mathbf{k}+\mathbf{q}+\mathbf{q}_1, i\omega + i\nu + i\nu_1) D(\mathbf{q}_1, i\nu_1).\end{aligned}$$

Comparing with Eq. (A.11), we note that

$$\begin{aligned}\delta\lambda^{(3)} &= -\lambda^3 \int \frac{d^2q_1}{(2\pi)^2}\, q_1^2 \int \frac{d\nu_1}{2\pi} G(\mathbf{k}+\mathbf{q}_1, i\omega + i\nu_1) G(\mathbf{k}+\mathbf{q}+\mathbf{q}_1, i\omega + i\nu + i\nu_1) D(\mathbf{q}_1, i\nu_1) \\ &= -\lambda^3 \int \frac{d^2q_1}{(2\pi)^2}\, q_1^2 \int \frac{d\nu_1}{2\pi}\, \frac{1}{(i\omega + i\nu_1 - \varepsilon_{\mathbf{k}+\mathbf{q}_1})(i\omega + i\nu_1 + i\nu - \varepsilon_{\mathbf{k}+\mathbf{q}+\mathbf{q}_1})} \left(\frac{1}{i\nu_1 - \omega_{\mathbf{q}_1}} - \frac{1}{i\nu_1 + \omega_{\mathbf{q}_1}}\right).\end{aligned}$$

The integration over ν_1 (closing the contour in the upper half of the complex plane) yields

$$\delta\lambda^{(3)} = \lambda^3 \int \frac{d^2q_1}{(2\pi)^2}\, \frac{q_1^2}{(i\omega - \omega_{\mathbf{q}_1} - \varepsilon_{\mathbf{k}+\mathbf{q}_1})(i\omega - \omega_{\mathbf{q}_1} + i\nu - \varepsilon_{\mathbf{k}+\mathbf{q}+\mathbf{q}_1})}. \tag{A.13}$$

We choose the fast modes to lie in the momentum shell $\mathcal{K}' < q_1 < \mathcal{K}$. The external momenta and frequencies (for the latter, we perform the analytic continuation $i\omega \to \omega$, $i\nu \to \nu$) are taken to be slow, such that $k, q \ll q_1$ and $\omega, \nu \ll \omega_{\mathbf{q}_1}, \varepsilon_{\mathbf{q}_1}$. Thus

$$\begin{aligned}\delta\lambda^{(3)} &= \lambda^3 \int \frac{d^2q_1}{(2\pi)^2}\, \frac{q_1^2}{(\omega_{\mathbf{q}_1} + \varepsilon_{\mathbf{q}_1})^2} \\ &= \frac{2\mu^2\lambda^3}{\pi} \int_{\mathcal{K}'}^{\mathcal{K}} \frac{dq_1}{q_1} \\ &= \frac{2\mu^2\lambda^3}{\pi} \ln\frac{\mathcal{K}}{\mathcal{K}'}.\end{aligned}$$

We introduce the cutoff scales with dimensions of energy $\Lambda = \mathcal{K}^2/2\mu$, $\Lambda' = (\mathcal{K}')^2/2\mu$; in this notation,

$$\delta\lambda^{(3)} = \frac{\mu^2\lambda^3}{\pi} \ln\frac{\Lambda}{\Lambda'}.$$

Considering an infinitesimal reduction of the cutoff, $\Lambda' = \Lambda e^{-dl}$ with $dl \ll 1$, we obtain the RG equation for the effective coupling constant

$$\frac{d\lambda}{dl} = \frac{\mu^2 \lambda^3}{\pi}.$$

In terms of the dimensionless coupling constant $\tilde{\lambda} = \mu\lambda$, we can write

$$\frac{d\tilde{\lambda}}{dl} = \frac{\tilde{\lambda}^3}{\pi}.$$

This β function implies that $\tilde{\lambda}$ flows to strong coupling. The solution for the renormalized coupling constant is

$$\tilde{\lambda}^2(\Lambda) = \frac{\tilde{\lambda}_0^2}{1 - (2\tilde{\lambda}_0^2/\pi)\ln(\Lambda_0/\Lambda)}, \tag{A.14}$$

where $\lambda_0 = \lambda(\Lambda_0)$ is the bare coupling constant. The perturbative result breaks down at energy scale $\Lambda \sim \Lambda_0 e^{-\pi/2\tilde{\lambda}_0^2}$. In terms of impurity momentum, the strong coupling regime sets in below $k \sim l^{-1} e^{-\pi/4\tilde{\lambda}_0^2}$. For small $\tilde{\lambda}_0$ it may be difficult to observe the full crossover to strong coupling in a finite size vortex lattice since the length scale above which $\tilde{\lambda}(\Lambda)$ becomes of order 1 is exponentially large. The line shape of the spectral function at the strong coupling fixed point is an open problem.

A.3 RG flow

We derived the RG equations for the non perturbative regime, considering high order correction diagrams and applying $G(\mathrm{k},\omega) = Z_\mathrm{k}/\omega$ for impurity Green function.

A.3.1 Field renormalization

The second order self-energy diagrams are → Rainbow diagram - (AI)

$$\sum_{AI} = \int \frac{d^2q}{(2\pi)^2}\,\frac{d^2q'}{(2\pi)^2}\,\frac{d\nu}{2\pi}\,\frac{d\nu'}{2\pi}\,\lambda^4\,q^2\,q'^2\,D(\nu,\omega_\mathbf{q})\,D(\nu',\omega_{\mathbf{q}'})\,G^2(\omega-\nu,\varepsilon_{\mathbf{k}-\mathbf{q}})\,G(\omega-\nu-\nu',\varepsilon_{\mathbf{k}-\mathbf{q}-\mathbf{q}'})$$
$$= -\int \frac{d^2q}{(2\pi)^2}\,\frac{d^2q'}{(2\pi)^2}\,\lambda^4\,q^2\,q'^2\,\left(\frac{1}{\omega-\omega_\mathbf{q}-\varepsilon_{\mathbf{k}-\mathbf{q}}+i\delta}\right)^2\frac{1}{\omega-\omega_\mathbf{q}-\omega_{\mathbf{q}'}-\varepsilon_{\mathbf{k}-\mathbf{q}-\mathbf{q}'}+i\delta}.$$

→ Vertex correction - (V)

$$\sum_{V} = \int \frac{d^2q}{(2\pi)^2}\,\frac{d^2q'}{(2\pi)^2}\,\frac{d\nu}{2\pi}\,\frac{d\nu'}{2\pi}\,\lambda^4\,q^2\,q'^2\,D(\nu,\omega_\mathbf{q})\,D(\nu',\omega_{\mathbf{q}'})\,G(\omega-\nu,\varepsilon_{\mathbf{k}-\mathbf{q}})\,G(\omega-\nu-\nu',\varepsilon_{\mathbf{k}-\mathbf{q}-\mathbf{q}'})$$
$$G(\omega-\nu',\varepsilon_{\mathbf{k}-\mathbf{q}'})$$
$$= -\int \frac{d^2q}{(2\pi)^2}\,\frac{d^2q'}{(2\pi)^2}\,\lambda^4\,q^2\,q'^2\,\frac{1}{\omega-\omega_\mathbf{q}-\varepsilon_{\mathbf{k}-\mathbf{q}}+i\delta}\,\frac{1}{\omega-\omega_\mathbf{q}-\omega_{\mathbf{q}'}-\varepsilon_{\mathbf{k}-\mathbf{q}-\mathbf{q}'}+i\delta}\,\frac{1}{\omega-\omega_{\mathbf{q}'}-\varepsilon_{\mathbf{k}-\mathbf{q}'}+i\delta}.$$

Together with the first order correction, applying $Z_\mathrm{k} = \left(1-\frac{\partial\Sigma(\mathrm{k},\omega)}{\partial\omega}\right)^{-1}\Big|_{\omega=0}$ we obtain

$$Z_\mathrm{k} \sim 1 - \frac{\lambda^2M^2}{\pi}\,Z_\mathrm{k}\,\ln\left(\frac{\Lambda}{\Lambda'}\right) - \frac{\lambda^4M^4}{\pi^2}\,Z_\mathrm{k}^3\,\ln\left(\frac{\Lambda}{\Lambda'}\right). \tag{A.15}$$

A.3.2 Higher order vertex diagrams

The high order vertex correction gives

$$\delta\lambda_{AI}^{(5)} = \lambda^5 \int \frac{d^2q_1}{(2\pi)^2}\,\frac{d^2q_2}{(2\pi)^2}\; q_1^2\; q_2^2\;\; \frac{1}{i\omega - \omega_{\mathbf{q}_1} - \varepsilon_{\mathbf{k}+\mathbf{q}_1}}\;\; \frac{1}{i\omega - \omega_{\mathbf{q}_1} - \omega_{\mathbf{q}_2} - \varepsilon_{\mathbf{k}+\mathbf{q}_1+\mathbf{q}_2}} \times \frac{1}{i\omega' - \omega_{\mathbf{q}_1} - \omega_{\mathbf{q}_2} - \varepsilon_{\mathbf{k}+\mathbf{q}+\mathbf{q}_1+\mathbf{q}_2}}\;\; \frac{1}{i\omega' - \omega_{\mathbf{q}_1} - \varepsilon_{\mathbf{k}+\mathbf{q}+\mathbf{q}_1}},$$

and

$$\delta\lambda_{V}^{(5)} = \lambda^5 \int \frac{d^2q_1}{(2\pi)^2}\,\frac{d^2q_2}{(2\pi)^2}\; q_1^2\; q_2^2\;\; \frac{1}{i\omega - \omega_{\mathbf{q}_2} - \varepsilon_{\mathbf{k}+\mathbf{q}_2}}\;\; \frac{1}{i\omega - \omega_{\mathbf{q}_1} - \omega_{\mathbf{q}_2} - \varepsilon_{\mathbf{k}+\mathbf{q}_1+\mathbf{q}_2}} \times \frac{1}{i\omega' - \omega_{\mathbf{q}_1} - \omega_{\mathbf{q}_2} - \varepsilon_{\mathbf{k}+\mathbf{q}+\mathbf{q}_1+\mathbf{q}_2}}\;\; \frac{1}{i\omega' - \omega_{\mathbf{q}_1} - \varepsilon_{\mathbf{k}+\mathbf{q}+\mathbf{q}_1}}.$$

As before, we assume $G(\mathrm{k},\omega) = Z_\mathrm{k}/\omega$ and include lower order corrections to have

$$\delta\lambda = \frac{\lambda^3\, M^2}{\pi}\; Z_\mathrm{k}^2\; \ln\left(\frac{\Lambda}{\Lambda'}\right) + \frac{\lambda^5 M^4}{\pi^2}\; Z_\mathrm{k}^4\; \ln\left(\frac{\Lambda}{\Lambda'}\right). \tag{A.16}$$

A.3.3 RG equations

In the perturbative regime ($Z \sim 1$), we did have the RG equations

$$\begin{aligned} \frac{dm}{d\ell} &= \frac{2\lambda^2\,\mu^3}{\pi}, \\ \frac{d\lambda}{d\ell} &= \frac{\lambda^3\,\mu^2}{\pi}. \end{aligned} \tag{A.17}$$

That can be solved to provide $\lambda(\ell) = \lambda_0\; \left(\frac{m(\ell)}{m_0}\right)^{1/2}\; e^{\left[\frac{m(\ell)-m_0}{2M}\right]}$.

According with the previous section, disregarding high order corrections, the general RG equations will be

$$\begin{aligned}
\frac{dm}{d\ell} &= \frac{2\lambda^2\,\mu^3}{\pi}, \\
\frac{d\lambda}{d\ell} &= \frac{\lambda^3\,\mu^2\,Z_{\rm k}^2}{\pi}, \\
\frac{dZ_{\rm k}}{d\ell} &= -\frac{\lambda^2\,\mu^2\,Z_{\rm k}}{\pi},
\end{aligned} \tag{A.18}$$

which have the solution $\lambda(\ell) = \lambda_0\, e^{1/2}\, e^{-Z(\ell)^2/2}$ and $Z(\ell) = \left(\frac{m_0}{m(\ell)}\right)^{1/2}\, e^{\left[-\frac{m(\ell)-m_0}{2M}\right]}$.

We can extract the asymptotic coupling $\lambda(Z \to 0) = e^{1/2}\lambda_0$, that is proportional to the bare interaction constant λ_0.

A.4 Residual impurity-phonon interaction

We start with

$$G(\mathbf{r},t) = \langle 0|T\Psi(\mathbf{r},t)\Psi^\dagger(\mathbf{0},0)\; e^{\alpha Y(\mathbf{r},t)}e^{-\alpha Y(\mathbf{0},0)}\; e^{-i\int dt_1 H_{int}(t_1)}|0\rangle \tag{A.19}$$

$$H_{int} = \frac{1}{\sqrt{S}}\sum_{\mathbf{k},\mathbf{q}} \lambda'\; q\; \hat{b}^\dagger_{\mathbf{k}+\mathbf{q}}\; \hat{b}_{\mathbf{k}}\; \hat{\phi}_{\mathbf{q}}$$
$$\hat{\phi}_{\mathbf{q}} = \hat{a}_{\mathbf{q}} + \hat{a}^\dagger_{-\mathbf{q}}$$

$$Y(\mathbf{r},t) = \frac{1}{\sqrt{S}}\sum_{\mathbf{q}} \frac{e^{i\mathbf{q}\cdot\mathbf{r}}}{q}\; \hat{\Pi}_{\mathbf{q}}$$
$$\hat{\Pi}_{\mathbf{q}} = \hat{a}_{\mathbf{q}} - \hat{a}^\dagger_{-\mathbf{q}}$$

Expanding Eq. (A.19) to second order in λ' as in Eq. (3.62), the second term provides the diagrams

→ Self-energy insertion

$$i^2\lambda'^2\frac{1}{S^2}\sum_{\mathbf{k}_1,\mathbf{q}_1} q_1^2\; e^{i\mathbf{k}_1\cdot\mathbf{r}}\; \frac{1}{(2\pi)^2}\int d\omega_1 d\nu_1\; e^{-i\omega_1 t}G^2(\mathbf{k}_1,\omega_1)G(\mathbf{k}_1+\mathbf{q}_1,\omega_1+\nu_1)D(\mathbf{q}_1,\nu_1)$$
$$\times\; \langle e^{\alpha Y(\mathbf{r},t)}e^{-\alpha Y(\mathbf{0},0)}\rangle$$

→ Connected phonon cloud

$$i^2\lambda'^2\;(-\alpha^2)\;\frac{1}{S^3}\sum_{\mathbf{k}_1,\mathbf{q}_1,\mathbf{q}_2} e^{i(\mathbf{k}_1+\mathbf{q}_1)\cdot\mathbf{r}}\;\frac{1}{(2\pi)^3}\int d\omega_1 d\nu_1 d\nu_2\; e^{-i(\omega_1+\nu_1)t}G(\mathbf{k}_1,\omega_1)G(\mathbf{k}_1+\mathbf{q}_1,\omega_1+\nu_1)$$
$$G(\mathbf{k}_1+\mathbf{q}_1+\mathbf{q}_2,\omega_1+\nu_1+\nu_2)F(\mathbf{q}_1,\nu_1)F(\mathbf{q}_2,\nu_2)\times\;\langle e^{\alpha Y(\mathbf{r},t)}e^{-\alpha Y(\mathbf{0},0)}\rangle$$

where

$$G(\mathbf{k},\epsilon) = \frac{1}{\epsilon-\epsilon_{\mathbf{k}}+i\delta}$$
$$D(\mathbf{q},\omega) = \frac{1}{\omega-\omega_{\mathbf{q}}+i\delta} - \frac{1}{\omega+\omega_{\mathbf{q}}-i\delta}$$
$$F(\mathbf{p},\nu) = -\frac{1}{\nu-\nu_{\mathbf{p}}+i\delta} - \frac{1}{\nu+\nu_{\mathbf{p}}-i\delta}$$